For Reference

NOT TO BE TAKEN FROM THIS ROOM

For Reference

NOT TO BE TAKEN FROM THIS ROOM

Ex libris
universitatis
albertaensis

QUAECUMQUE VERA

The University of Alberta
Printing Department
Edmonton, Alberta

[illegible]

[illegible]

[illegible]

by

© [illegible]

[illegible]

[illegible]

[illegible]

[illegible]

[illegible]

[illegible]

[illegible]

THE UNIVERSITY OF ALBERTA

A STUDY OF ^{30}P STATES BELOW 5 MeV VIA THE REACTION ^{28}Si(^{3}He, p)^{30}P

by

©

Clifford William Harvey Vermette

A THESIS
SUBMITTED TO THE FACULTY OF GRADUATE STUDIES
IN PARTIAL FULFILMENT OF THE REQUIREMENTS FOR THE DEGREE
OF DOCTOR OF PHILOSOPHY

DEPARTMENT OF PHYSICS
EDMONTON, ALBERTA

Sept., 1967

UNIVERSITY OF ALBERTA

FACULTY OF GRADUATE STUDIES

The undersigned certify that they have read, and recommend to the Faculty of Graduate Studies for acceptance, a thesis entitled A STUDY OF ^{30}P STATES BELOW 5 MeV VIA THE REACTION ^{28}Si(^{3}He, p)^{30}P, submitted by Clifford William Harvey Vermette in partial fulfilment of the requirements for the degree of Doctor of Philosophy.

ABSTRACT

Spins of sixteen excited states of ^{30}P have been investigated in conjunction with multipole mixing and branching ratios of a number of transitions via the reaction $^{28}Si(^{3}He, p)^{30}P$ (Q = 6.34 MeV). Spin assignments are consistent with those of other investigators in all cases except for the 4.92 MeV level. The branching ratios for this level are also in disagreement with those previously reported. Assuming, as suggested by the present results, a transition to the 0.68 MeV level rather than to the 0.71 MeV level, a unique assignment of J = 1 is made to the 4.92 MeV level. A probable new assignment of J = 1 has been made to the 3.74 MeV level. Also, the previously unstudied 2.84, 3.84, 3.93 and 4.73 MeV levels have been assigned possible spin values together with branching ratios and multipole mixing ratios for their decay transitions. Branching ratios for transitions from the 3.74, 3.84, 3.93 and 4.50 MeV levels are in serious disagreement with those of previous studies. Using shell model wave functions, calculations of lifetimes, multipole mixing ratios and branching ratios corresponding to five low lying states showed agreement with experimental values for only the first two excited states.

ACKNOWLEDGEMENTS

I would like to thank my supervisor, Dr. W. C. Olsen, for his cooperation, assistance and interest throughout the course of this work.

I wish to extend a very special thanks to my two colleagues, Mr. D. A. Hutcheon and Mr. D. H. Sykes for their competent help, enthusiastic support and many illuminating discussions.

Appreciation is also extended to Mr. J. J. W. Bogaards Jr. for his help during the development stages of this work, Dr. W. K. Dawson and Mr. J. F. Easton for writing SDS computer programs, Dr. D. M. Sheppard for his help in the data collection, Dr. G. Roy for his help in making the silicon targets and Mr. T. H. Hsu for photographic services.

I am grateful to Messrs. Mr. J. B. Elliott, C. Green, L. Holm and the rest of the technical staff of the Nuclear Research Center for their help.

Thanks are due to Mrs. W. Johnson for her able, expeditious efforts in typing the thesis.

Finally, I wish to thank the University of Alberta for their financial support during the course of this research.

TABLE OF CONTENTS

Page

CHAPTER I INTRODUCTION 1

- a Summary of Previous Work 1
- b Model Applications 3

CHAPTER II EXPERIMENTAL METHOD 6

- a Theory 6
- b Method of Analysis 12
- c Description of Apparatus 17
- d Electronics 23
- e Target Preparation 30
- f Spectrum Analysis 31

CHAPTER III EXPERIMENTAL RESULTS 37

- a Yield Curves 37
- b The 0.68 and 0.71 MeV Levels 50
- c The 1.45 MeV Level 53
- d The 1.97 MeV Level 53
- e The 2.54 MeV Level 65
- f The 2.72 MeV Level 70
- g The 2.84 MeV Level 70
- h The 2.94 MeV Level 82
- i The 3.02 MeV Level 82
- j The 3.74 MeV Level 87
- k The 3.84 MeV Level 94
- l The 3.93 MeV Level 101

Page

m The 4.14 and 4.18 MeV Levels 101

n The 4.23 MeV Level 111

o The 4.50 MeV Level 111

p The 4.62 MeV Level 128

q The 4.73 MeV Level 128

r The 4.92 MeV Level 138

CHAPTER IV MODEL CALCULATIONS 148

CHAPTER V CONCLUSION 152a

REFERENCES 153

APPENDIX 1 LEAST-SQUARES ANALYSIS 156

APPENDIX 2 CALCULATION OF REDUCED MATRIX ELEMENTS FOR TRANSITIONS BETWEEN TWO-PARTICLE STATES 160

LIST OF SYMBOLS 173

TABLES

Page

3-1 Branching Ratios of ^{30}P States. 40

3-2 A_2 and A_4 Coefficients from Legendre Polynomial Fits to the Angular Distributions. 42

3-3 Summary of Spin Assignments and Mixing Ratio Solutions. 43

A2-1 Multipole Expansion Coefficients 161

A2-2 Summary of I(L) Values for Harmonic Oscillator Wave Functions as a Function of a Parameter b. 164

A2-3a Proton Single-Particle Matrix Elements $\langle \ell_1 \; \tfrac{1}{2} \; j_1 || (Q_L)_{eff} || \ell_2 \; \tfrac{1}{2} \; j_2 \rangle$ 168

A2-3b Single-Particle Matrix Elements $\langle \ell_1 \; \tfrac{1}{2} \; j_1 || Q'_L || \ell_2 \; \tfrac{1}{2} \; j_2 \rangle$ 169

A2-3c Proton Single-Particle Matrix Elements $\langle \ell_1 \; \tfrac{1}{2} \; j_1 || M_L || \ell_2 \; \tfrac{1}{2} \; j_2 \rangle$ 171

A2-3d Single-Particle Matrix Elements $\langle \ell_1 \; \tfrac{1}{2} \; j_1 || M'_L || \ell_2 \; \tfrac{1}{2} \; j_2 \rangle$ 170

A2-4a E2 Two-Particle Matrix Elements for T + T' Even in the $2s_{\frac{1}{2}}$ and $1d_{\frac{3}{2}}$ Shells. 171

A4-4b M1 Two-Particle Matrix Elements for T + T' Even in the $2s_{\frac{1}{2}}$ and $1d_{\frac{3}{2}}$ Shells. 172

A2-5 Shell Model Two-Particle Configurations of Predicted ^{30}P States. 172

FIGURES

Page

Figure 2-1 Hypothetical χ^2-versus arc tan (mixing ratio) least-squares fit. 16

Figure 2-2 Photograph of the Goniometer and Target Chamber. 22

Figure 2-3 Electronics. 25

Figure 2-4 Photograph of 8 Gamma-ray Bins Taken from the SDS 920 Computer Display Unit. 29

Figure 3-1 Summary of Spin Assignments and Branching Ratios for ^{30}P Levels. 39

Figure 3-2a Yield Curves for 10 States of ^{30}P. 47

Figure 3-2b Coincident Charged-Particle Spectrum from ^{3}He on a Natural Silicon Target. at 6.2 MeV Bombarding Energy. 49

Figure 3-3 Angular Distribution and χ^2-Versus Arc tan x for the 0.71 → 0 MeV Transition that Arises from the 1.97 → 0.71 → 0 MeV Cascade. 52

Figure 3-4 Gamma-ray Spectrum for the 1.45 MeV Level of ^{30}P. 55

Figure 3-5 Angular Distribution and χ^2-Versus Arc tan x for the 1.45 → 0 MeV Transition. 57

Figure 3-6 Gamma-ray Spectrum for the 1.97 MeV Level of ^{30}P. 60

Figure 3-7 Angular Distribution and χ^2-Versus Arc tan x for the 1.97 → 0 MeV Transition. 62

Figure 3-8 Angular Distribution and χ^2-Versus Arc tan x for the 1.97 → 0.71 MeV Transition. 63

Page

Figure 3-9 Gamma-ray Spectrum for the 2.54 MeV Level of ^{30}P. 67

Figure 3-10 Angular Distribution and χ^2-Versus Arc tan x for the 2.54 → 0 MeV Transition. 69

Figure 3-11 Gamma-ray Spectrum for the 2.72 MeV Level of ^{30}P. 72

Figure 3-12 Angular Distribution and χ^2-Versus Arc tan x for the 2.72 → 0 MeV Transition. 74

Figure 3-13 Gamma-ray Spectrum for the 2.84 MeV Level of ^{30}P. 76

Figure 3-14 Angular Distribution and χ^2-Versus Arc tan x for the 2.84 → 0.71 MeV Transition. 79

Figure 3-15 Angular Distribution and χ^2-Versus Arc tan x for the 2.84 → 0 MeV Transition. 81

Figure 3-16 Gamma-ray Spectrum for the 2.94 MeV Level of ^{30}P. 84

Figure 3-17 Gamma-ray Spectrum for the 3.02 MeV Level of ^{30}P. 86

Figure 3-18 Angular Distribution for the 3.02 MeV Level of ^{30}P. 89

Figure 3-19 Gamma-ray Spectrum for the 3.74 MeV Level of ^{30}P. 91

Figure 3-20 Angular Distribution and χ^2-Versus Arc tan x for the 3.74 → 0 MeV Transition. 93

Figure 3-21 Gamma-ray Spectrum for the 3.84 MeV Level of ^{30}P. 96

Page

Figure 3-22 Angular Distribution and χ^2-Versus Arc tan x for the 3.84 → 2.94 MeV Transition. 98

Figure 3-23 Estimated Time Coincidence Peak for a State with a 20 nsec Lifetime. 99

Figure 3-24 Gamma-ray Spectrum for the 3.93 MeV Level of ^{30}P. 103

Figure 3-25 Angular Distribution and χ^2-Versus Arc tan x for the 3.93 → 2.94 MeV Transition. 105

Figure 3-26 Gamma-ray Spectrum for the 4.14 → 4.18 MeV Levels of ^{30}P. 108

Figure 3-27 Angular Distribution and χ^2-Versus Arc tan x for the 4.14 → 0 MeV Transition. 110

Figure 3-28 Gamma-ray Spectrum for the 4.23 MeV Level of ^{30}P. 113

Figure 3-29 Gamma-ray Spectrum for the 4.50 MeV Level of ^{30}P. 115

Figure 3-30 Angular Distribution and χ^2-Versus Arc tan x for the 4.50 → 0 MeV Transition. 118

Figure 3-31 Angular Distribution and χ^2-Versus Arc tan x for the 4.50 → 1.45 MeV Transition. 120

Figure 3-32 Angular Distribution for the 1.45 → 0 MeV Transition Arising from the 4.50 → 1.45 → 0 MeV Cascade. 122

Figure 3-33 Minimum in χ^2-Versus Arc tan x (mixing 124

Page

Ratio of 4.50 → 1.45 MeV Transition) for 1.45 → 0 MeV Transition that Arises from the 4.50 → 1.45 → 0 MeV Cascade. J(4.50) = 1 is Assumed.

Figure 3-34 Simultaneous Least-Squares Fit to the 4.50 → 1.45 and 1.45 → 0 MeV Transitions for the 4.50 MeV Level of ^{30}P. 127

Figure 3-35 Gamma-ray Spectrum for the 4.62 MeV Level of ^{30}P. 130

Figure 3-36 Angular Distribution and χ^2-Versus Arc tan x for the 4.62 → 1.45 MeV Transition. 132

Figure 3-37 Angular Distribution and χ^2-Versus Arc tan x for the 4.62 → 2.94 MeV Transition. 134

Figure 3-38 Gamma-ray Spectrum for the 4.73 MeV Level of ^{30}P. 136

Figure 3-39 Angular Distribution and χ^2-Versus Arc tan x for the 4.73 → 2.94 MeV Level of ^{30}P. 137

Figure 3-40a Simultaneous Least-Squares Fit to the 4.73 → 2.94 and 2.94 → 0.68 MeV Transitions. 139

Figure 3-40b Angular distribution and χ^2-versus Arc tan x for the 2.94 → 0.68 MeV transition Arising from the 4.73 → 2.94 → 0.68 Cascade. 140

Figure 3-41 Gamma-ray Spectrum for the 4.92 MeV Level of ^{30}P. 142

Page

Figure 3-42 Angular Distributions of the 4.92 → 0.68 and 4.92 → 2.94 MeV Transitions. 144

Figure 3-43 Least-Squares Fit to an Assumed 4.92 → 0.71 MeV Transition for the 4.92 MeV Level of ^{30}P. 146

Figure 4-1 A Comparison of Experimental and Calculated Multipole Mixing Ratios, Branching Ratios and Lifetimes for 5 Low Lying States of ^{30}P. 151

CHAPTER I INTRODUCTION

a. Summary of Previous work

This report describes a study of level spins and gamma-ray mixing and branching ratios for levels of ^{30}P below 5 MeV using the particle-gamma angular correlation method of Litherland and Ferguson (Li 61).

The first major investigations of the self-conjugate nucleus ^{30}P were carried out using the $^{32}S(d, \alpha)^{30}P$ reaction (En 58) and the $^{29}Si(p, \gamma)^{30}P$ reaction (Va 58). Using the former reaction, Endt and Paris accurately located the energies of 30 excited states in ^{30}P (to ±10 keV) in a region of excitation up to 5.8 MeV. They also observed a number of $T = 1$ states in violation of the isospin selection rule which allows only $T = 0$ states to be excited in this reaction. Using the $^{29}Si(p, \gamma)^{30}P$ reaction, Van der Leun and Endt (En 58) made the following spin, parity and isospin assignments to states of excitation energy E_x (denoted by $E_x(J^\pi, T)$):

Ground $(1^+, 0)$; 0.68 $(0^+, 1)$; 0.71 $(1^+, 0)$; 1.45 $(2^+, 0)$; 2.94 $(2^+, 1)$; 4.18 $(2^+, 1)$; 5.88 $(2^-, 1)$; 5.96 $(1^-, 0)$; 6.23 $(1^-, 1)$; and 6.27 $(3^-, 0)$.

In addition, they found the isospin selection rule forbidding E1 transitions between levels of the same T in self-conjugate nuclei to be valid in four resonance level decays that went

predominantly to either T = 0 or T = 1 states. Work on the same reaction by Baart et al. (Ba 62) gave the following spin and parity assignments:

Ground (1^+); 0.71 (1^+); 1.45 (2^+); 1.97 (3^+); 2.54 (2^+, 3^+); 2.72 (2^+, (1^+)); 2.94 (2^+); 3.02 (1^+, (1^-)); 4.18 (2^+, (2^-)); 5.89 (2^-); 6.00 (1^-, (1^+)); 6.27 (2^+); 6.31 (3^-, (3^+)); 6.52 (1^+, (1^-)); and 6.53 (2^+).

The less probable of two possible assignments has been enclosed in parentheses. Also using the ^{29}Si(p, γ)^{30}P reaction, Moore (Mo 63) provided additional branching ratio information and the following five spin and parity assignments:

2.54 (3^+); 4.23 (2^+); 6.84 (1^+); 7.04 (2^+); and 7.21 (2^+).

Further work by Harris and Hyder (Ha 66B, Ha 67B) on the same reaction led to the following eight unique spin and parity assignments:

0.71 (1^+); 1.45 (2^+); 1.97 (3^+); 2.54 (3^+); 4.23 (4^-); 4.47 (0^+); 4.63 (3^-); 4.93 (3^-); and 7.04 (4^-).

It is seen that the spins of the 4.23 and 7.04 MeV levels are in disagreement with the assignments by Moore (Mo 63) who assumed that formation of such a strong resonance by g- or f-wave protons as required for a resonance spin of 4 is unlikely. Using a 2 c.c. Ge(Li) detector,

Harris and Hyder (Ha 67A) investigated decay schemes of 7 resonances in the ^{29}Si(p, γ)^{30}P reaction and provided an accurate energy determination (±2 keV to ±4 keV) of 17 bound levels of ^{30}P. They found a weak 3% transition from the J = 4^-, 4.23 MeV level to the $J^\pi = 1^+$ ground state and a strong transition from the $J^\pi = 3^-$, 4.92 MeV level to the $J^\pi = 1^+$, 0.71 MeV level. Finally, lifetime measurements of the 0.680 and 0.709 MeV states by Kennedy et al. (Ke 67) yielded values of $\tau = (1.55 \pm 0.30) \times 10^{-13}$ sec and $\tau \leq 3.0 \times 10^{-12}$ sec, respectively. They also reported slightly revised energies of 677 ± 1 and 709.1 ± 1 keV for these levels.

b. Model Applications

To date relatively few attempts have been made to interpret ^{30}P theoretically. It is of interest, therefore, to investigate the applicability of different models by considering past calculations on nuclei in this mass region. Successful theoretical interpretation of many nuclei in the region $19 \leq A \leq 29$ in terms of a rotational collective model has been possible. For example, all observed states in the mirror pair Al^{25} and Mg^{25} (Li 58) up to 4 MeV can be described by the latter model. Bromley (Br 57) showed that many of the properties of ^{29}Si and ^{31}P can be explained by a rotational collective model. Baart et al. (Ba 62) investigated the applicability of a rotational model

to ^{30}P and found it inadequate to explain the energy levels of ^{30}P. Picard and Pinho (Pi 66) applied a strong-coupling unified model with a Soper two-body force to ^{30}P but satisfactorily predicted the position of only the first two excited states. Thankappan and Pandya found that a weak-coupling unified model explained electromagnetic transitions in ^{31}P better than did a strong-coupling unified model (Th 60). Encouraged by this discovery he applied the former model to ^{30}Si and obtained fair agreement with the observed properties (Th 62). Arima (Ar 58), on the basis of a j-j coupling shell model which assumed an inert ^{28}Si core and neglected configuration mixing, investigated nuclei in the mass region A = 29 to 40. In the case of ^{30}P his predicted energy level positions showed only fair agreement with the experimentally observed level positions. Later shell model calculations by Glaudemans *et al.* (Gl 64) which included configuration mixing produced better agreement with observed level positions in the case of ^{30}P. A comparison of the latter model with observed radiative properties is made in Chapter IV. Employing an intermediate coupling model, Bouten *et al.* (Bo 67) calculated energy levels as a function of a parameter measuring the relative strength of spin-orbit and central forces for almost all nuclei in the mass region $18 < A < 38$. In the case of ^{30}P their predicted energy level positions

show only fair agreement with the observed energy level positions.

CHAPTER II EXPERIMENTAL METHOD

a. Theory

The measurement technique used in this work involved the detection of charged particle reaction products emitted near 180° in an axially mounted annular, silicon surface-barrier detector. Gamma rays in coincidence with these protons were detected by a NaI(Tl) counter between angles of 0° and 90°. For this arrangement the gamma-ray angular distributions can be expressed in terms of an expansion of even Legendre polynomials and are, therefore, symmetric about 90°. Because of the charged-particle detector's axial symmetry, the angular distribution will also be symmetric about 0°. Litherland and Ferguson (Li 61) have shown that detection of the outgoing particles, y, from a reaction A(x, y)B* by a point counter on the beam axis limits the maximum number of magnetic substates of the residual nucleus B* that can be populated according to

$$|\alpha|_{max} \leq S_A + S_x + S_y$$

where α is a magnetic quantum number of B* and S_A, S_x and S_y are the maximum z-components of spin of the target, bombarding and outgoing particles, respectively. This restriction arises basically from the fact that the

orbital angular momenta contained in plane waves have only zero projection along their direction of propagation. A further condition on the population parameters results from the alignment of the state B*. If $P(\alpha)$ denotes the population of the α^{th} substate relative to the other substates then alignment as opposed to polarization of B* implies that $P(\alpha) = P(-\alpha)$. Thus, for the reaction $^{28}Si(^{3}He, p)^{30}P$, (Q - 6.344 MeV) studied in this work the highest substate populated is given by $|\alpha|_{max} = 1$. Consequently, the populations of the three substates $\alpha = -1$, 0 and 1 are fully specified by the ratio $P(\pm 1)/P(0)$ together with the normalization condition $\sum_{\alpha} P(\alpha) = 1$. An important feature of the above technique is that, generally, B* will be a bound state of definite spin and parity. All information about the nature of the reaction mechanism is contained in the population parameters which are treated as unknowns in the analysis.

The effect of the non-zero size of the particle detectors is to populate substates higher than $|\alpha|_{max}$. Litherland and Ferguson investigated this problem (Li 61) and found that the corrections can be calculated only with a knowledge of the details of the reaction. They showed, moreover, that corrections in lowest order are proportional to ξ^2, ξ being the half-angle subtended by the counter. For an annular detector at 180°, ξ^2 is

replaced by $(\xi_2^2 - \xi_1^2)$ where ξ_1 and ξ_2 are the angles (measured from 180°) which are subtended at the target by the inner and outer edges of the counter. Since the corrections occur because of the nonzero projection of the outgoing orbital angular momentum on the beam axis it is expected that higher angular momenta for the outgoing particles will lead to larger corrections to the population parameters.

Following the formalism of Poletti and Warburton (Po 65) the angular distribution of gamma-rays arising from the decay of a state 'a' to a state 'b' is given by

$$W(\theta) = \sum_{\substack{k \\ k \text{ even}}} a_k P_k(\cos\theta) = \sum_k \rho_k(a) F_k(ab) Q_k P_k(\cos\theta) \tag{1-1}$$

where θ is the angle between the direction of emission of the gamma rays and the axis of alignment. The Q_k are attenuation coefficients for the gamma-ray detector, the $\rho_k(a)$ are statistical tensors which describe the alignment of the initial state, and the $F_k(ab)$ depend specifically on the gamma-ray cascade and are independent of nuclear alignment.

The statistical tensors $\rho_k(a)$ can be expressed in terms of a weighted sum of the population parameters of the 2a + 1 magnetic substates of 'a' by

$$\rho_k(a) = \sum_\alpha \rho_k(a, \alpha) P(\alpha) \tag{1-2}$$

Alignment of the state 'a' implies $P(\alpha) = P(-\alpha)$, and the normalization is such that $\sum_{\alpha} P(\alpha) = 1$. If the sum in equation 2 is limited to positive α then

$$\rho_k(a, \alpha) = (2 - \delta_{\alpha o}) \frac{(a\alpha a{-}\alpha|ko)}{(a\alpha a{-}\alpha|oo)} \qquad (1\text{-}3)$$

where the symbol $(a\alpha a{-}\alpha|ko)$ represents a Clebsh-Gordan coefficient. Values of $\rho_k(a, \alpha)$ for integer values of a between 1 and 6 and for half-integer values of a between 3/2 and 11/2 are listed in the paper of Poletti and Warburton (Po 65). The $F_k(ab)$ are given by

$$F_k(ab) = \sum_{LL'} i^{L'-L+\pi-\pi'} x_L x_{L'} F_k(LL'ba)/\sum_{L} x_L \qquad (1\text{-}4)$$

where L, L' are integers ranging from a-b to a+b (with the restriction L, L' $\neq$ 0), π and π' are associated with L and L', respectively; π is 0 for electric and 1 for magnetic radiation. The sign convention is that of Litherland and Ferguson (Li 61). The quantities x_L and $x_{L'}$ are given by ratios of reduced matrix elements as

$$x_L = \frac{<b||L||a>}{<b||L_m||a>} \; ; \quad x_{L'} = \frac{<b||L'||a>}{<b||L_m||a>} \qquad (1\text{-}5)$$

The reduced matrix elements are real and L_m is the lowest allowed value of L. The $F_k(LL'ba)$ are given by

$$F_k(LL'ba) = (-)^{b-a-1}[(2L+1)(2L'+1)(2a+1)]^{\frac{1}{2}}(L1L'-1|ko)$$

$$\times\ W(aa\ LL';\ ko) \qquad (1\text{-}6)$$

They have the symmetry property $F_k(LL'ba) = F_k(L'Lba)$, and the normalization $F_o(LL'ba) = \delta_{LL'}$. The triangular conditions on the Racah coefficient, $W(aa\ LL';\ ko)$, in equation 6 limit k to $k \leq \min(2L, 2L', 2a)$. Values of the $F_k(LL'ba)$ are tabulated in the paper of Poletti and Warburton (Po 65), and in the Argonne National Laboratory report, ANL 5324, by M. Ferentz and N. Rozenzweig.

Often the second gamma ray in a cascade a → b → c provides useful information either in conjunction with the first transition or by itself. The angular distribution of the second gamma ray is given by

$$W(\theta) = \sum_k \rho_k(a)U_k(ab)F_k(bc)Q_kP_k(\cos\theta) \qquad (1\text{-}7)$$

where

$$U_k(ab) = \sum_L x_L^2 U_k(Lab)/\sum_L x_L^2 \qquad (1\text{-}8)$$

The $U_k(Lab)$ are given by

$$U_k(Lab) = \frac{W(abab;\ Lk)}{W(abab;\ Lo)} \qquad (1\text{-}9)$$

so that $U_o(Lab) = 1$ and $U_k(Lab) = U_k(Lba)$. Equation 7 can be generalized to give the angular distribution of the n^th^ gamma ray in a cascade as

$$W(\theta) = \sum_k \rho_k(a)U_k(ab)U_k(bc)\ldots U_k(xy)F_k(yz)Q_kP_k(\cos\,\theta) \tag{1-10}$$

which contains the product of n-1 U_k coefficients.

Rarely is it necessary to include more than two multipoles in equations 4 and 8. For only two multipoles present equations 4 and 8 become

$$F_k(ab) = \frac{F_k(LLba) - (-)^{\sigma}2xF_k(LL'ba) + x^2F_k(L'L'ba)}{1 + x^2} \tag{1-11}$$

and

$$U_k(ab) = \frac{U_k(Lab) + x^2U_k(L'ab)}{1 + x^2} \tag{1-12}$$

where L is the lowest allowed multipole and L' = L + 1. The denominator $1 + x$ provides a convenient normalization. It is sometimes useful to express equations 11 and 12 in terms of an angle ϕ given by $\phi = \text{arc tan } x$. In these equations the mixing parameter x is given by

$$x = \frac{\langle b||L+1||a\rangle}{\langle b||L||a\rangle} \tag{1-13}$$

so that the x_L and $x_{L'}$ of equation 5 have become $x_L \equiv 1$, $x_{L'} \equiv x$. The Litherland-Ferguson sign convention takes $\sigma = 0$ for an EL+1/ML mixture and $\sigma = 1$ for an ML+1/EL mixture. The Rose and Brink convention (Ro 67) corresponds with the case $\sigma = 0$ independent of the type of multipole mixing. The latter convention is used throughout this

report. Values of U_k(Lab) are tabulated in the paper of Poletti and Warburton (Po 65).

b. Method of Analysis

The general problem of analysis involves fitting the equation

$$W(\theta) = \sum_{k\alpha} \rho_k(a, \alpha)P(\alpha)F_k(ab)Q_kP_k(\cos\theta) \quad (1\text{-}1)$$

to a measured angular distribution. The computer program used in the present work treats the population parameters $P(\alpha)$ as unknowns and, for each of a series of discrete values of the mixing ratio (contained in $F_k(ab)$) and assumed values for the spin(s), does a least-squares fit to the measured points in the angular distribution. The best fit corresponds to those values of the population parameters which give the lowest value of χ^2 where

$$\chi^2 = \frac{1}{N}\sum_i \frac{(Y(\theta_i) - W(\theta_i))^2}{E^2(\theta_i)} \quad (1\text{-}14)$$

The quantity $E(\theta_i)$ is the estimated uncertainty in the measured gamma-ray yield $Y(\theta_i)$ at angle θ_i and N is the number of degrees of freedom. One condition that the function defined by 1-14 must satisfy for it to be a χ^2-distribution function is that the denominator should equal the variance. A good approximation to the variance is made if one assumes Poisson statistics and takes the number of counts in a peak for $E^2(\theta_i)$. However, in the

present work $E^2(\theta_i)$ includes not only the uncertainty in the peak area but also uncertainties due to background. A problem arises with equation 14, namely, that of defining the correct number of degrees of freedom. For example, one may carry out the fitting of $W(\theta)$ to the observed gamma-ray yields, $Y(\theta_i)$, in two different ways. One way would be to vary both the population parameters and the mixing ratio together. Another way would be to step through all possible values of the mixing ratio and for each value fit $W(\theta)$ to the yields, $Y(\theta_i)$. The net result of both procedures is a solution for the mixing ratio and the population parameters on the basis of a minimum value of χ^2. However, if one takes the number of degrees of freedom as the number of data points minus the number of free parameters then in the first case there is one less degree of freedom than in the second case. Moreover, no account has been taken of the effectiveness in changing $W(\theta)$ of each of these free parameters. For instance, in fitting the angular distribution from a spin zero state only the mean of the data points is unknown. In fitting a nearly isotropic angular distribution with an assumed spin of 1 for the initial state, one will obtain a small $k = 2$ term that can be fitted with a number of different mixing ratios and population parameters. This effect occurs because the $k = 2$ term is

of the form

$$A_2 = 2F(x^0, x^1, \dots x^p)[P(1) - P(0)]$$

where x is the mixing ratio and p is an integer such that $p \leq 3$. It can be seen that for a given normalization (i.e. a given value of P(0) + 2P(1)) it is possible to produce a small A_2 for a wide range of mixing ratios. This situation is equivalent to fitting the distribution with the Legendre expansion $A_0 + A_2P_2 (\cos \theta)$. In the latter case both A_0 and A_2 are uniquely predicted and the number of degrees of freedom can be unambiguously shown to be N-2 (N is the number of data points). Thus, the three parameters x, P(0) and P(1) and the number of data points result in the same number of degrees of freedom as the two parameters A_0 and A_2 and the number of data points. In the opposite extreme, however, there are many cases where a fit leads to unique values of x, P(0) and P(1) in which case all three of these parameters are 'fully effective'. Determination of the correct number of degrees of freedom, r, can be the difference between a given solution being at the 10% confidence limit for r = 1 or at the 50% confidence limit for r = 2.

In the present work the population parameters are treated as unknowns and a least-squares fit is carried out for a discrete number of assumed mixing ratios.

The number of degrees of freedom is taken as the number of data points minus the number of allowed population parameters. Clearly, of the possible alternatives, the above choice will give the highest values of χ^2 and, therefore, in the sense of rejecting possible solutions, this choice will be the most conservative one. Moreover, spin zero solutions and those arising from isotropic angular distributions for spin 1 will have fewer degrees of freedom than they should have.

For a correct solution the value of χ^2 should be near the expected value of unity. The probability that for a correct solution the value of χ^2 obtained will be greater than a given value can be read from probability tables.[a] In the present work, solutions which did not dip below the 0.1% confidence limit were rejected.

In the reaction ^{28}Si(^{3}He, p)^{30}P (Q = 6.34 MeV) both P(0) and P(1) were allowed. Effects of the finite size of the annular charged-particle detector were estimated by including a fraction of the next highest substate. One fit was done with P(±2) = 0.025 P(0) and another with P(±2) = 0.05 P(±1). The curve having the greatest effect on the solution was plotted together with the curve for P(2) = 0. Limits on the mixing ratio solution were taken at the extremes of these curves as shown by the

---

[a] D. R. Whitney, Elements of Mathematical Statistics, (Henry Holt and Company, New York, 1959).

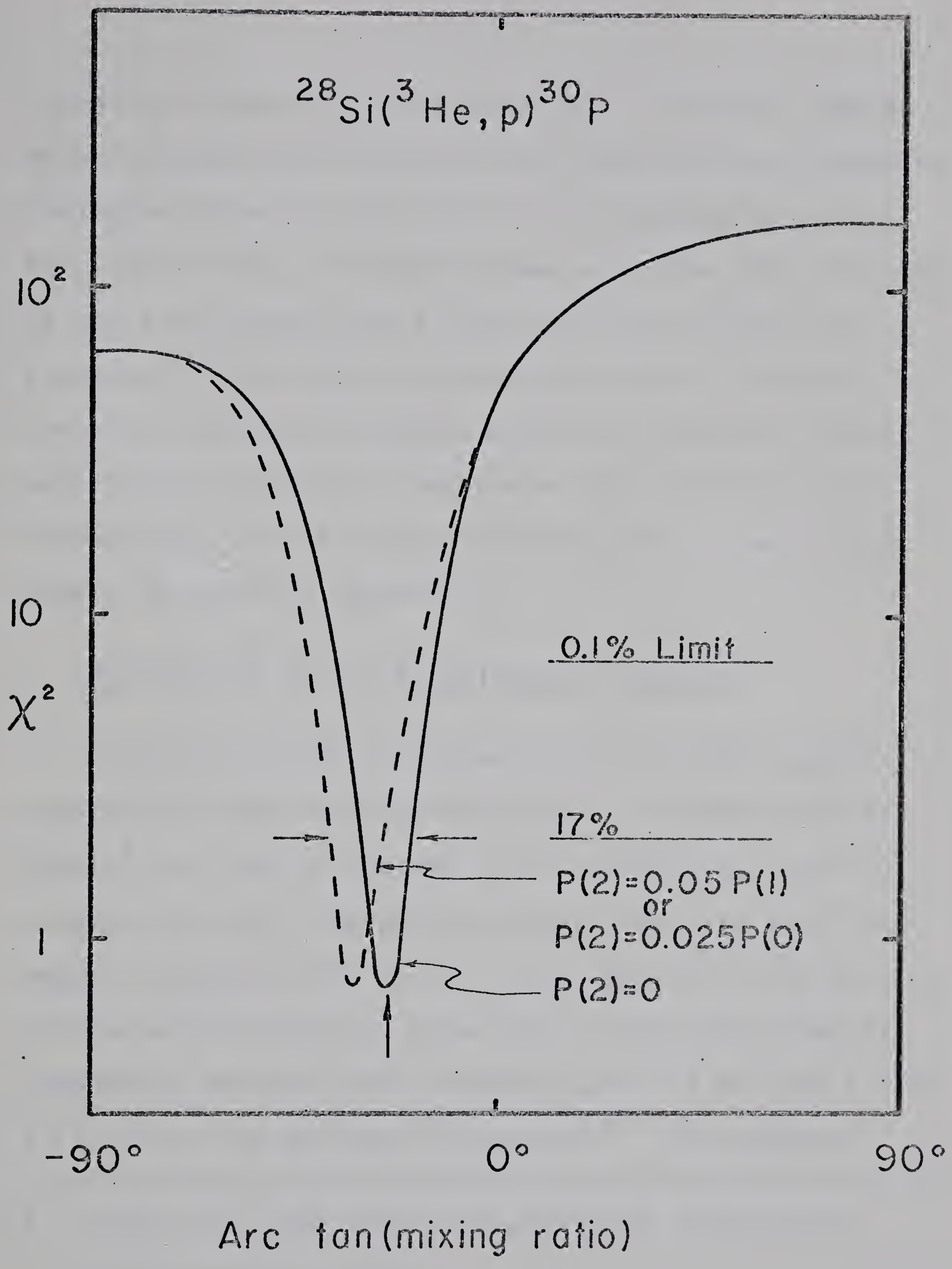

Figure 2-1 Hypothetical χ^2-versus arc tan (mixing ratio) least-squares fit.

[illegible]

[illegible]

arrows in Figure 2-1. The value of χ^2 at which limits on the mixing ratio solution were taken were one standard deviation above the 50% limit if the minimum was at or below this level. If the minimum was above the 50% limit, it was first normalized to the 50% limit and the uncertainty limits taken as mentioned above. In cases for which excessive normalization was required, limits were taken at the 0.1% confidence limit without first normalizing. A more detailed discussion of the fitting theory is given in Appendix I.

c. Description of the Experimental Apparatus

Approximately 0.2 microamperes of 6.2 MeV singly-charged ^{3}He beam from the University of Alberta Van de Graaff[b] was used to bombard a self-supporting target of natural silicon. Charged particles scattered into the angular range of 170° to 173° were detected by an annular silicon surface barrier detector[c] in the 180° geometry. Gamma rays were observed between angles of 30° and 90° by a (7.6 cm × 7.6 cm) NaI(Tl) detector[d]. The charged-

---

[b] Model CN, High Voltage Engineering, Burlington, Massachusetts, U.S.A.

[c] Nuclear Diodes, 10,000Ω-cm, 750 microns depletion depth at 200 volts bias.

[d] Harshaw "Integral Line' Assembly type 12S12/3.

particle beam originating from the radio frequency ion source first passed through a terminal analyzing magnet which sorted out the undesired mass components from the beam. The particles were then accelerated and bent through 90° by a double focusing sector magnet of radius 28.5 in. Four feet from the exit port of the analyzing magnet the beam passed through a pair of energy stabilizing slits. The current balance on these slits was maintained by a feedback circuit controlling the impedance of the corona loading of the accelerator terminal. This system limited the energy spread of the beam at the target to less than 5 keV. The beam then passed through a carbon trap, switching magnet and quadrupole lens. Since the straight through port was used only a small switching magnetic field was necessary to steer the beam into the quadrupole lens. A tantalum collimator with a 1/4 in. diameter hole was placed at the entrance to the quadrupole to ensure axial alignment with the beam. Approximately 9 feet from the exit of the quadrupole, the beam passed through a second tantalum collimator with a 3/8 in. diameter hole backed by a 1½ in. long lead cylinder of ½ in. inner diameter. This collimator served to define the beam entrance into a 9 in. long tantalum shielded, copper carbon trap of 3/4 in. inner diameter. This carbon trap minimized carbon buildup on the collimators and target. Following this trap were four more tantalum collimators

holes of 1/4, 1/8, 1/16 and 3/32 in. in that order. The first three collimators were each backed by a 1½ in. long lead cylinder of 1/4 in. inner diameter. The last collimator was placed on the end of the last lead cylinder and functioned as an antiscattering shield. The latter four collimators were spaced over a length of approximately 1 foot. A final collimator consisting of a tantalum sheet with a 3/32 in. diameter hole followed by a 1 in. long lead block having a hole slightly larger than that in the tantalum was situated in the target chamber immediately behind the annular charged-particle detector. This collimator prevented the detector resolution from being affected by intense low energy gamma rays that would otherwise arise from the beam hitting the tantalum shield on the back of the detector and spraying on the sides of the hole through the detector. After passing through the target, the beam was stopped in a tantalum lined beam catching tube approximately 1 metre long. This arrangement reduced 180° elastic scattering into the charged-particle detector to a negligible amount.

Angular changes in the gamma detector were made by moving a rotatable arm onto which the NaI(Tl) detector was mounted. The arm rotated about the center of an aluminum frame which, in turn, was bolted to the concrete floor. The entire counter support assembly,

or goniometer, was modeled after a similar design at Brookhaven National Laboratory. The target chamber was supported by the center post of the goniometer and was estimated to be within ½ mm of the axis of the rotatable arm that held the gamma-ray detector. A photograph of the target chamber mounted on the goniometer is shown in Figure 2-2.

The gamma-ray detector was placed at a distance of 10cm from the target and had a resolution of 6.2% (FWHM) for the 1.45 MeV gamma ray of ^{30}P. Specifications for this detector listed a maximum gain shift of less than 1% for a counting rate change from 1000 c/sec to 10,000c/sec and a drift of less than 1% over a 24 hour period for a counting rate of 1000 c/sec. An 1/8 in. lead sheet was placed over the detector face in order to reduce the intensity low energy gamma radiation. For this experiment the gamma detector was set at angles of 31°, 45°, 60° and 90°. Interference of the beam catching tube prevented the gamma detector from being set at angles less than 31°. Eight runs were made with two runs at each angle. The runs were typically 6 hours long.

The charged-particle detector was placed approximately 2 cm from the target. Particles were detected in a sensitive region of the detector having a 1 mm wide annulus of 5.5 mm inner diameter. For 10 MeV protons

Figure 2-2 Photograph of the Goniometer and Target Chamber

Only the top portion of the goniometer can be seen. The final lead collimator, annular detector, target holder, part of the beam catching tube and the half-moon shaped rotatable arm that supports the gamma-ray counter can all be seen.

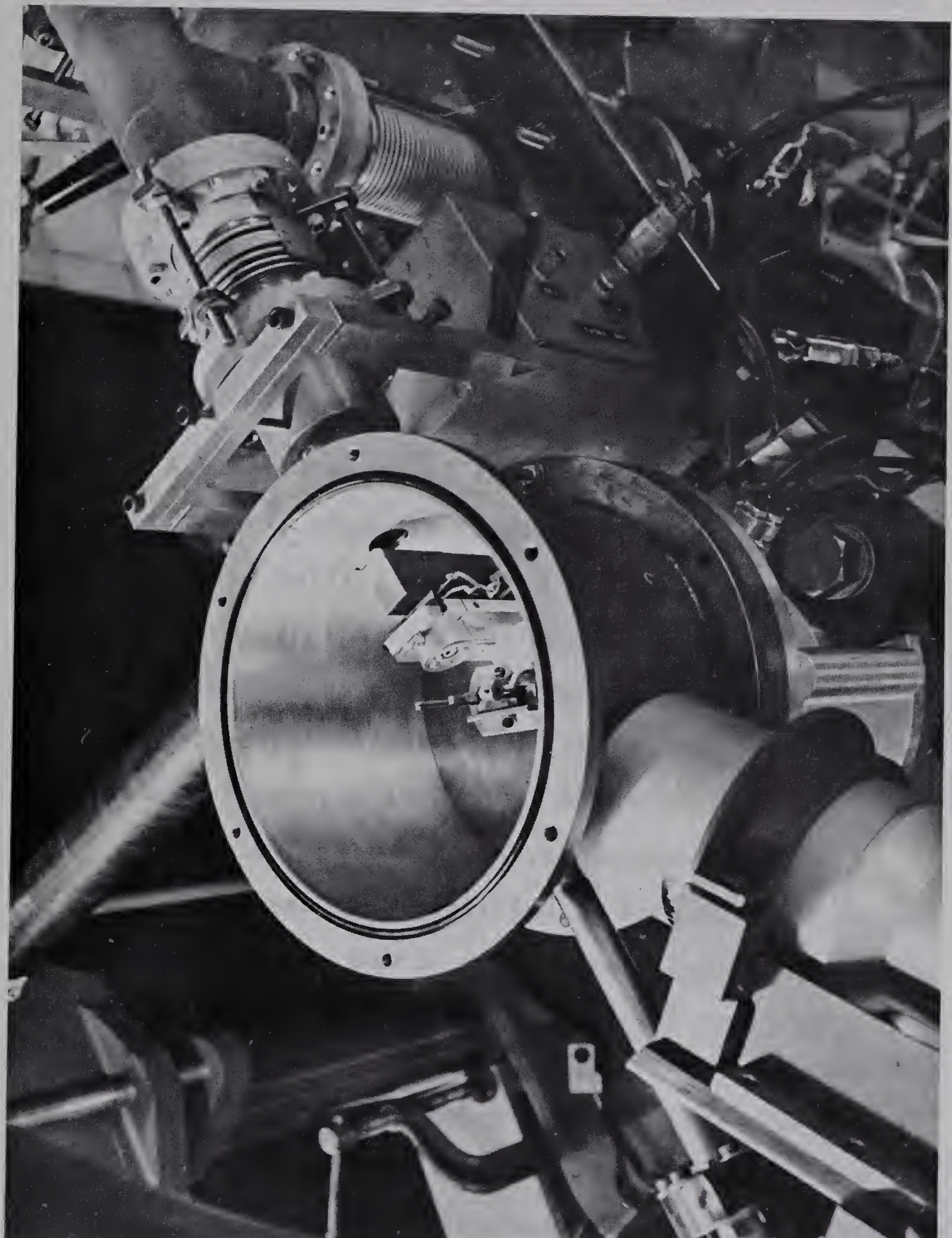

this detector exhibited a resolution of close to 65 keV. This figure includes the effect of target thickness.

System isotropy was checked using the $J^{\pi} = 0^{+}$, 2.32 MeV level of ^{14}N formed by the ^{12}C(^{3}He, p)^{14}N (Q = 4.779 MeV) reaction. The difference between the normalized number of counts at any angle and the mean, normalized number of counts was zero to within the 2% statistical uncertainty.

d Electronics

A block diagram of the electronics used in this experiment is shown in Figure 2-3. Fast coincidences between the NaI(Tl) gamma-ray and annular surface barrier charged-particle detectors were used to gate the analog pulses from these detectors into two independent analog-to-digital converters (ADC's) which were interfaced on-line with an SDS 920 computer.

Signals from the gamma-ray detector were preamplified[e] and then amplified by a shaping amplifier[f] operating in the double delay line clipping mode. The bipolar output was fanned out to the F input of a 4096 channel ND-161F Dual Analog to Digital Converter[g] (ADC) through an adjustable delay line for pulse height analysis, and to a cross-over pickoff circuit[h] for timing purposes. The (20 nsec wide, 0.5 volt after dif-

---

[e] Ortec Model 113 Scintillation Preamplifier.

[f] Ortec Model 410 Multimode Amplifier.

[g] Nuclear Data Inc., Palatine, Illinois.

[h] Ortec Model 407 Cross-over Pickoff.

Figure 2-3 Electronics.

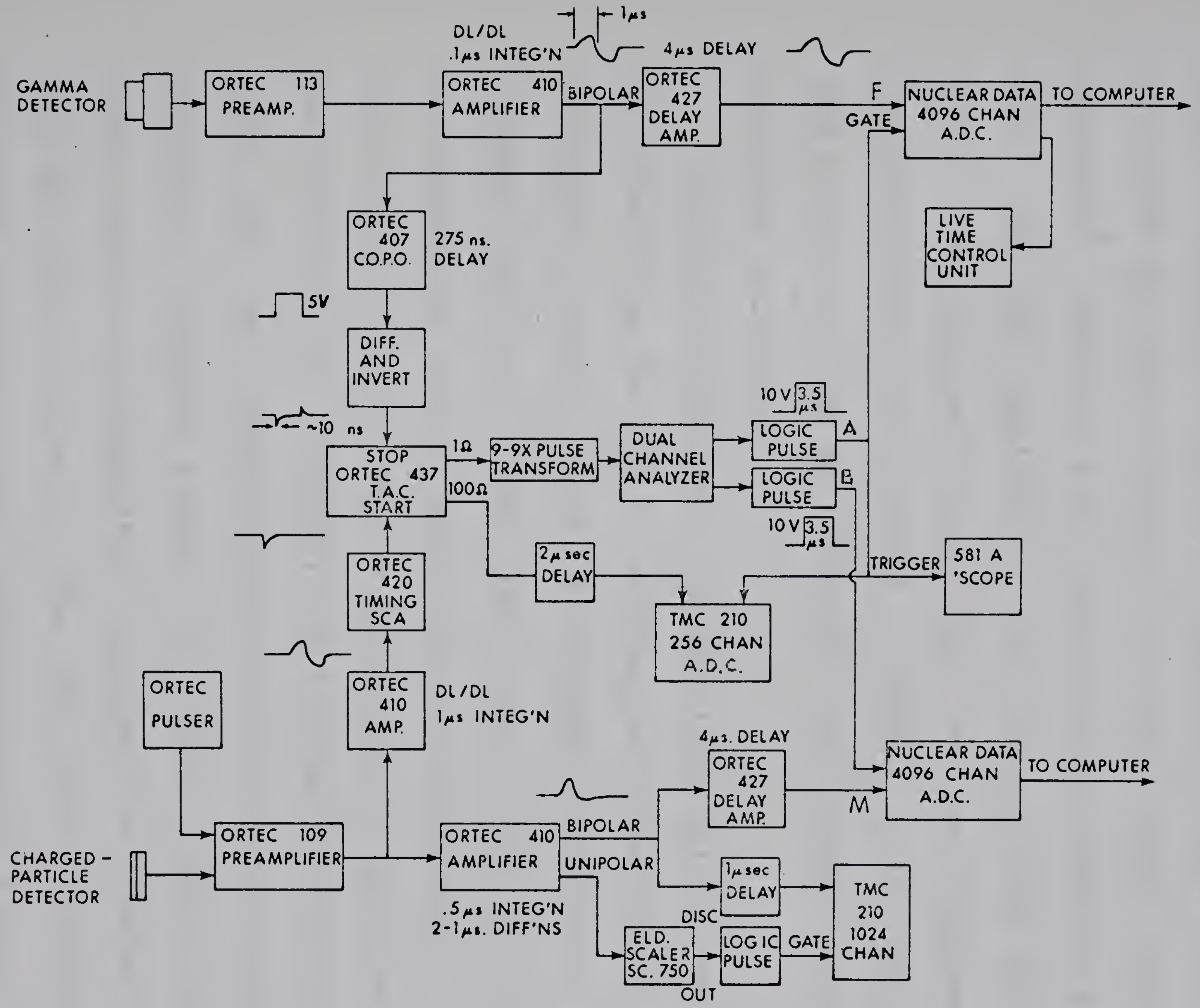

ELECTRONICS

ferentiating) output of the latter circuit provided the stop input to a time-to-amplitude converter[i] (TAC).

Signals from the solid state charged-particle detector were preamplified[j] and then fanned out to two main shaping amplifiers in parallel. One of these amplifiers, operating with double delay line shaping, provided the input pulses to a timing single channel analyzer[k] which in turn fed the start input of the TAC. The other amplifier[f] was operated with RC shaping of 0.5 microseconds integration and two 1 microsecond differentiations to present a suitable pulse shape to the M input of the ND-161F ADC[g]) for optimum charged-particle resolution.

The fast-coincidence gating logic pulses were obtained from the TAC by setting two 40 nanosecond wide, contiguous windows around its output by means of a dual channel analyzer[ℓ]. The logic output from this unit corresponding to the lower window corresponded to true plus random coincidences and was used to gate the F ADC and interrupt the computer for sorting of the coincident gamma-ray and charged-particle pulses into certain regions of computer memory. The logic output from the upper window corresponded to random coincidences only and was used to interrupt the computer for sorting of the random gamma-ray and charged-particle pulses into other regions of computer memory.

---

[i] Ortec Model 437 Time-to-Pulse Height Converter.

[j] Ortec Model 109 Transitor Preamplifier

[k] Ortec Model 420 Timing Single Channel Analyzer.

[l] F. S. Goulding and R. A. M^cNaught, Nucl. Instr. and Methods 9(1960) 282.

The gated gamma rays associated with the decay of a certain level or excited state of the final nucleus were sorted into bins by the computer by setting a window around the particle group feeding that level. Each such window generated a bin consisting of a 256 channel true-plus-random gamma-ray spectrum followed by a 256 channel associated random gamma-ray spectrum. Sixteen such bins were set allowing the simultaneous investigation of the decay of 16 excited states of the final nucleus. Also was recorded a 256 channel spectrum of the total unsorted true-plus-random coincident gamma rays, followed by a 256 channel spectrum of the corresponding total random coincident gamma rays and the true-plus-random coincident charged-particle spectrum (1024 channels) followed by its corresponding random spectrum (1024 channels).

Up to eight bins at a time could be viewed on the computer display unit while the experiment was in progress. A photograph of such a display is shown in Figure 2-4. The data for each run were stored on magnetic tape and processed off-line on the University of Alberta IBM 7040 Computer.

Monitoring of the experiment was accomplished by recording a self-gated charged particle spectrum on a separate 1024 channel pulse height analyzer[m] . Normalization of the data for each run was determined from the area

---

[m] Technical Measurements Corp. Model 210 256 Channel Pulse Height Analyzer.

Figure 2-4 Photograph of 8 Gamma-ray Bins Taken from the SDS 920 Computer Display Unit.

The trues plus randoms are in the first 256 channels of each bin followed by randoms only in the last 256 channels.

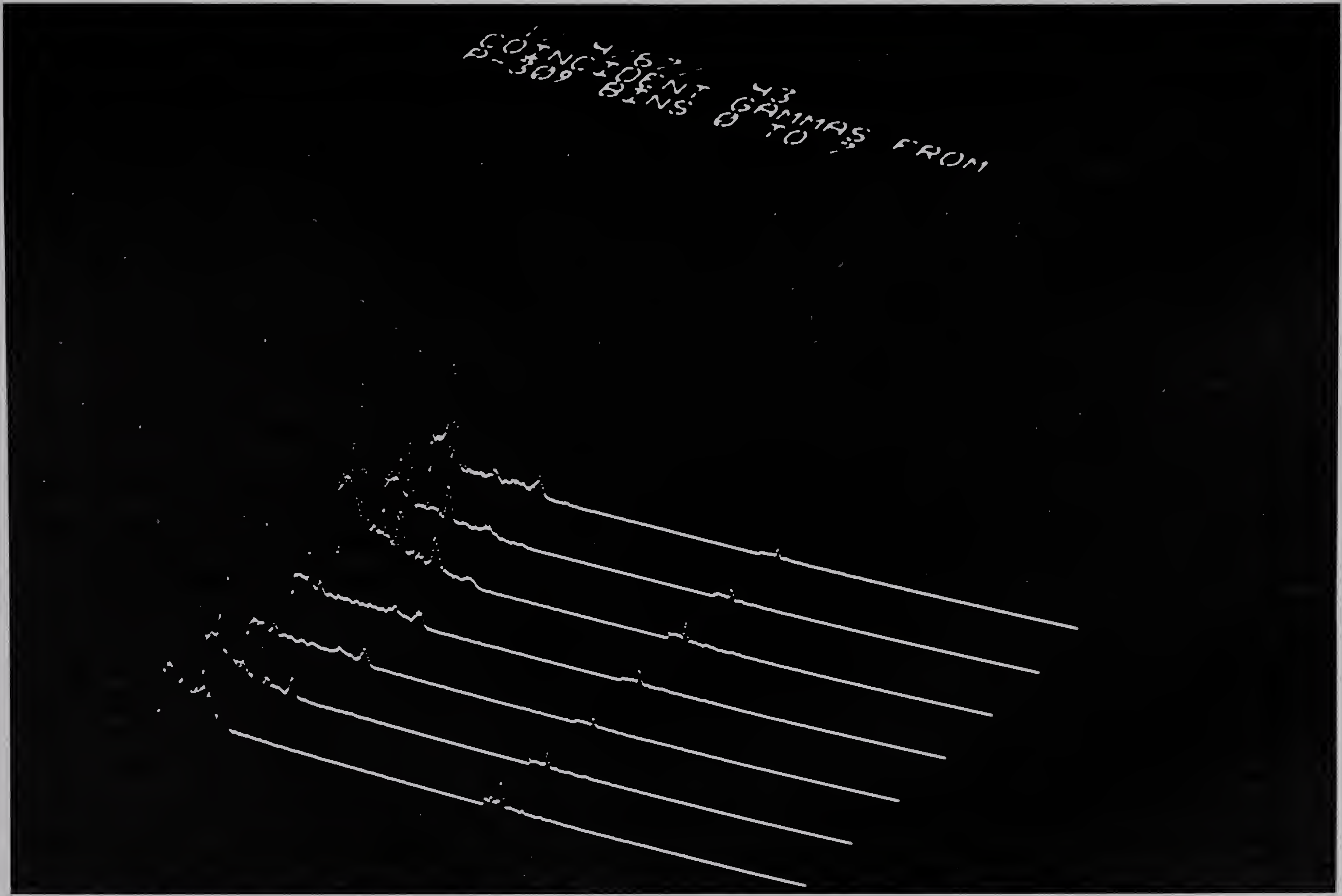
4.6 43
COINCIDENT GAMMAS FROM
P-309 BINS 0 TO 3

of selected peaks in the monitor spectrum.

e. Target Preparation

The self-supporting targets used in this work were prepared by evaporation of natural silicon. The procedure involved first evaporating NaCl onto glass slides. These slides were then placed at varying distances from the crucible of an electron gun evaporator[o]. Silicon was evaporated using an electron current of 100 ma at 3500 volts in a vacuum of less than 10^{-6} torr pressure. A slow evaporation was necessary to avoid sputtering from the molten silicon metal. After evaporation, the silicon films were floated off the glass slides onto distilled water and then picked up on aluminum target frames. In this way self-supporting targets ranging in thickness from approximately 30 to 200 $\mu g/cm^2$ were made. Measurements of target contamination and thickness were obtained by elastically scattering 3 MeV alpha particles from several of the targets. For the target used resolutions of 56 and 47 keV (FWHM) were obtained for scattering from silicon and oxygen, respectively. Using an estimated value of 35 keV for

---

[o] Model no. 980-0001 Single Crucible e-Gun Evaporation source, Varian Associates, Palo Alto, California.

detector plus electronics resolution, these figures correspond to thicknesses of approximately 55 μg/cm^2 and 30 μg/cm^2 for silicon and oxygen, respectively. All other contaminants below approximately A = 40 gave elastic scattering peak areas less than 0.1% of the area of the oxygen peak.

f. Spectrum Analysis

Gamma rays can interact with a detector crystal by Compton scattering, photoelectric absorption or pair production. The probability of interaction by each of these processes depends on the gamma-ray energy. At low energies photoelectric absorption is the dominant process and gives rise to a single peak or photopeak corresponding to absorption of the full gamma-ray energy. Compton scattering is present at all energies and results in a broad distribution beginning at slightly below the full energy peak and extending down to zero energy. It is also possible for the Compton scattered photon to be absorbed in the crystal and, in this way, contribute to the full energy peak. The relative importance of the latter process depends on gamma-ray energy and crystal size. At gamma-ray energies above 1.02 MeV pair production becomes energetically possible. The probability for interaction by pair production increases with increasing energy while that for photoelectric absorption decreases. The probability for interaction by Compton

scattering also decreases with increasing energy but less rapidly than it does for photoelectric absorption. At energies above approximately 1.5 MeV three other peaks, in addition to the photopeak, are observed. These peaks result from the interaction of the photons by pair production in either the crystal or the surrounding material. The positrons resulting from the pair-production process annihilate with electrons producing two 0.511 MeV photons. If the positrons are produced in the crystal, one or both of the annihilation photons can escape from the crystal. If only one photon escapes, a single peak 0.511 MeV lower in energy than the photopeak is produced while if both photons escape, a peak 1.02 MeV lower in energy than the photopeak is produced. The 0.511 MeV peak results from the detection of annihilation radiation produced in the surrounding material and not from the primary interactions in the detector. Thus, the response to or 'line shape' of a given gamma ray is due to the crystal dimensions and a combination of the above three basic processes.

To obtain branching ratios from a gamma-ray spectrum one must extract the relative intensities of the different energy gamma rays present. With spectra obtained by NaI(Tl) detectors these intensities are usually obtained from photopeak areas corrected for photopeak efficiency as

a function of energy[p]. Thus, one is usually concerned with unfolding contributions from a mixture of a number of different gamma-ray 'line shapes'. In this work gamma rays of interest extended from 0.68 MeV up to 4.50 MeV. Standard line shapes were constructed from the gamma rays originating from the 1.45, 1.97, 2.72, 3.73, 4.14 and 4.93 MeV levels of ^{30}P. From these 'line shapes' curves were constructed giving the ratio of the photopeak height to the heights of the first valley, Compton shoulder, first escape peak, second valley, second escape peak and asymptotic Compton tail, respectively, as a function of gamma-ray energy. A graph of full width at half maximum (FWHM) as a function of energy was also constructed. Using these, self-consistent stripping of the spectra was accomplished.

It was found that slight gain changes often occurred between runs, partly because of the large count rate change that resulted from turning off the beam and partly because of the 1/2 to 1 hour of shutdown necessary to carry out routine operations. For this reason a program was written in SDS 920 machine language to shift the counts in channel x of a spectrum to a new position x' given by x'=Gx+B. The shifting was done so as to make corresponding peaks in the different sets of spectra coincide. This program uses linear interpolation and

---

[p] R. L. Heath et al., IDO-17017 (1965) A.E.C. Research and Development Report.

was found to preserve areas to better than 1 part in 500. A more detailed discussion of the program's format and general features is given in an internal report.[g]

In determining branching ratios from spectra of gamma rays that de-excite one level only, usually only a few gamma rays are present. In these cases the analysis is usually relatively simple. Moreover, a self-consistent check is usually available in that corrected intensities of gamma rays in a given cascade must be consistent with each other and with the branching ratios of lower lying levels. Thus, analysis must start from the lower excited states and proceed successively towards the higher lying levels.

Photopeak areas in this work were determined from plotted spectra by summing the number of counts under a given peak and subtracting off the estimated background due to higher energy gamma rays. The line shapes of these higher energy peaks were constructed using the parameters of standard line shapes mentioned previously. The consistency of this method was checked by comparison with areas of several peaks as determined by a modified gaussian peak fitting program[h]. Uncertainties

---

[g] C. Vermette, University of Alberta Internal Report, 1967.

[h] M. Putnam et al., IDO-17016 (1965) A.E.C. Research and Development Report.

were estimated by taking the square root of the total number of counts under a peak including background. An additional uncertainty associated with defining the background was also included. Uncertainties in the branching ratios were computed from corrected photopeak areas according to the expression

$$\delta B_i = \sqrt{\sum_j \left(\frac{\partial B_i}{\partial A_j}\right)^2 (\delta A_j)^2}$$

$$= \frac{B_i}{A_i}\sqrt{(1-B_i)^2(\delta A_i)^2 + B_i^2\Big(\sum_{\substack{j \\ j\neq i}} \delta A_j\Big)^2} \qquad (1\text{-}16)$$

where B_i is the branching ratio of the i^{th} transition ($\sum_j B_j = 1$), A_i is the photopeak area corrected for relative efficiency of the gamma ray corresponding to this transition and δA_i is the uncertainty in A_i. Branching ratios were determined from the summed spectra of runs at 45° and 60°. Because the intensity of each gamma ray has an angular distribution of the form

$$W(\theta) = A_0 + A_2P_2(\cos\theta) + A_4P_4(\cos\theta) \qquad (1\text{-}17)$$

where the P_k (k even) are Legendre polynomials, branching ratios determined in the above mentioned way must be suitably corrected. The total intensity of gamma-ray emission into a solid angle of 4π steradians, because of the axial symmetry and symmetry about 90°, is proportional

to

$$I \alpha \int_{0^\circ}^{90^\circ} W(\theta)d\theta = A_0$$

By normalizing both the data and $W(\theta)$ to $A_0 = 100$ correction factors to the branching ratios were determined by summing the values of the data at 45° and 60°, dividing by 2 and taking the reciprocal. Except for a few distributions having large A_4 terms, correction factors were usually within 5% of unity.

CHAPTER III EXPERIMENTAL RESULTS

The following is a detailed discussion of experimental results. Results discussed in subsections a to r are summarized in tables 3-1, 3-2 and 3-3. A summary of existing information on levels of ^{30}P below 5 MeV together with spin assignments and branching ratios obtained in the present work is given in figure 3-1.

a. Yield Curves

To determine the best ^{3}He bombarding energy a charged-particle yield curve using doubly-charged ^{3}He was run over an energy range of 4.7 to 10 MeV in steps of 100 keV. The greatest variation in proton yield took place in the neighborhood of 5.5 to 6.5 MeV. Yield curves for protons corresponding to ^{30}P levels of the most interest are given in figure 3-2a for an energy range of 4.7 to 7.2 MeV. Because only general trends in the yield curve rather than accurately known areas were required, the points in these curves taken as the maximum number of counts in a peak measured from the background level for 10 microcoulombs of integrated beam current. A bombarding energy of 6.2 MeV was chosen since most of the curves in figure 3-2a exhibit a maximum or near maximum at this energy. A coincident charged-particle spectrum taken at a ^{3}He energy of 6.2 MeV is shown in figure 3-2b.

Figure 3-1 Summary of Spin Assignments and Branching Ratios for ^{30}P Levels.

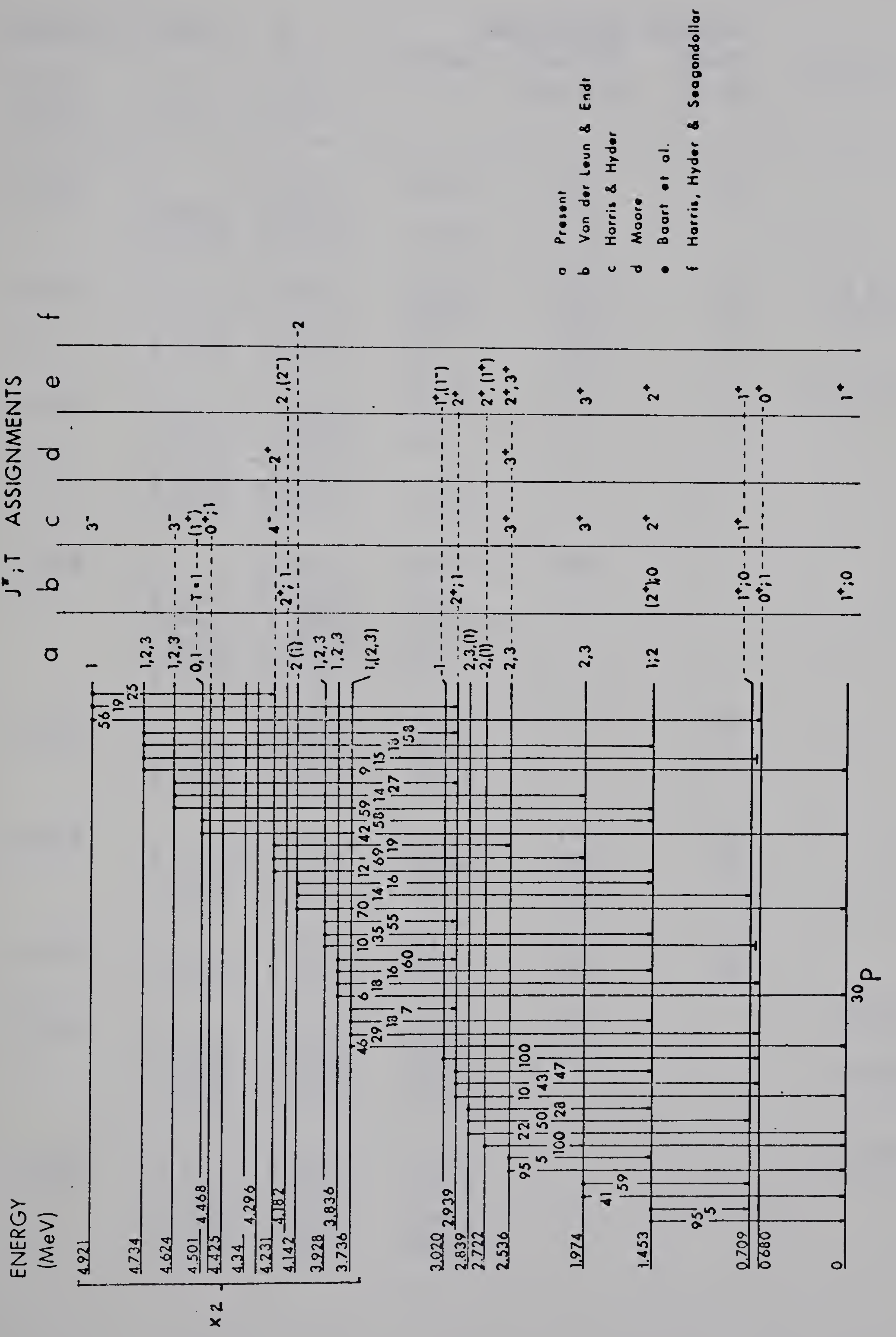
ENERGY (MeV)
Jπ;T ASSIGNMENTS
a
b
c
d
e
f
4.921
4.734
4.624
4.501
4.468
4.425
4.34
4.296
4.231
4.182
4.142
3.928
3.836
3.736
3.020
2.939
2.839
2.722
2.536
1.974
1.453
0.709
0.680
0
x 2
30P
a Present
b Van der Leun & Endt
c Harris & Hyder
d Moore
e Baart et al.
f Harris, Hyder & Seagondollar

Table 3-1 Branching Ratios of ^{30}P States.

Initial State	Final State	E_γ (MeV)	Branching Ratios Present	Harris *et al.*	Baart *et al.*	Others
1.453	0	1.453	95±4	$\geq$96	100	
	0.680	0.773		$\leq$ 3		
	0.709	0.744	5±4	$\leq$ 3		
1.974	0	1.974	41±5	34±2	40	56 (Va 58)
	0.709	1.263	59±5	53±2	47	44 (Va 58)
	1.453	0.521	<4	13±2	13	
2.536	0	2.536	95±4	$\geq$85	95	100 (Mo 63)
	0.680	1.856	<9		5	
	0.709	1.827				
	1.453	1.083	5±4			
	1.974	0.562	<10			
2.722	0	2.722	100	$\geq$80		
	0.680	2.042	<2			
	0.709	2.013				
	1.453	1.269	<3			
	1.974	0.748	<2			
2.839	0	2.839	22±3		100	
	0.709	2.130	50±4			
	1.453	1.386	28±4			
2.939	0	2.939	10±6	19±2	15	
	0.680	2.259	43±6	37±2	42	
	1.453	1.486	47±6	44±2	43	
3.020	0	3.020	<1	$\leq$ 5	11	
	0.680	2.340	100	$\geq$95	89	
3.736	0	3.736	46±6	$\geq$80		53 (Mo 63)
	0.680	3.056	29±5			
	1.453	2.283	18±6			47 (Mo 63)
	2.939	0.797	7±3			
3.836	0	3.836	6±3			100 (Mo 63)
	0.680	3.156	18±9			
	1.453	2.383	16±4			
	2.939	0.897	60±6			

Table 3-1 (cont'd)

Initial State	Final State	E (MeV)	Branching Ratios Present	Harris *et al.*	Baart *et al.*	Others
3.928	0	0	<6			
	0.680	3.248	10±6			
	0.709	3.219				
	1.453	2.475	35±6	(100)		
	2.939	0.989	55±6			
4.142	0	4.142	70±4	88±4		87 (Mo 63)
	0.709	3.433	14±5	12±4		
	1.453	2.689	16±5			12 (Mo 63)
4.182	0	4.182		19±3	6	
	0.709	3.473		81±3	62	
	2.939	1.243			32	
4.231	0	4.231	<10	3±1		
	1.453	2.778	12±5			
	1.974	2.257	69±4	69±2		64 (Mo 63)
	2.536	1.695	19±4	28±2		26 (Mo 63)
4.501	0	4.501	42±5	70±8	66	
	0.709	3.792	≤9			
	1.453	3.048	58±5	30±8		
	3.020	1.481			34	
4.624	0.680	3.915	<11			14 (Mo 63)
	0.709					
	1.453	3.171	59±7	71±3		86 (Mo 63)
	1.974	2.650	14±6	5±2		
	2.939	1.685	27±5	24±3		
4.734	0	4.734	9±5			
	0.680	4.054	15±5			
	0.709	4.025				
	1.453	3.281	18±5			
	2.939	1.794	58±6			
4.921	0.680	4.241	56±7			
	0.709	4.212		63±5		
	1.453	3.468		37±5		
	2.939	1.982	19±3			
	4.231	0.690	25±4			

Table 3-2 A_2 and A_4 Coefficients from Legendre Polynomial Fits to the Angular Distribution.

Energy Level (MeV)	Decay Transition	A_2	A_4	χ^2
1.453	1.453→0	0.83±0.03	0.00±0.05	0.7
1.974	1.974→0	0.29±0.10	-0.38±0.16	1.7
	1.974→0.709	0.29±0.08	-0.15±0.14	0.2
	0.709→0	0.37±0.07	0.10±0.12	0.7
2.536	2.536→0	0.29±0.10	-0.52±0.15	0.2
2.722	2.722→0	0.42±0.10	0.36±0.14	<0.1
2.839	2.839→0	0.47±0.11	-0.10±0.17	<0.1
	2.839→0.709	0.50±0.15	-0.37±0.23	0.4
3.020	3.020→0.680	0.74±0.14	-0.11±0.23	0.5
	0.680→0	0.01±0.03	-0.00±0.05	0.2
3.736	3.736→0	1.16±0.22	-0.22±0.31	0.5
	0.680→0	-0.03±0.06	-0.01±0.11	0.5
3.836	3.836→2.939	0.32±0.12	-0.23±0.19	0.1
	0.680→0	0.10±0.10	0.05±0.15	1.4
3.928	3.928→2.939	0.39±0.09	-0.06±0.16	0.4
	0.680 0.709 →0	-0.07±0.08	-0.10±0.15	<0.1
4.142	4.142→0	-0.43±0.03	-0.07±0.05	1.0
4.501	4.501→0	-0.01±0.03	0.09±0.05	2.1
	4.501→1.453	0.04±0.13	-0.10±0.21	<0.1
	1.453→0	-0.15±0.07	-0.06±0.12	1.8
4.624	4.624→1.453	0.27±0.07	-0.05±0.11	0.5
	4.624→2.939	0.10±0.27	0.42±0.43	<0.1
4.734	4.734→2.939	-0.27±0.07	0.14±0.11	0.6
	2.939→0.680	+0.25±0.17	-0.26±0.25	0.1
4.921	4.921→2.939	-0.11±0.11	-0.09±0.17	0.1
	4.921→0.680	-0.55±0.03	0.01±0.06	<0.1
	0.680 0.690 →0	-0.03±0.04	-0.01±0.06	0.3

Table 3-3 Summary of Spin Assignments and Mixing Ratio Solutions.

Energy Level (MeV)	Decay Transition	Assumed Spin Sequence	χ^2 min	Solutions of Mixing Ratio, x
1.453	1.453→0	1→1	.7	$-2.36 \leq x \leq -.45$ or $.58 < x < 1.73$
		2→1	.7	$.14 < x < 1.19$
1.974	1.974→0	2→1	1.7	$x \geq 6.3$ or $x \leq -0.40$
		3→1	1.7	$x \geq -.14$
	1.974→0.709	2→1	.3	$x \leq -6.3$ or $x \geq 19$ or $x = -(0.49^{+0.17}_{-0.11})$
		3→1	.2	$x = +(0.21^{+0.30}_{-0.26})$ or $x = +(2.5^{+5.1}_{-1.2})$
	1.974→0.709 0.709→0 1.974→0	3→1→1	.8	$x(0.709 \to 0) = -(0.25^{+0.33}_{-0.21})$ or $= -(4.01^{+19}_{-2.28})$
2.536	2.536→0	2→1	.2	$x < -.42$ or $x > 28$
		3→1	.2	$x = +(.23^{+0.39}_{-0.20})$ or $x = +(2.36^{+1.97}_{-.70})$
2.722	2.722→0	1→1	3.5	(x=Undefined)
		2→1	.1	$x = -(11^{+\infty}_{-6.3})$
			1.5	$x = -(.34^{+.33}_{-.10})$
2.839	2.839→0	1→1	.4	$x \leq 0$ or $x = +(1.00^{+0.92}_{-0.48})$ or $x \geq 23$
		2→1	.1	$x = -(5.7^{+17}_{-3.3})$ or $x = -(0.65^{+0.45}_{-0.18})$
		3→1	.1	$x = +(5.7^{+\infty}_{-2.6})$ or $x = -(0.03^{+0.31}_{-0.15})$ or $x \leq -5.7$
	2.839→0.709	1→1	2.4	$x \leq .04$
			3.2	$x = +(1.00^{+2.08}_{-.68})$
		2→1	.4	$-23 \leq x \leq -0.67$
		3→1	.4	$x = +(0.03^{+0.29}_{-0.19})$ or $x = +(4.5^{+15}_{-2.6})$
3.020	3.020→0.680	1→0	.6	$x \equiv 0$
	0.680→0	0→1	.2	$x \equiv 0$
3.736	3.736→0	1→1	.5	$-8 \leq x \leq -0.13$
		2→1	2.5	$-4.33 \leq x \leq -0.60$
		3→1	2.2	$x < .04$ or $x \geq 4.5$
3.836	3.836→2.939	1→2	.9	$x \leq -.21$ or $.23 \leq x \leq 1.54$

Table 3-3 (cont'd)

Energy Level (MeV)	Decay Transition	Assumed Spin Sequence	$\chi^2_{\min}$	Solutions of Mixing Ratio, x
		2→2	.1	$x=-(2.9^{+3.4}_{-1.7})$
			.9	$-0.58\leq x\leq +0.38$
		3→2	1.1	$x=-(0.47^{+0.15}_{-0.11})$ or
			2.0	$x=-(3.7^{+25}_{-2.3})$
		4→2	.1	$x<-19$ or $x=+(0.11\pm 0.23)$ or $x=+(6.3^{+\infty}_{-3.8})$
3.928	3.928→2.939	1→2	.4	$x\leq -.12$ or $x\geq 5.7$
		2→2	.4	$0.55\leq x\leq 6.3$
		3→2	.4	$x=(0.^{+.14}_{-.06})$
			1.2	$x=+(3.49^{+2.18}_{-0.74})$
4.142	4.142→0	1→1	2.2	$-29<x<-.05$ or $.31<x<3.17$
		2→1	1.0	$x=+(2.14^{+0.22}_{-0.30})$
			1.6	$x=+(.15^{+.40}_{-.22})$
4.501	4.501→0	0→1	2.9	$x\equiv 0$
		1→1	3.5	(x=Undefined)
		2→1	2.3	$x=+(5.7^{+3.84}_{-1.34})$
			3.8	$x=-(.18\pm .11)$
	4.501→1.453	0→2	.1	$x\equiv 0$
		1→2	.2	(x=Undefined)
		2→2	.1	$x=+(5.7^{+1.44}_{-1.16})$
			.2	$x=-(.19^{+.11}_{-.08})$
	4.501→1.453 1.453→0	0→2→1	1.4	(x(1.453→0)=Undefined)
		1→2→1	.7	(x(1.453→0)=Undefined)
4.624	4.624→1.453	1→2	.6	$x<-.05$
			1.0	$x=+(.75^{+.44}_{-.30})$
		2→2	.6	$x=+(.62^{+.35}_{-.13})$ or $x=+(5.7^{+19}_{-3.0})$
		3→2	.8	$x=-(.04\pm .08)$
			2.0	$x=+(5.7^{+8.6}_{-3.0})$

Table 3-3 (cont'd)

Energy Level (MeV)	Transition	Assumed Spin Sequence	χ^2 min	Solutions of Mixing Ratio,x	
	4.624→2.939	1→2	0.5	(x=Undefined)	
		2→2	.1	$x=-(5.7^{+\infty}_{-4.9})$ or $x\ge-0.29$	
		3→2	.1	$x=-(0.16^{+0.33}_{-.07})$ or $x\ge6.3$ or $x\le4.0$	
4.734	4.734→2.939	1→2	1.3	$x\le0$ or $x>3.5$	
			3.0	$.\overline{2}8\le x\le1.57$	
		2→2	.6	$.65\overline{<}x\overline{<}9.5$	
		3→2	1.3	$x=+\overline{(}.\overline{0}2\pm0.05)$	
			1.0	$x=+(4.4^{+1.9}_{-1.4})$	
4.734	4.734→ 2.939→0	1→2→0	0.7	$\lvert x\rvert\le0.78$ or $\lvert x\rvert\ge1.9$	X = X(4.734→ 2.939)
		2→2→0	0.1	$\lvert x\rvert\le0.70$	
		3→2→0	0.5	$\lvert x\rvert\le1.54$	
	4.734→2.939	1→2→0	.7	$x=-(.27^{+.18}_{-.09})$	
	2.939→0.680	2→2→0	1.2	$x=4.33^{+\infty}_{-3.68})$	
		3→2→0	.7	For x=0.02	
4.921	4.921→.709	1→1	.1	$-4.5\le x\le.23$ or $.34\le x\le2.25$	
		2→1	.1	$x=+(.11^{+.36}_{-.11})$ or $x=+(1.73\pm0.32)$	
	4.921→.680	1→0	.1	x=0	
	4.921→2.939	1→2	.2	(x=Undefined)	
		2→2	.3	$x=+(.51^{+.08}_{-.26})$	
			.1	$\lvert x\rvert\ge14.$	

Figure 3-2a Yield Curves for 10 States of ^{30}P.

The points correspond to the maximum number of counts in a peak with background subtracted for 10 microcoulombs of charge.

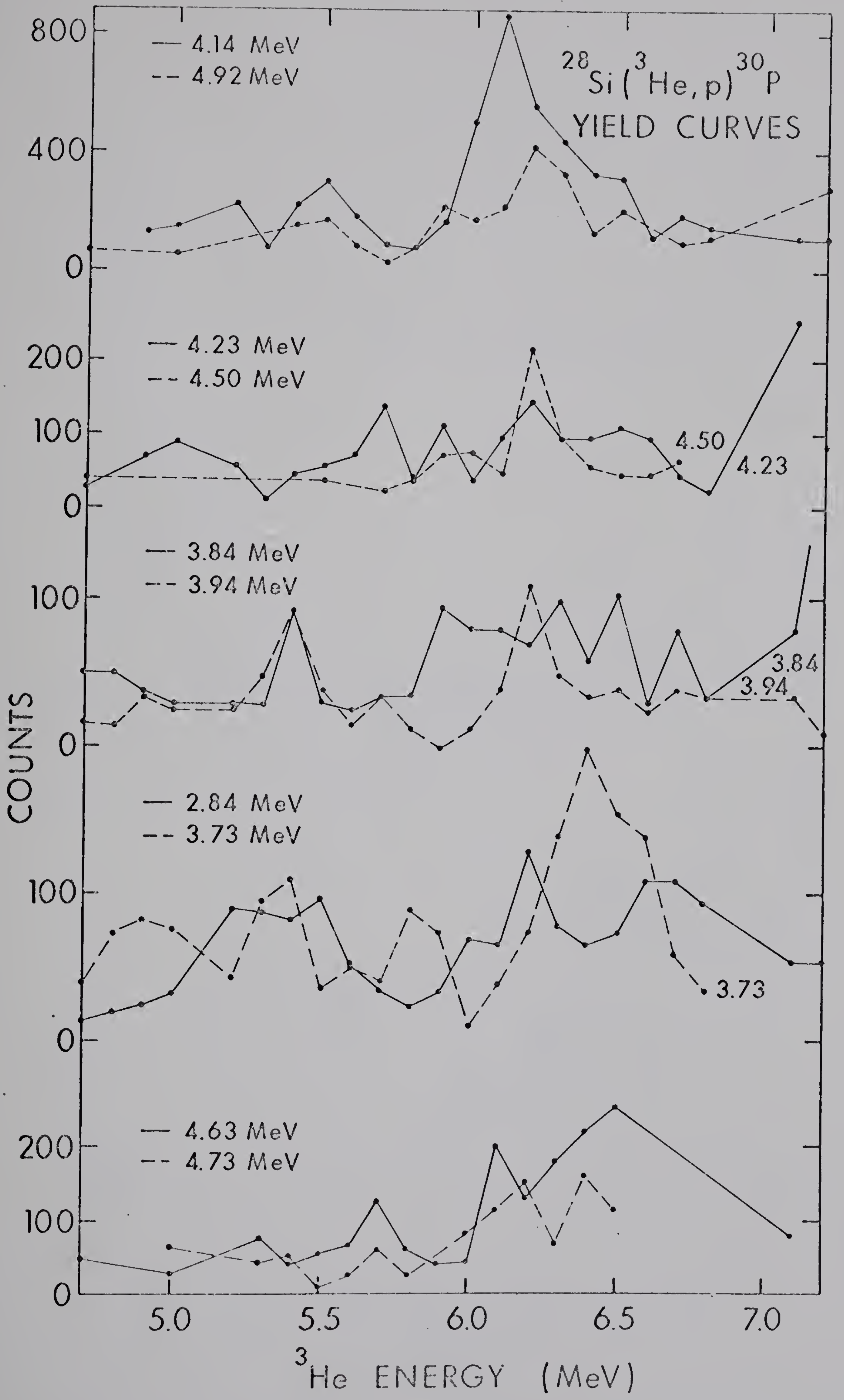

$^{28}Si(^{3}He,p)^{30}P$
YIELD CURVES
— 4.14 MeV
-- 4.92 MeV
— 4.23 MeV
-- 4.50 MeV
4.50
4.23
— 3.84 MeV
-·- 3.94 MeV
3.84
3.94
— 2.84 MeV
-- 3.73 MeV
3.73
— 4.63 MeV
-- 4.73 MeV
800
400
0
200
100
0
100
0
100
0
200
100
0
COUNTS
5.0
5.5
6.0
6.5
7.0
^{3}He ENERGY (MeV)

Figure 3-2b Coincident charged-particle spectrum from ^{3}He on a natural silicon target at 6.2 MeV bombarding energy.

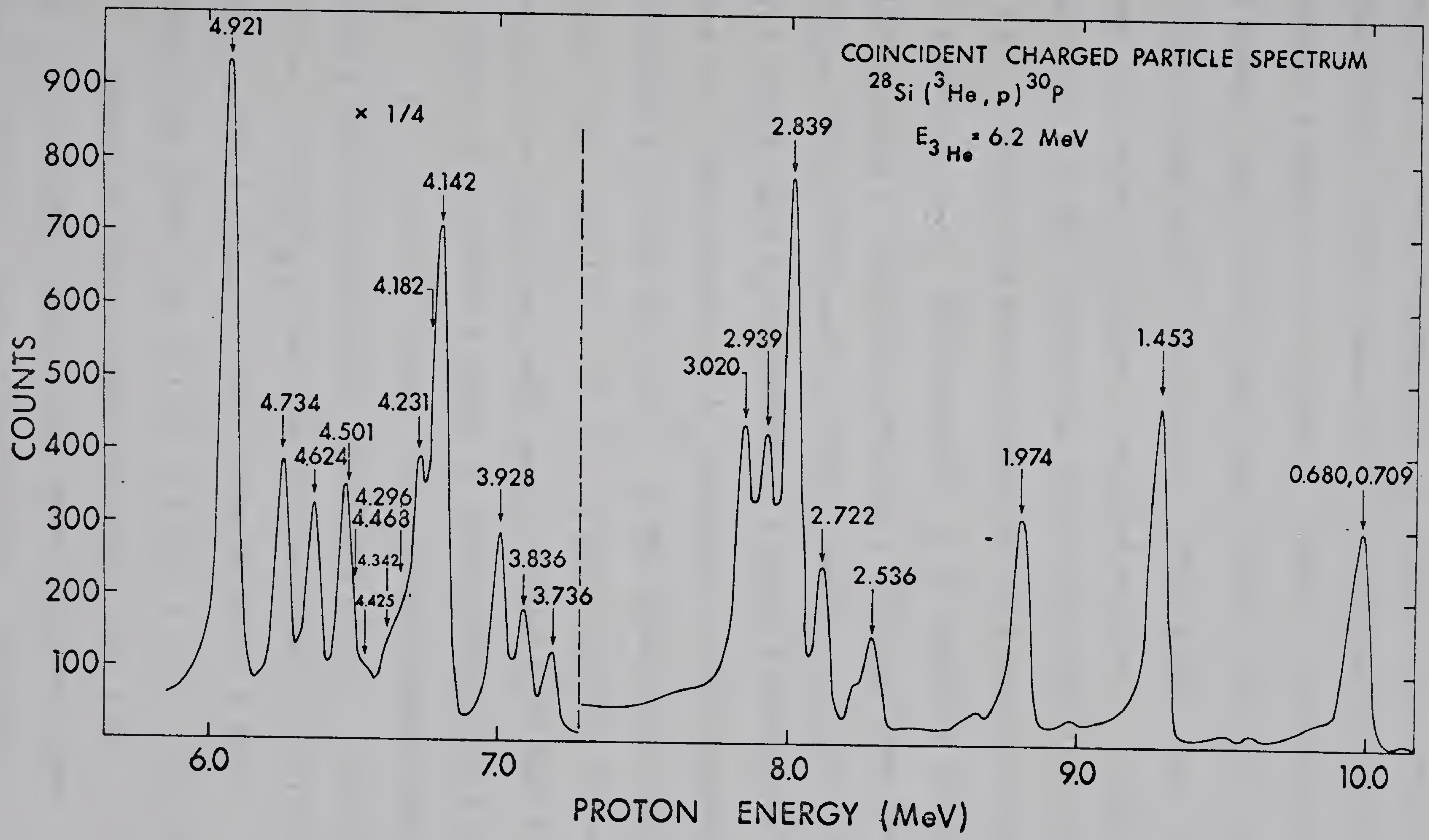
COINCIDENT CHARGED PARTICLE SPECTRUM
$^{28}Si(^{3}He, p)^{30}P$
$E_{^3He} = 6.2$ MeV
× 1/4
4.921
4.734
4.624
4.501
4.296
4.468
4.342
4.425
4.231
4.182
4.142
3.928
3.836
3.736
3.020
2.939
2.839
2.722
2.536
1.974
1.453
0.680,0.709
COUNTS
900
800
700
600
500
400
300
200
100
6.0
7.0
8.0
9.0
10.0
PROTON ENERGY (MeV)

b. The 0.68 and 0.71 MeV Levels

Because of the small energy separation of this doublet, it was not possible to study these levels by observation of the gamma rays in coincidence with the protons forming these states. However, correlations of gamma rays de-exciting these levels could be studied by observing known 0.68 and 0.71 MeV gamma rays arising from the decay of higher excited states. In this way, the 0.68 → 0 MeV transition resulting from the 3.02 → 0.68 → 0 MeV cascade was found to be isotropic with a χ^2 value of 0.2. Furthermore, in a Legendre Polynomial fit suspected 0.68 MeV gamma-rays arising from the decay of the 3.74, 3.84 and 4.92 MeV levels all gave values of zero for A_2 and A_4 to within a standard deviation. From the large value of A_2 obtained in the Legendre Polynomial fit to the 0.71 → 0 MeV transition that arises from the 1.97 → 0.71 → 0 MeV cascade, it was possible to rule out spin zero for the 0.71 MeV level. In figure 3-3 curve A shows a simultaneous fit to the 1.97 → 0.71, 0.71 → 0 and 1.97 → 0 MeV transitions which yields mixing ratio solutions of $x = -(0.25^{+0.33}_{-0.21})$ or $x = -(4.01^{+19}_{-2.28})$ for the 0.71 → 0 MeV transition while curve B shows a fit to the 0.709 → 0 MeV transition alone for $x(1.97 \pm 0.71) = 0.21$. In this fit, values of the mixing ratios for the 1.97 → 0.71 and 1.97 → 0 MeV transitions were obtained from separate fits to these transitions. Although χ^2-fits to the 1.97 → 0.71 MeV transition gave a large region

Figure 3-3 Angular Distribution and χ^2-Versus Arc tan x for the 0.71 → 0 MeV Transition that Arises from the 1.97 → 0.71 → 0 MeV Cascade.

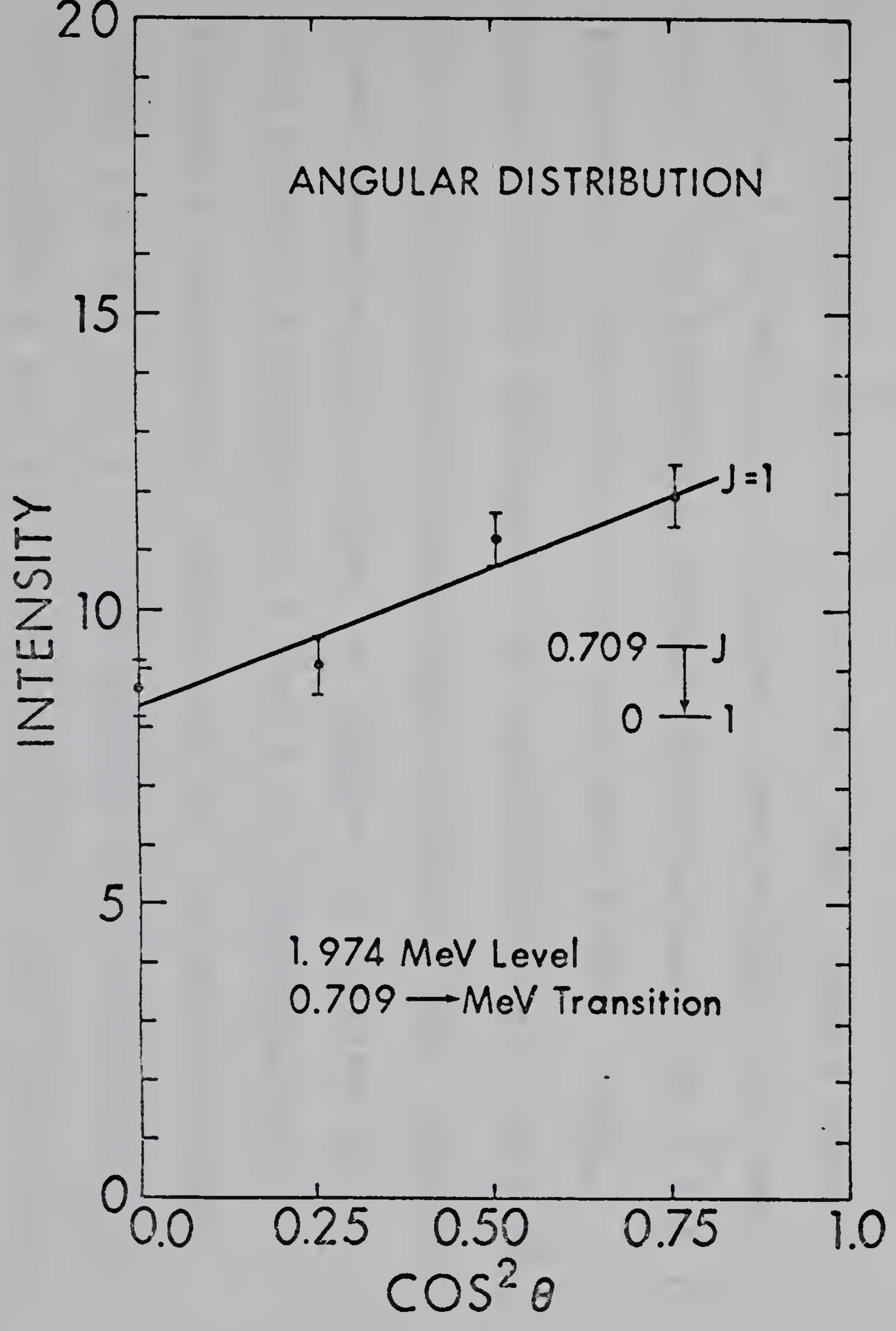
ANGULAR DISTRIBUTION
INTENSITY
20
15
10
5
0
0.0
0.25
0.50
0.75
1.0
COS² θ
J=1
0.709
J
0
1
1.974 MeV Level
0.709 ⟶ MeV Transition

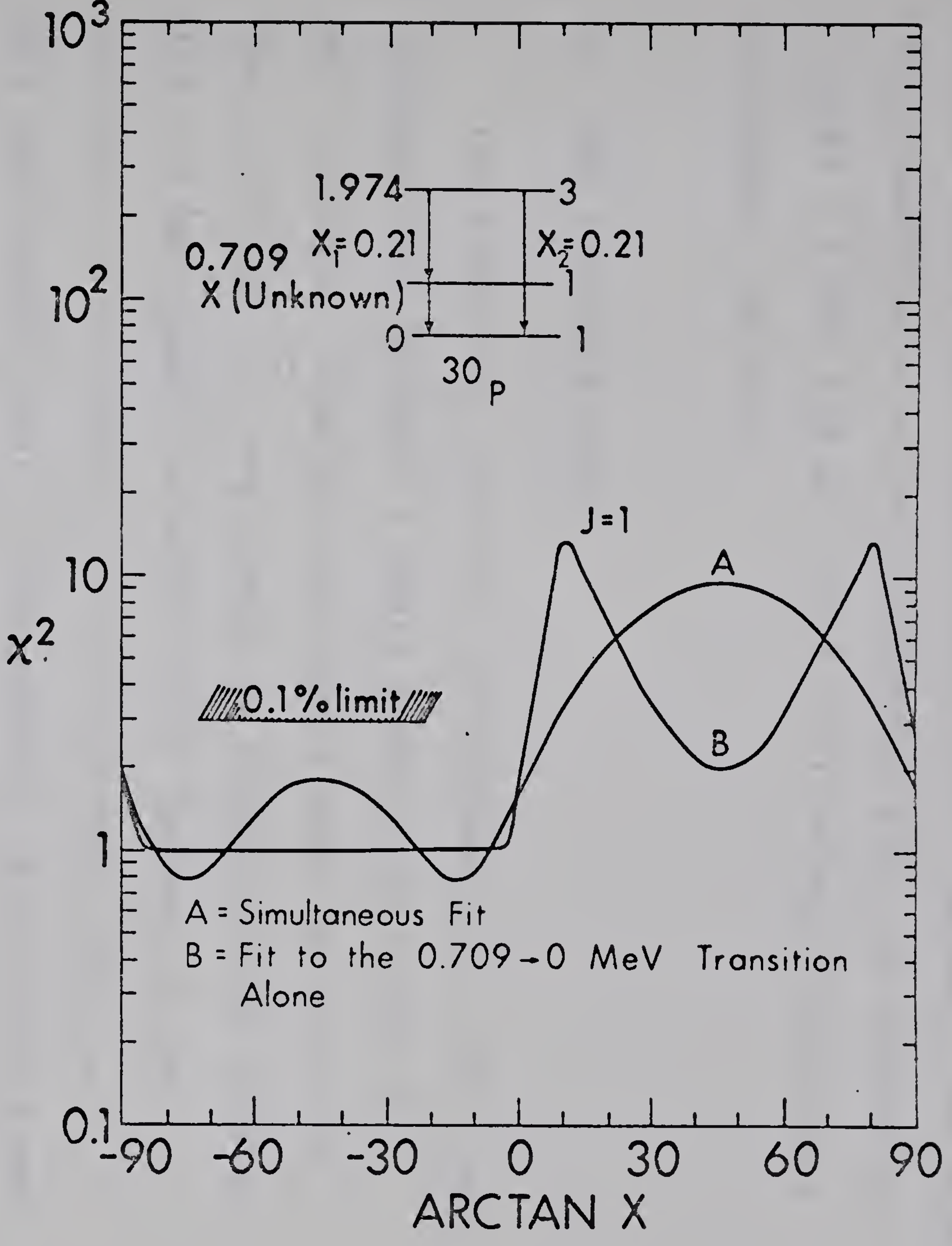
10³
10²
10
1
0.1
χ²
-90
-60
-30
0
30
60
90
ARCTAN X
1.974
3
X₁=0.21
X₂=0.21
0.709
X (Unknown)
1
0
1
30p
J=1
A
B
0.1% limit
A = Simultaneous Fit
B = Fit to the 0.709→0 MeV Transition Alone

of acceptable values for the mixing ratio of this transition, only the value x = 0.21 corresponding to the minimum with the largest quadrupole component was used. Our results are in fair agreement with the values x = -(0.48 ± 0.04) and x = -(2.0 ± 2) measured by Harris and Hyder (Ha 67A).

c. The 1.45 MeV Level

The gamma-ray spectrum corresponding to this level (figure 3-4) reveals a small transition to the 0.7 MeV doublet. From the accurately known position of the 0.68 and 0.71 MeV gammas as obtained from fits to the 0.7 MeV gammas of other level decays, it was possible to accurately fix the position where a 0.77 MeV peak would occur. The weakness of any such gamma ray indicated that the 1.45 MeV level decays mainly to the 0.71 MeV level, rather than to the 0.68 MeV level. The branching ratios obtained are (95 ± 4)% to ground and (5 ± 4)% to the 0.71 MeV level. These values include estimates of overlap with the tail of the proton peak corresponding to the 0.7 MeV doublet. Least-squares fits shown in figure 3-5 failed to distinguish between J = 1 and J = 2 assignments. Previous assignments (Va 58, Ba 62, Ha 66A) to this level are all $J = 2^+$. The mixing ratio solution for J = 2, $0.14 \leq x \leq 1.19$, is consistent with the value measured by Harris and Hyder (Ha 66B) of x = +(0.21 ± 0.03). Uncertainties have been taken at the 17% confidence limit.

d. The 1.97 MeV Level

Figure 3-4 Gamma-ray Spectrum for the 1.45 MeV Level of ^{30}P.

The points in the simultaneous randoms spectrum are indicated by open circles.

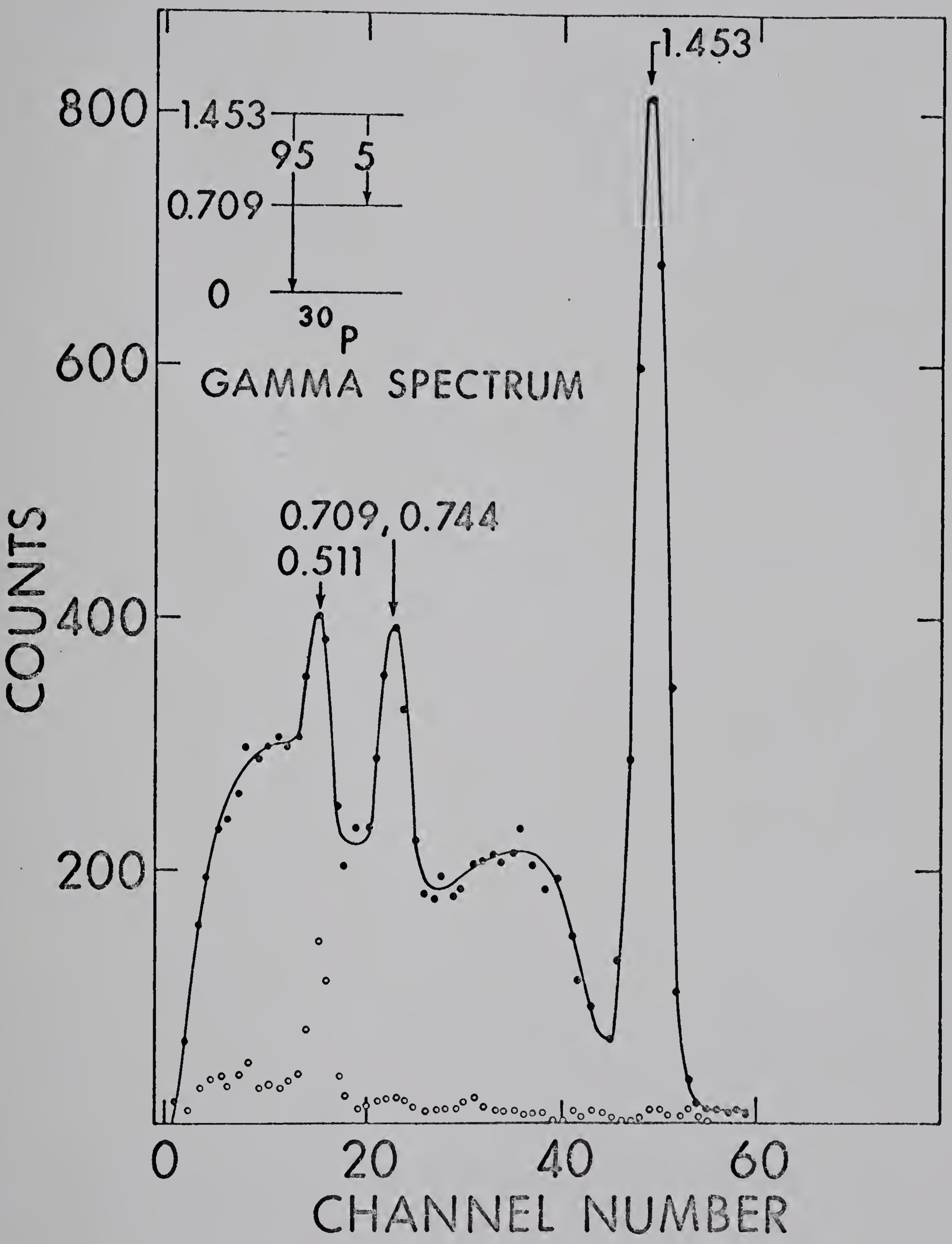

1.453
800
1.453
95
5
0.709
0
30P
600
GAMMA SPECTRUM
0.709, 0.744
0.511
400
COUNTS
200
0
20
40
60
CHANNEL NUMBER

Figure 3-5 Angular Distribution and χ^2-Versus Arc tan x for the 1.45 → 0 MeV Transition.

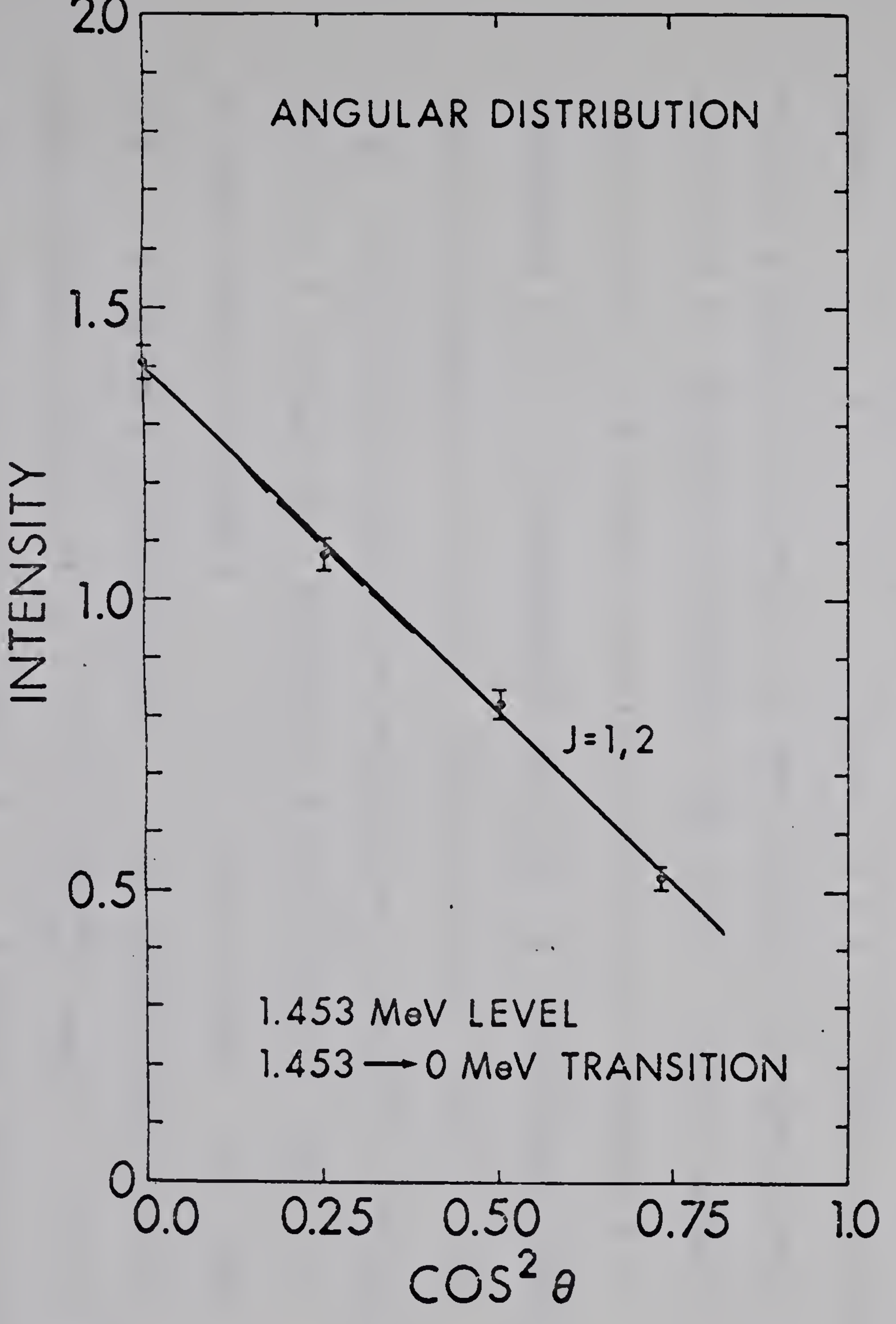
ANGULAR DISTRIBUTION
INTENSITY
2.0
1.5
1.0
0.5
0
0.0
0.25
0.50
0.75
1.0
COS² θ
J=1,2
1.453 MeV LEVEL
1.453 ⟶ 0 MeV TRANSITION

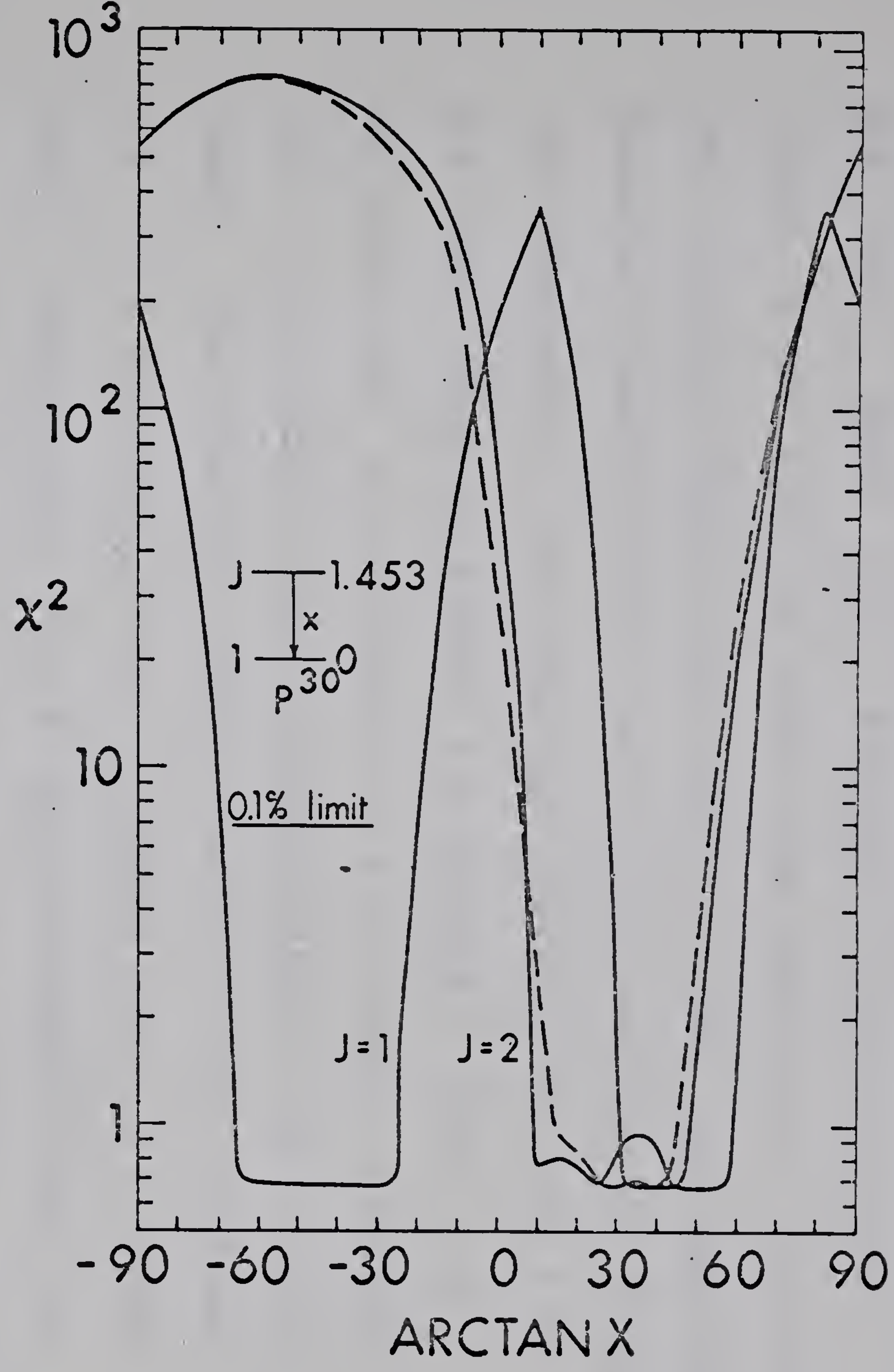
χ²
10³
10²
10
1
J — 1.453
x
1 — 0
P³⁰
0.1% limit
J=1
J=2
-90
-60
-30
0
30
60
90
ARCTAN X

$^{29}Si(p, \gamma)^{30}P$ reaction, both Moore (Mo 63) and Harris and Hyder (Ha 67A) have found a 13% branch to the 1.45 MeV level. Baart _et al_. assigned an uncertain 14% branch to the 1.45 MeV level from analysis of the 695 keV resonance decay scheme while Van der Leun and Endt found no branch to this level after examination of the same resonance. The gamma-ray spectrum for the 1.97 MeV level shown in figure 3-6 reveals a small 1.45 MeV peak that is attributed to a 3% overlap with the tail of the proton peak corresponding to the 1.45 MeV level. The branching ratio results of (41 ± 5)% and (59 ± 5)% for transitions to ground and the 0.71 MeV level, respectively, are in poor agreement with the values (34 ± 2)%, (53 ± 2)% and (13 ± 2)% for branching to the ground 0.71 and 1.45 MeV states, respectively, measured by Harris and Hyder (Ha 67A). Least-squares fits to the 1.97 MeV transition shown in figure 3-7 excluded a $J = 1$ assignment at the 1% confidence limit. Shown in figure 3-8 is the least-squares fit to the 1.97 → 0.71 MeV transition which gave possible solutions for $J = 1$, 2 and 3. Previous investigators (Ba 62, Ha 66A) have assigned $J = 3^+$ to this level. For the 1.97 → 0.71 MeV transition a $J = 3$ least-squares fit gave mixing ratios of $x = +(0.21^{+0.30}_{-0.26})$ and $x = +(2.5^{+5.1}_{-1.2})$ with an 83% probability while a $J = 3$ fit to the 1.97 → 0 MeV transition gave an allowed region for the mixing ratio of $x > -0.14$ with a 99.9% probability. No other

Figure 3-6 Gamma-ray Spectrum for the 1.97 MeV Level of ^{30}P.

The points in the simultaneous randoms spectrum are indicated by open circles.

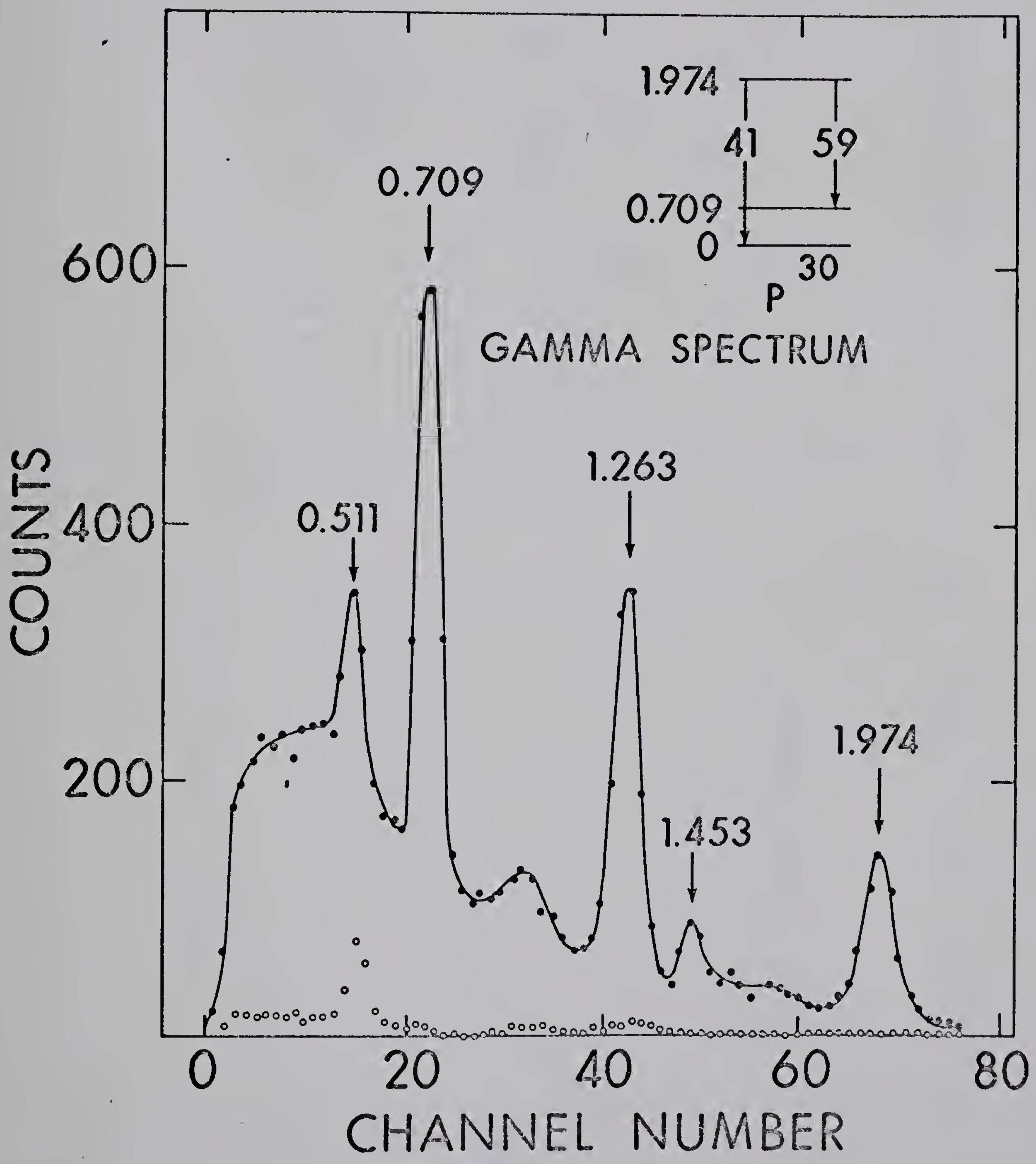
1.974
41
59
0.709
0
P^{30}
GAMMA SPECTRUM
0.709
0.511
1.263
1.974
1.453
COUNTS
600
400
200
0
20
40
60
80
CHANNEL NUMBER

Figure 3-7 Angular Distribution and χ^2-Versus Arc tan x for the 1.97 → 0 MeV Transition.

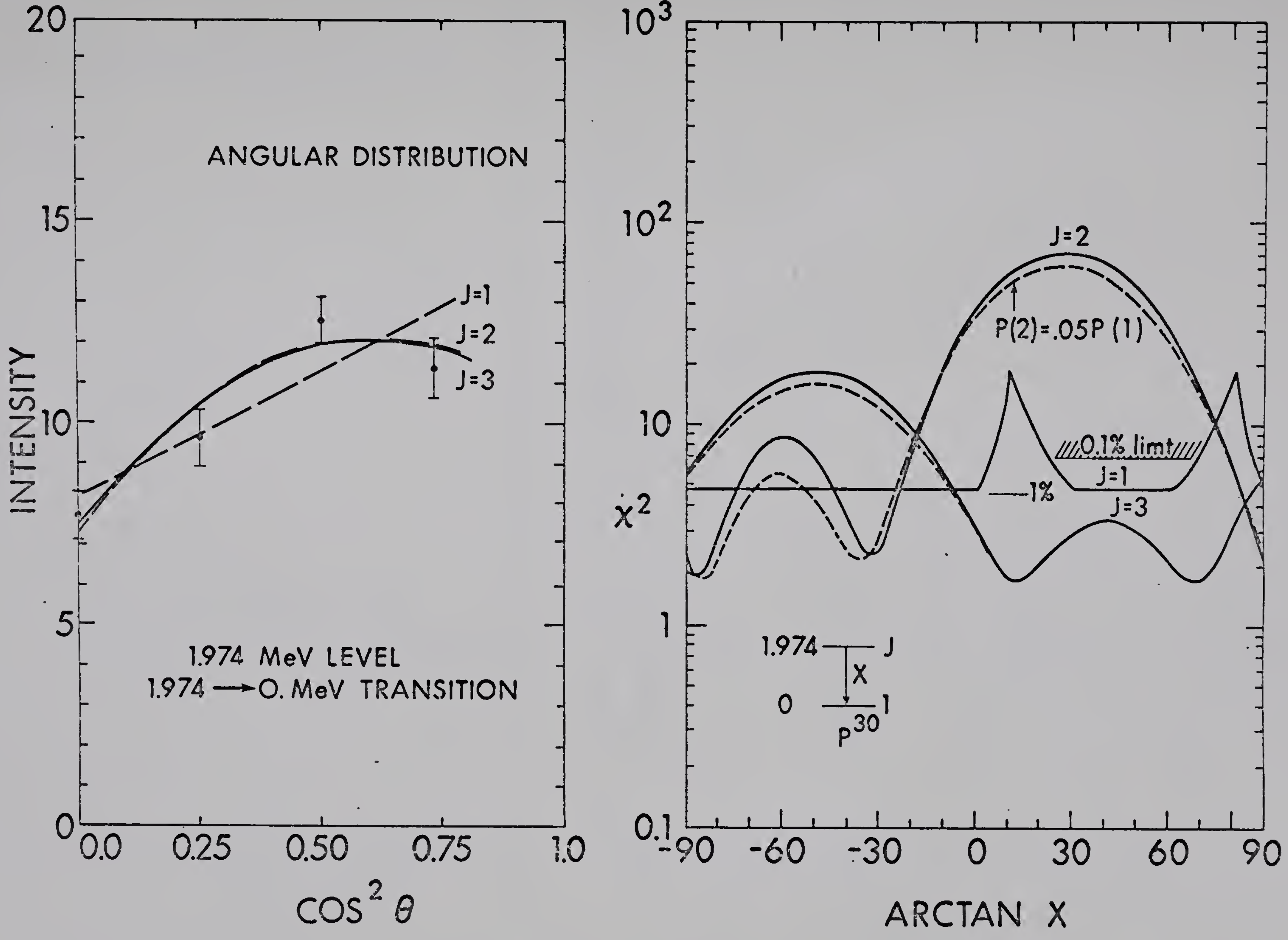
ANGULAR DISTRIBUTION
INTENSITY
20
15
10
5
0
0.0
0.25
0.50
0.75
1.0
$\cos^2\theta$
J=1
J=2
J=3
1.974 MeV LEVEL
1.974 ⟶ O. MeV TRANSITION
10^3
10^2
10
1
0.1
χ^2
-90
-60
-30
0
30
60
90
ARCTAN X
J=2
P(2)=.05P (1)
0.1% limt
J=1
1%
J=3
1.974
J
X
0
1
P^{30}

Figure 3-8 Angular Distribution and χ^2-Versus Arc tan for the 1.97 → 0.71 MeV Transition.

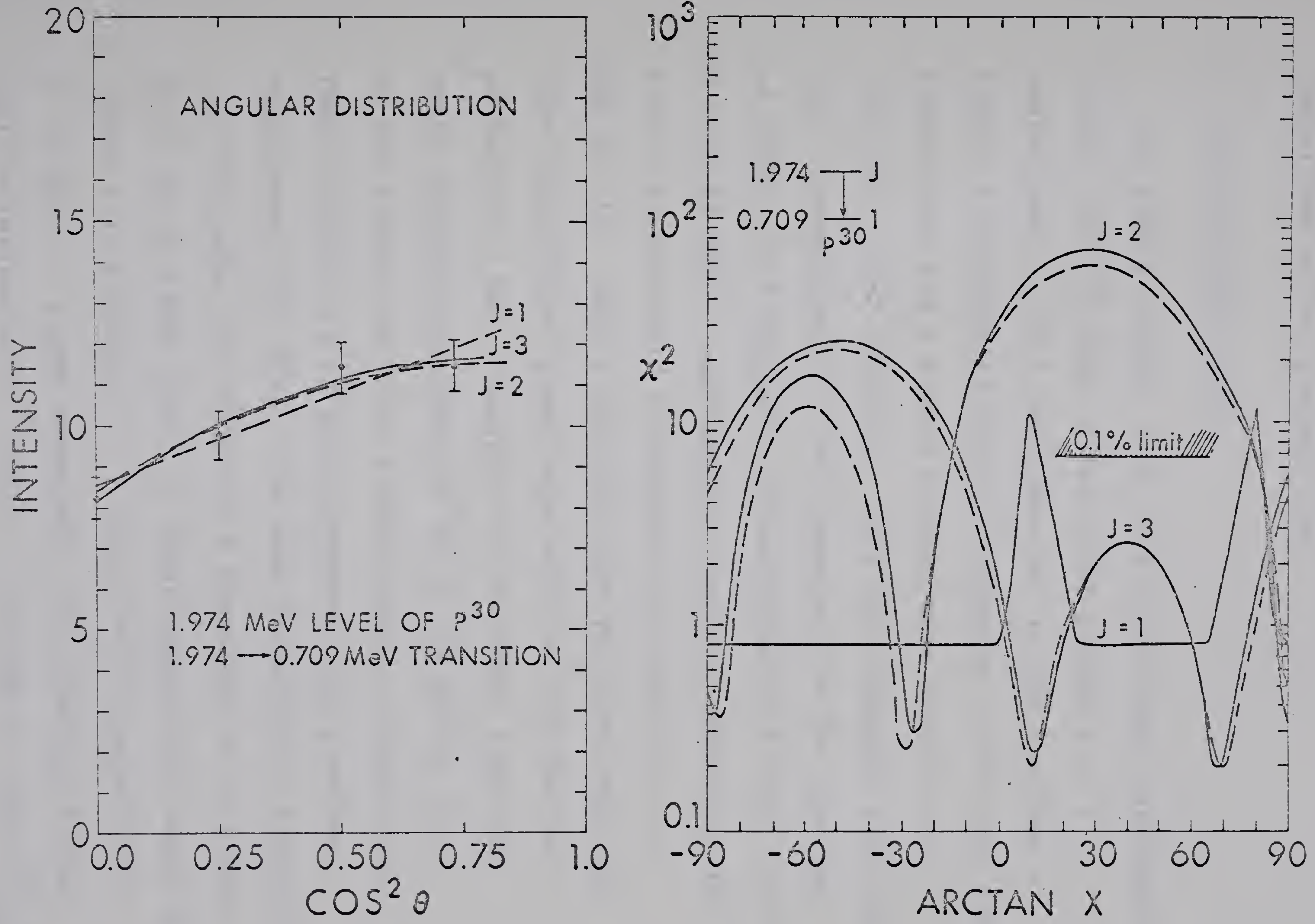
ANGULAR DISTRIBUTION
INTENSITY
20
15
10
5
0
0.0
0.25
0.50
0.75
1.0
COS² θ
J=1
J=3
J=2
1.974 MeV LEVEL OF P³⁰
1.974 ⟶ 0.709 MeV TRANSITION
10³
10²
10
1
0.1
x²
1.974 J
0.709 1
P³⁰
J=2
J=3
J=1
0.1% limit
-90
-60
-30
0
30
60
90
ARCTAN X

mixing ratios for these transitions are available for comparison at the present time.

e. The 2.54 MeV Level

As seen in figure 3-2b, the proton peak corresponding to the 2.54 MeV level reveals the presence of a contaminant. A 3.1 MeV gamma ray in the spectrum of figure 3-9 indicates that the reaction of ^{3}He with this contaminant has a higher Q value than that for the ^{28}Si(^{3}He, p)^{30}P reaction. This fact together with the large unexplained 1.26 MeV gamma ray in the spectrum of figure 3-10 suggests the contaminant is ^{29}Si(^{29}Si(^{3}He, p)^{31}P Q = 10.18 MeV). Calculations, however, show that the particle peak would correspond to a state at 6.76 MeV in ^{31}P. Such a state has not yet been reported. Other unexplained gamma rays occur at 0.92 MeV and probably 0.7 MeV. Analysis of the other gamma-ray peaks yielded branchings of (95 ± 4)% and (5 ± 4)% to the ground and first excited states, respectively. These results are in good agreement with previous measurements (Ha 67A). The weak intensity of a possible 1.83 MeV gamma ray indicates a branching of less than 5% to the 0.7 MeV level. A least-squares fit shown in figure 3-10 excluded J = 1 with a 99.7% probability. Both J = 2 and J = 3 gave acceptable fits yielding mixing ratio solutions of $x < -0.42$, $x > 28$ and $x = +(0.23^{+0.39}_{-0.20})$,

Figure 3-9 Gamma-ray Spectrum for the 2.54 MeV Level of ^{30}P.

The points in the simultaneous randoms spectrum are indicated by open circles.

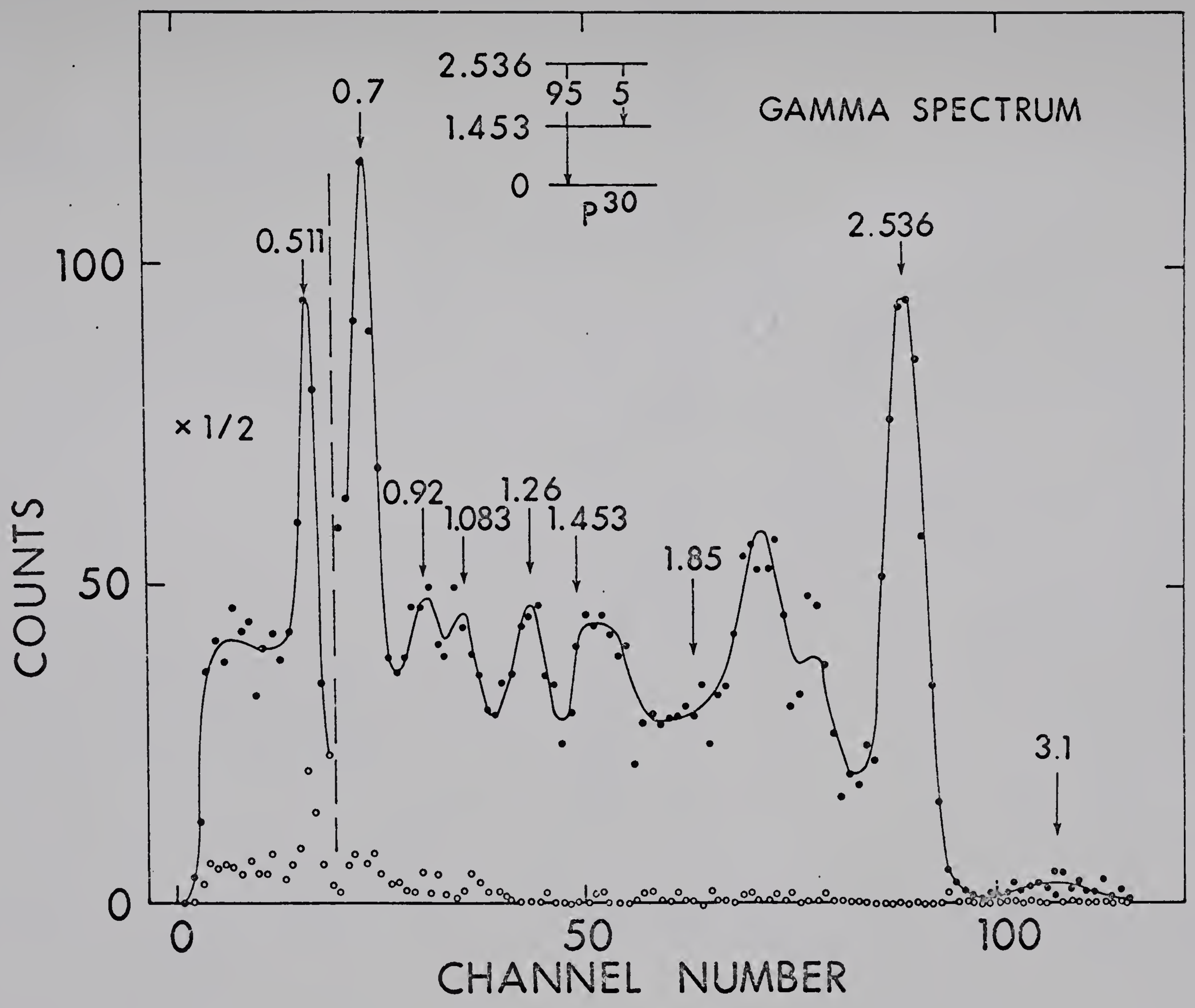
GAMMA SPECTRUM
2.536
95
5
1.453
0
P^{30}
0.7
0.511
×1/2
0.92
1.083
1.26
1.453
1.85
2.536
3.1
COUNTS
100
50
0
CHANNEL NUMBER
0
50
100

Figure 3-10 Angular Distribution and χ^2-Versus Arc tan x for the 2.54 → 0 MeV Transition.

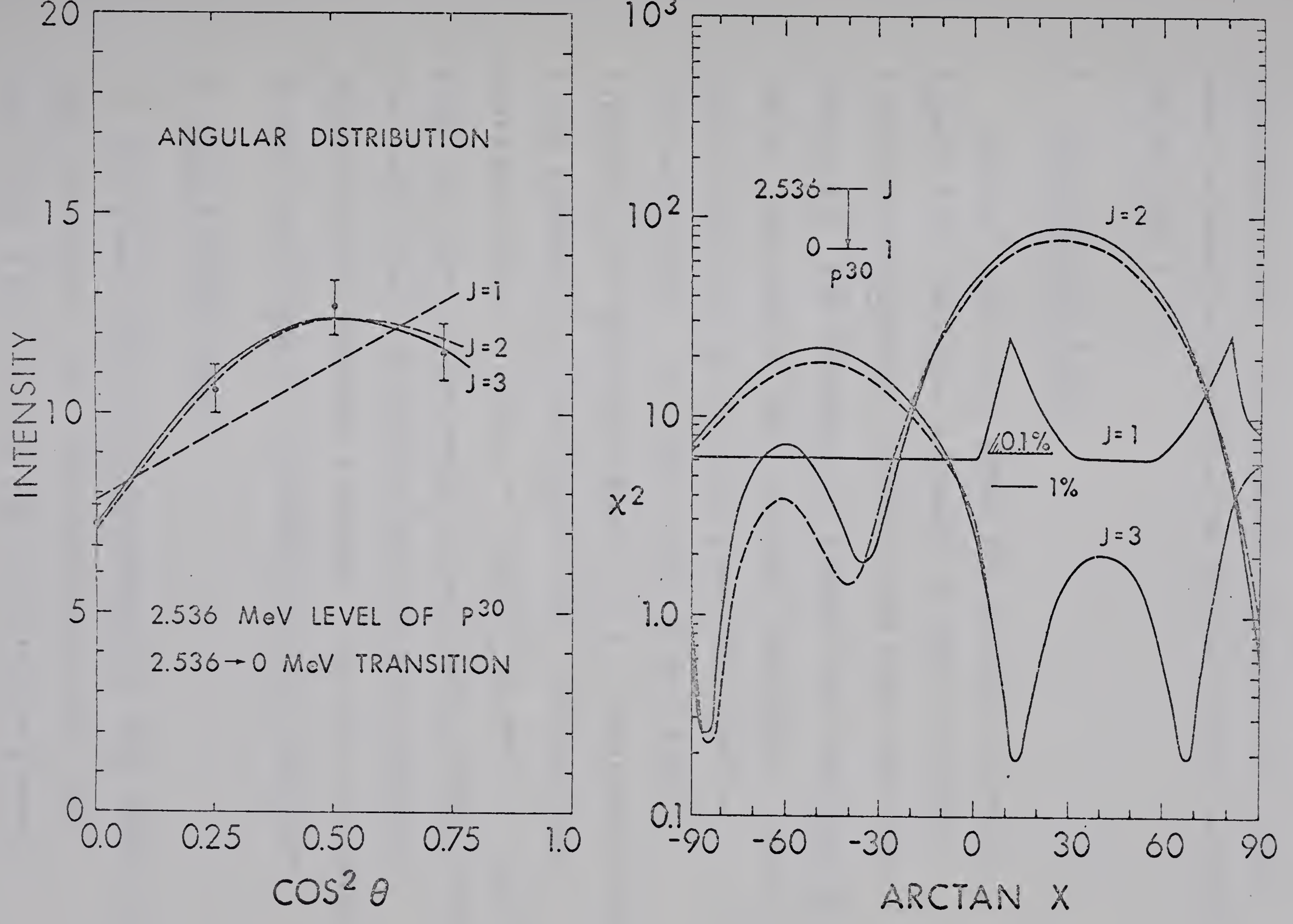
ANGULAR DISTRIBUTION
2.536 MeV LEVEL OF P^{30}
2.536→0 MeV TRANSITION
J=1
J=2
J=3
INTENSITY
20
15
10
5
0
0.0
0.25
0.50
0.75
1.0
$\cos^2\theta$
2.536
J
0
1
P^{30}
J=2
J=1
J=3
0.1%
1%
χ^2
10^3
10^2
10
1.0
0.1
-90
-60
-30
0
30
60
90
ARCTAN X

$x = +(2.36^{+1.97}_{-0.70})$ for J = 2 and 3, respectively. For J = 4, pure octupole radiation is rejected at the 0.1% confidence limit. The previous assignment for this level as measured by Moore (Mo 63) and Harris and Hyder (Ha 66B) is $J = 3^+$.

f. The 2.72 MeV Level

The 2.72 MeV level gamma-ray spectrum shown in figure 3-11 indicates a branch of 100% to ground. Previous measurements by Harris and Hyder (Ha 67A) indicate a 80% branching to ground while Baart et al. (Ba 62) obtained a 100% to ground branching. Previous work by Baart et al. (Ba 62) gave this level a $J = 2^+$, (1^+) assignment. χ^2- fits to the $2.72 \rightarrow 0$ MeV transition of this work reject a J = 1 assignment with a 96% probability (see figure 3-12). Mixing ratio solutions for J = 2 are $x = -(11.4^{+\infty}_{-6.3})$ and $x = -(0.34^{+0.33}_{-0.10})$ with the former value being 4 times more probable than the latter one. In view of the positive parity indicated by the previous assignment (Ba 62) the results of this work suggest a predominantly E2 transition.

g. The 2.84 MeV Level

The gamma spectrum corresponding to this level is shown in figure 3-13. The branching ratios are (22 ± 3)%, (50 ± 4)% and (28 ± 4)% to the ground,

Figure 3-11 Gamma-ray Spectrum for the 2.72 MeV Level of ^{30}P.

The points in the simultaneous randoms spectrum are indicated by open circles.

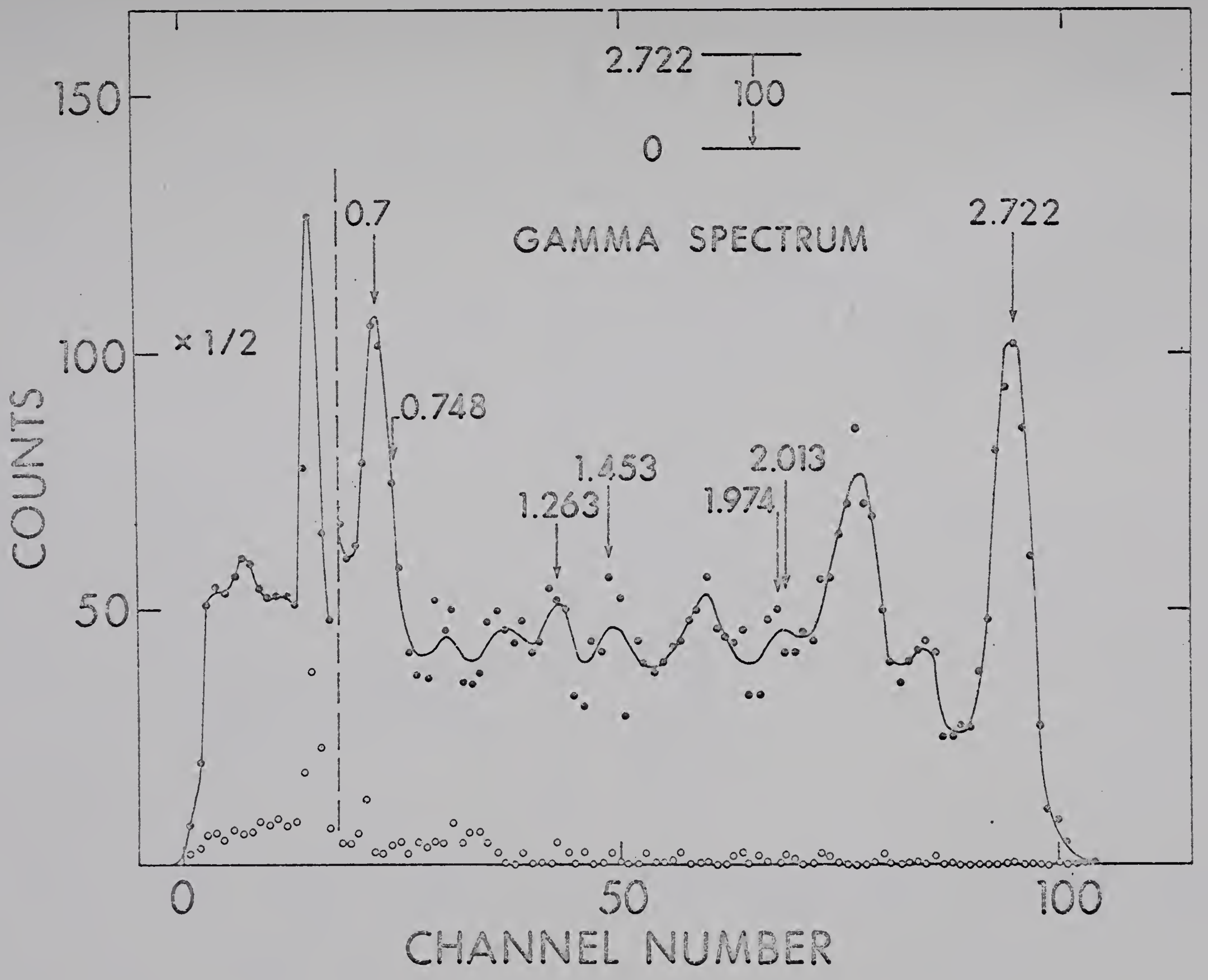
2.722
100
0
GAMMA SPECTRUM
0.7
2.722
× 1/2
0.748
1.453
1.263
2.013
1.974
150
100
50
COUNTS
0
50
100
CHANNEL NUMBER

Figure 3-12 Angular Distribution and χ^2-Versus Arc tan x for the 2.72 → 0 MeV Transition.

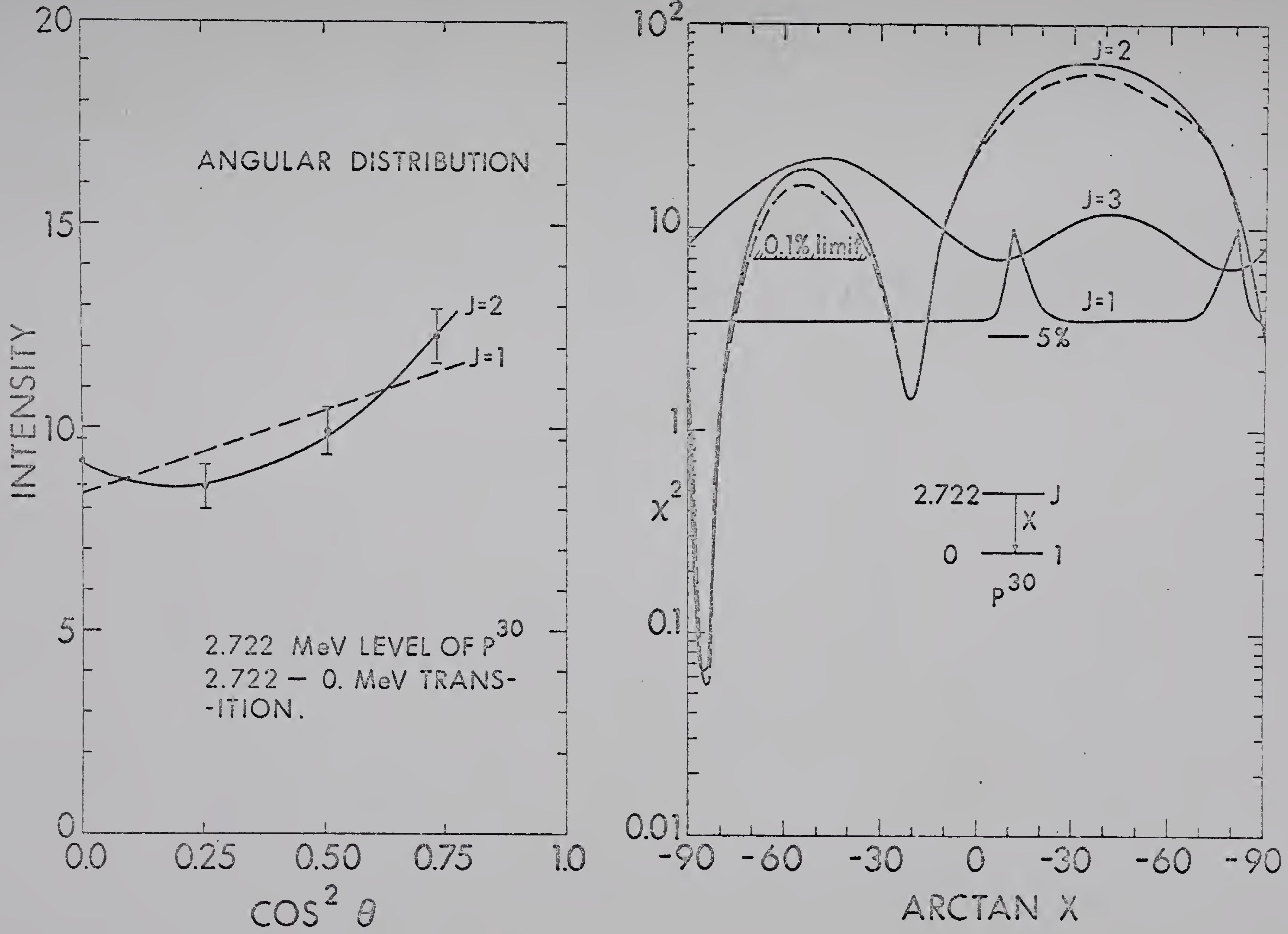
ANGULAR DISTRIBUTION
2.722 MeV LEVEL OF P^{30}
2.722 — 0. MeV TRANS-
-ITION.
INTENSITY
20
15
10
5
0
0.0
0.25
0.50
0.75
1.0
COS^2 θ
J=2
J=1
10^2
10
1
0.1
0.01
X^2
-90
-60
-30
0
-30
-60
-90
ARCTAN X
J=2
J=3
J=1
0.1% limit
5%
2.722
J
X
0
1
P^{30}

Figure 3-13 Gamma-ray Spectrum for the 2.84 MeV Level of ^{30}P.

The points in the simultaneous randoms spectrum are indicated by open circles.

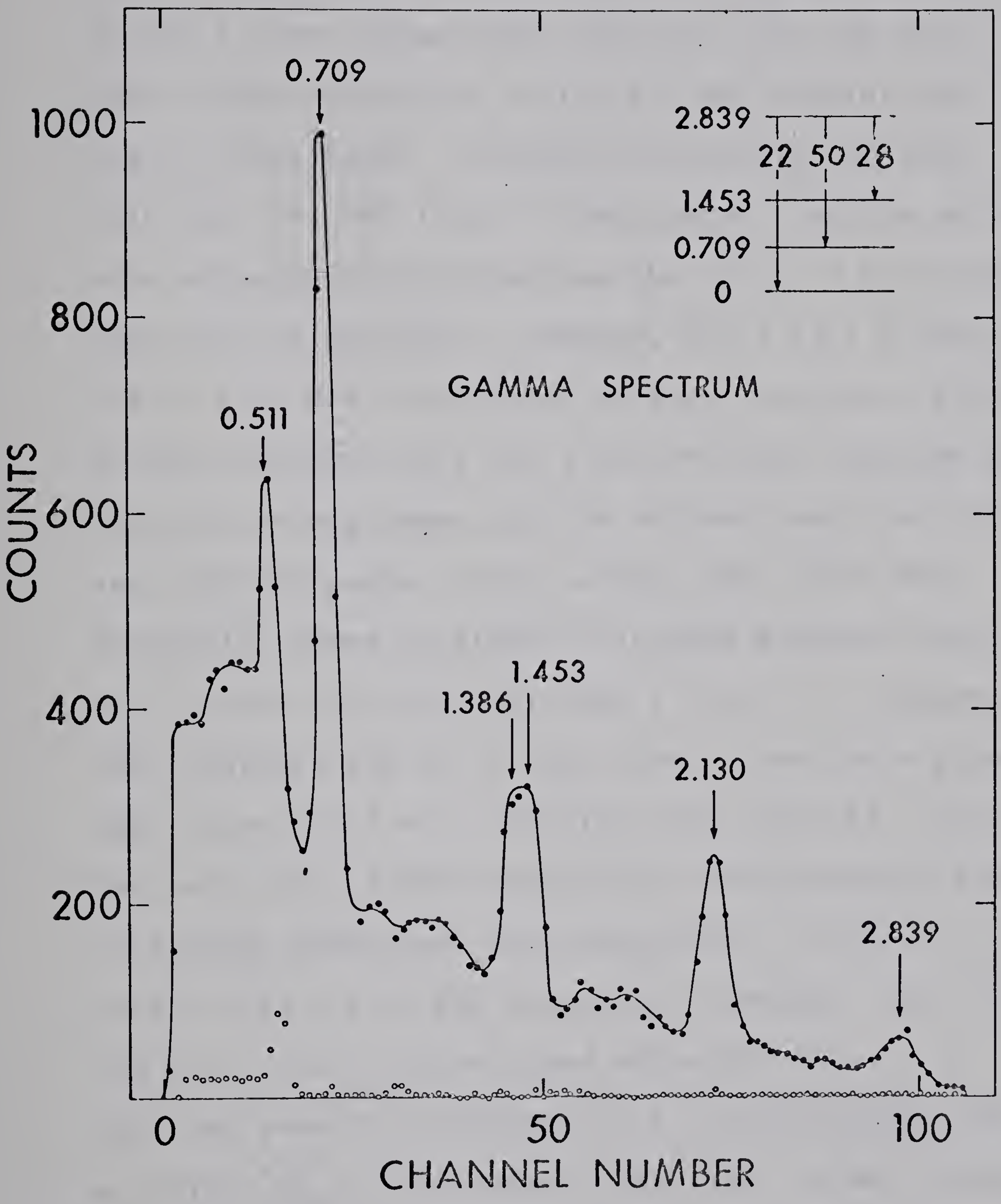
0.709
1000
800
600
400
200
COUNTS
0.511
1.386
1.453
2.130
2.839
GAMMA SPECTRUM
2.839
22
50
28
1.453
0.709
0
0
50
100
CHANNEL NUMBER

0.7 MeV and 1.45 MeV levels, respectively. These values are in disagreement with the 100% to ground branch indicated by Moore (Mo 63). The position of the 0.7 MeV gamma peak indicates that the major part of the transition to the 0.7 MeV doublet goes to the 0.71 MeV level. Because of extensive overlap with the 2.94 MeV level in the proton spectrum extraction of a reliable correlation for the 0.71 → 0 MeV transition was not possible. However, the 2.84 → 0 MeV and 2.84 → 0.71 MeV transitions were not seriously affected by this overlap since the 2.94 MeV level spectrum does not give strong gamma rays in regions near the 2.13 and 2.84 MeV peaks. Fits to the 2.84 → 0.71 MeV transition shown in figure 3-14 gave minimum values of χ^2 below the 0.1% limit for $J = 1, 2, 3$. However, the solutions for $J = 2$ and 3 are 3 times more probable than those for $J = 1$. Fitting both the 2.84 → 0.71 MeV and 2.84 → 0 MeV transitions simultaneously failed to provide additional discrimination. In the $J = 2$ fit to the 2.84 → 0.71 MeV transition a mixing ratio of $-23 \leq x \leq -0.67$ was obtained while for the $J = 3$ fit, two possible solutions of $x = +(0.03^{+0.29}_{-0.19})$ and $x = +(4.5^{+15}_{-2.6})$ were found. The 2.84 → 0 MeV transition shown in figure 3-15 yielded solutions of $x = -(5.7^{+17}_{-3.3})$ $x = -(0.65^{+0.45}_{-0.18})$ for $J = 2$ and $x = +(5.7^{+\infty}_{-2.6})$ $x=-(0.03^{+0.31}_{-0.15})$ and $x \leq -5.7$ for $J=3$. No previous spin assignments

Figure 3-14 Angular Distribution and χ^2-Versus Arc tan x for the 2.84 → 0.71 MeV Transition.

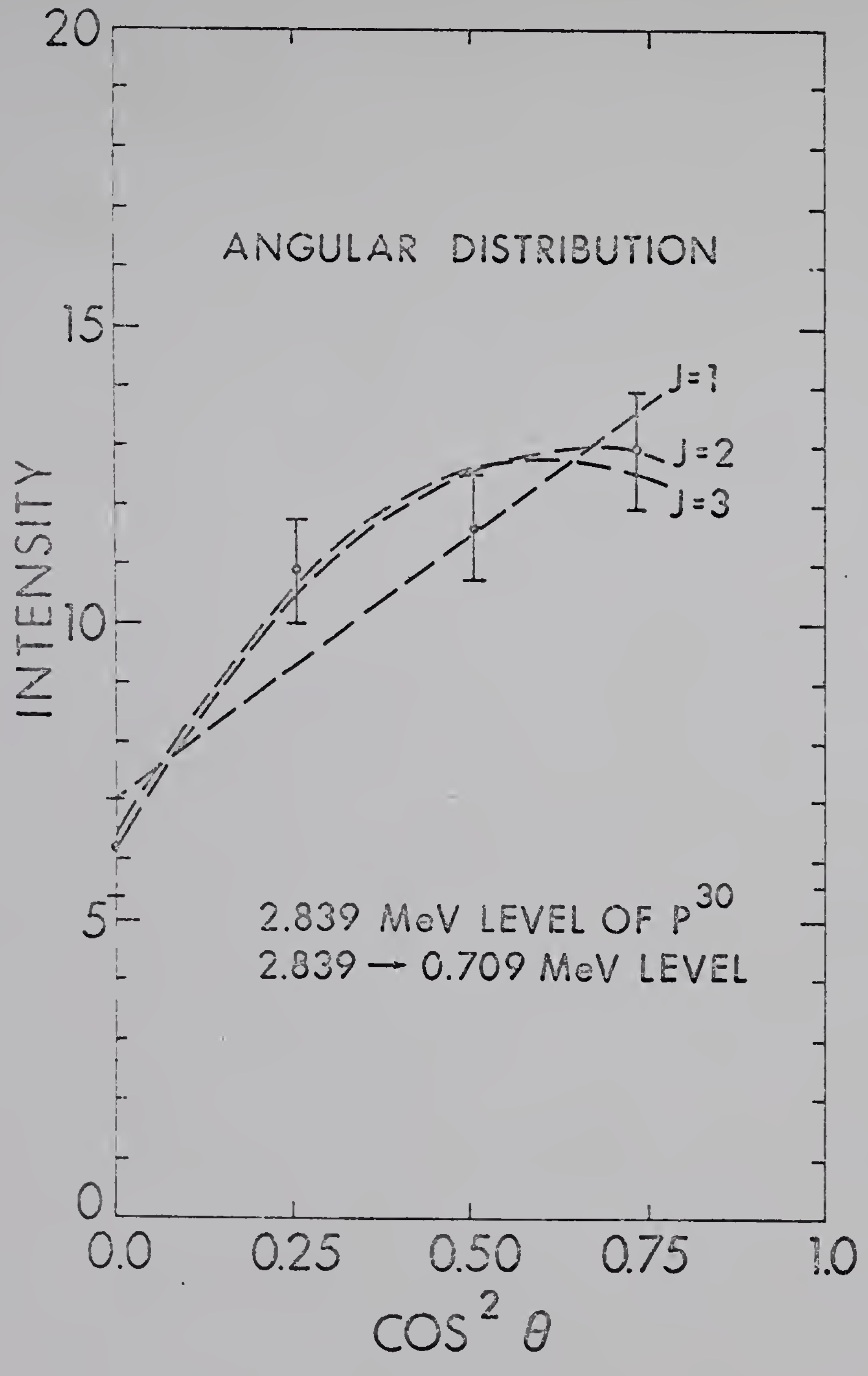
ANGULAR DISTRIBUTION
INTENSITY
20
15
10
5
0
0.0
0.25
0.50
0.75
1.0
COS ^{2} θ
J=1
J=2
J=3
2.839 MeV LEVEL OF P^{30}
2.839 → 0.709 MeV LEVEL

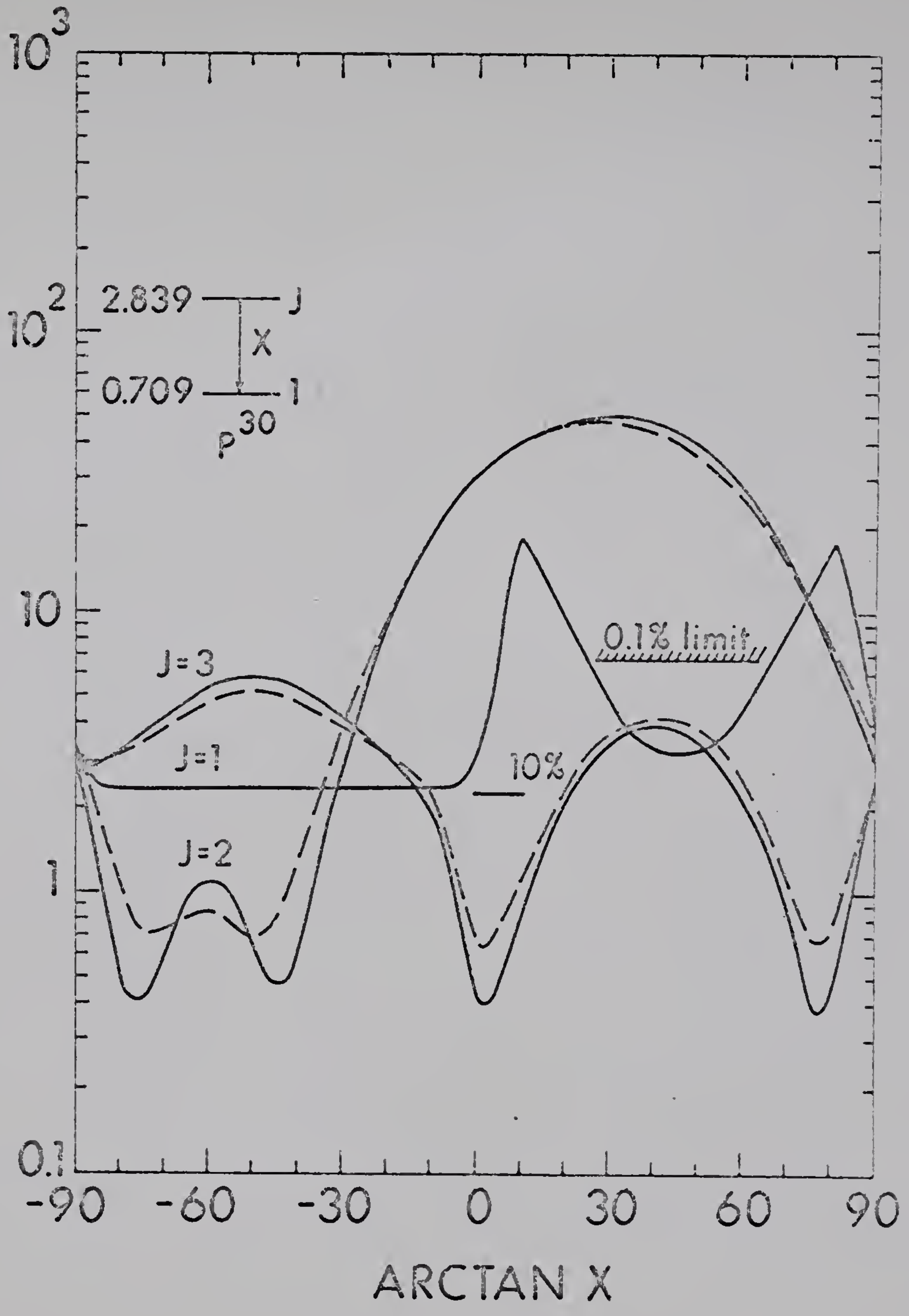
10^3
10^2
10
1
0.1
-90
-60
-30
0
30
60
90
ARCTAN X
2.839
J
X
0.709
1
P^{30}
J=3
J=1
J=2
10%
0.1% limit

Figure 3-15 Angular Distribution and χ^2-Versus Arc tan x for the 2.84 → 0 MeV Transition.

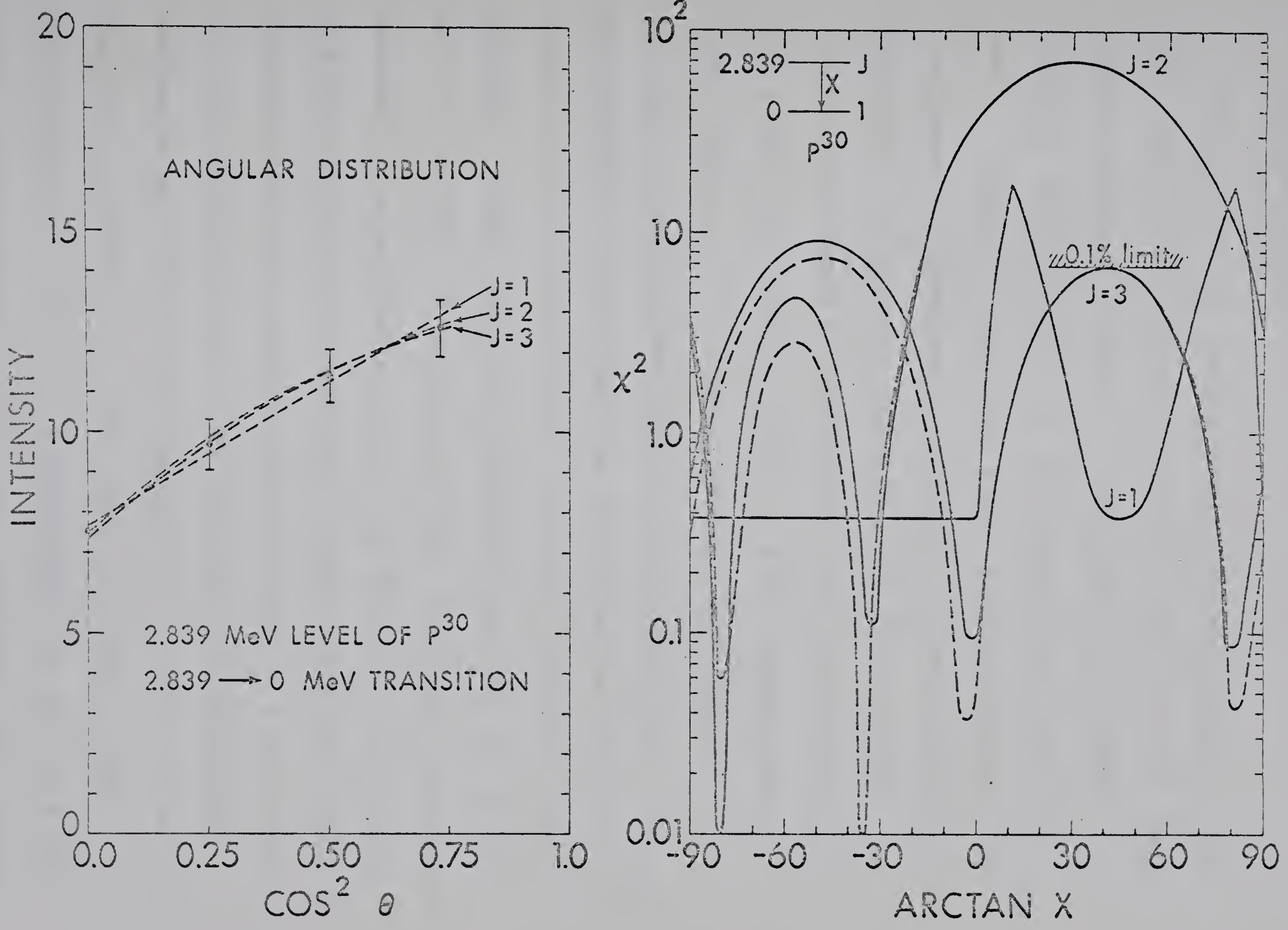
ANGULAR DISTRIBUTION
J = 1
J = 2
J = 3
2.839 MeV LEVEL OF P30
2.839 ⟶ 0 MeV TRANSITION
INTENSITY
20
15
10
5
0
0.0
0.25
0.50
0.75
1.0
COS2 θ
2.839
J
X
0
1
P30
J=2
0.1% limit
J=3
J=1
X2
10^2
10
1.0
0.1
0.01
-90
-60
-30
0
30
60
90
ARCTAN X

h. 2.94 MeV Level

Overlap of the proton peaks corresponding to the 3.02 and 2.84 MeV levels, and the nature of the decay scheme combined to make it impossible to extract reliable correlations for the gamma rays from this level. However, branching ratio determinations from the gamma-ray spectrum of figure 3-16 were possible. Decays to the ground, the 0.68, and the 1.45 MeV levels were found to take place with the branching of (10 ± 6)%, (43 ± 6)%, and (47 ± 6)%, respectively. These values are in fair agreement with those of previous investigators (Ba 62, Mo 63, Ha 67A). It was not possible in this work to determine to which of the levels of the doublet at 0.7 MeV the 2.94 MeV level decayed. Thus, based on previous work (Va 58, Ba 62, Mo 63, Ha 67A) a transition to the 0.680 MeV level was assumed. As pointed out by A. R. Poletti[s] it is surprising that an E2 transition to the 0.680 MeV level is favoured over an isotopic spin allowed M1 transition to the 0.709 MeV level. On the basis of Weisskopf estimates an $\Gamma(E2)/\Gamma(M1)$ ehnancement of $\sim 10^4$ is required for this to be so. Van der Leun and Endt (Va 58) have made a $J^\pi = 2^+$, $T = 1$ assignment to the 2.94 MeV level. Baart _et al_ (Ba 62) have confirmed the latter J^π assignment.

i. The 3.02 MeV Level

The gamma-ray spectrum for this level shown in figure 3-17 indicates a 20 to 30% overlap of the charged particles feeding this level with those feeding the 2.94 MeV level. This value is supported by estimates based on the coincident charged-particle spectrum. Fortunately only 15% of the total area of the strong 2.34 MeV gamma peak consisted of the 2.26 MeV gamma

---

[s] A. R. Poletti, Private communication, 1967.

Figure 3-16 Gamma-ray Spectrum for the 2.94 MeV Level of ^{30}P.

The points in the simultaneous randoms spectrum are indicated by open circles.

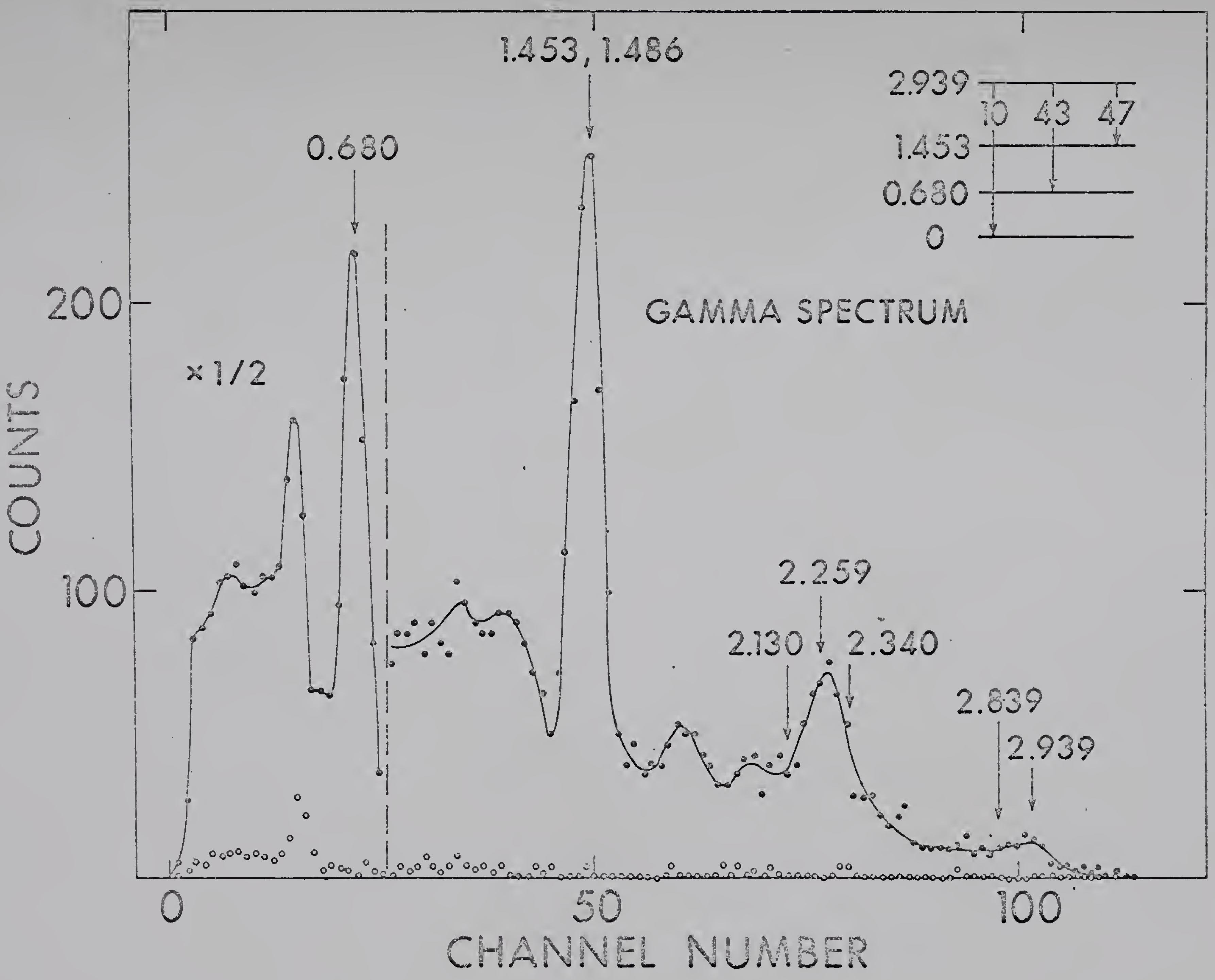
1.453, 1.486
0.680
2.939
1.453
0.680
0
10
43
47
GAMMA SPECTRUM
× 1/2
200
100
COUNTS
2.259
2.130
2.340
2.839
2.939
0
50
100
CHANNEL NUMBER

Figure 3-17 Gamma-ray Spectrum for the 3.02 MeV Level of ^{30}P.

The points in the simultaneous randoms spectrum are indicated by open circles.

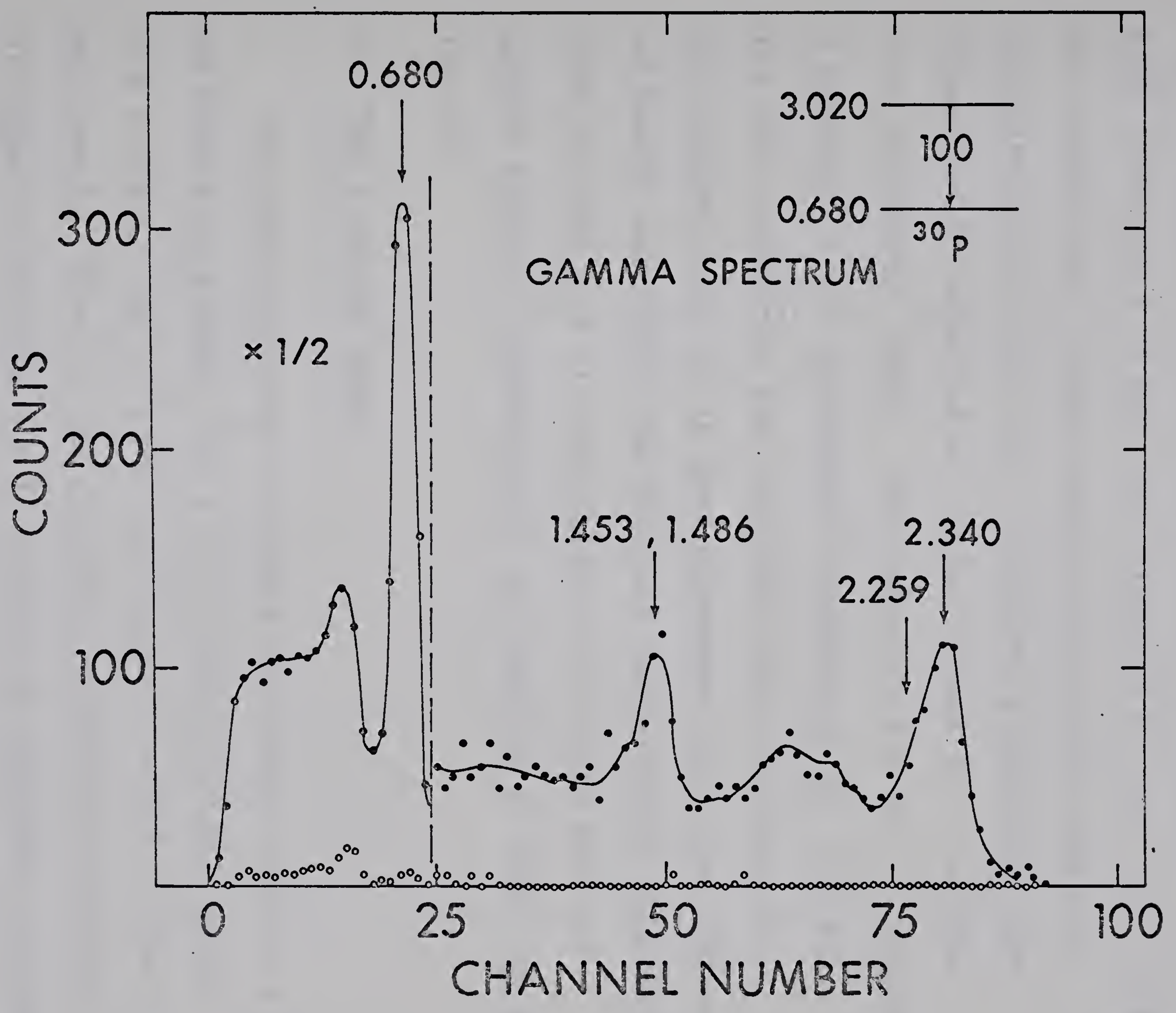
0.680
3.020
100
0.680
^{30}P
GAMMA SPECTRUM
× 1/2
300
200
100
COUNTS
1.453 , 1.486
2.259
2.340
0
25
50
75
100
CHANNEL NUMBER

ray arising from the decay of the 2.94 MeV level to the 0.68 MeV level. An approximate correlation of this 2.26 MeV gamma ray was used in subtracting off this peak from the 2.34 MeV peak produced by the 3.02 → 0.68 MeV transition. Least-squares fits to the angular distribution of the 3.02 → 0.68 MeV transition (see figure 3-18) rejected all spins except J = 1 at the 0.1% confidence limit. The value of 0.6 for χ^2 confirms a previous J = 1 assignment by Baart et al. (Ba 62). The 100% branch to the 0.68 MeV level obtained in the present work is in good agreement with the 95% result of Harris and Hyder (Ha 67A) but shows poorer agreement with the 89% and 11% branching to the 0.68 MeV and ground states, respectively, as reported by Baart et al. (Ba 62).

j. The 3.74 MeV Level

The gamma spectrum of figure 3-19 shows a (46 ± 6)% of branch to ground, (29 ± 5)% to the 0.68 MeV level, (18 ± 6)% to the 1.45 MeV level and (7 ± 3)% to the 2.94 MeV level. Fits to the crossover transition as shown in figure 3-20 give J = 1, 2 and 3 as possible solutions with J = 1 : 2 : 3 in the likelihood ratio of 5 : 1 . 5 : 1. The mixing ratio for the J = 1 solution of this transition is in the region $-8 \leq x \leq -0.13$. No previous spin assignments have been made to this level.

Figure 3-18 Angular Distribution for the 3.02 MeV Level of ^{30}P.

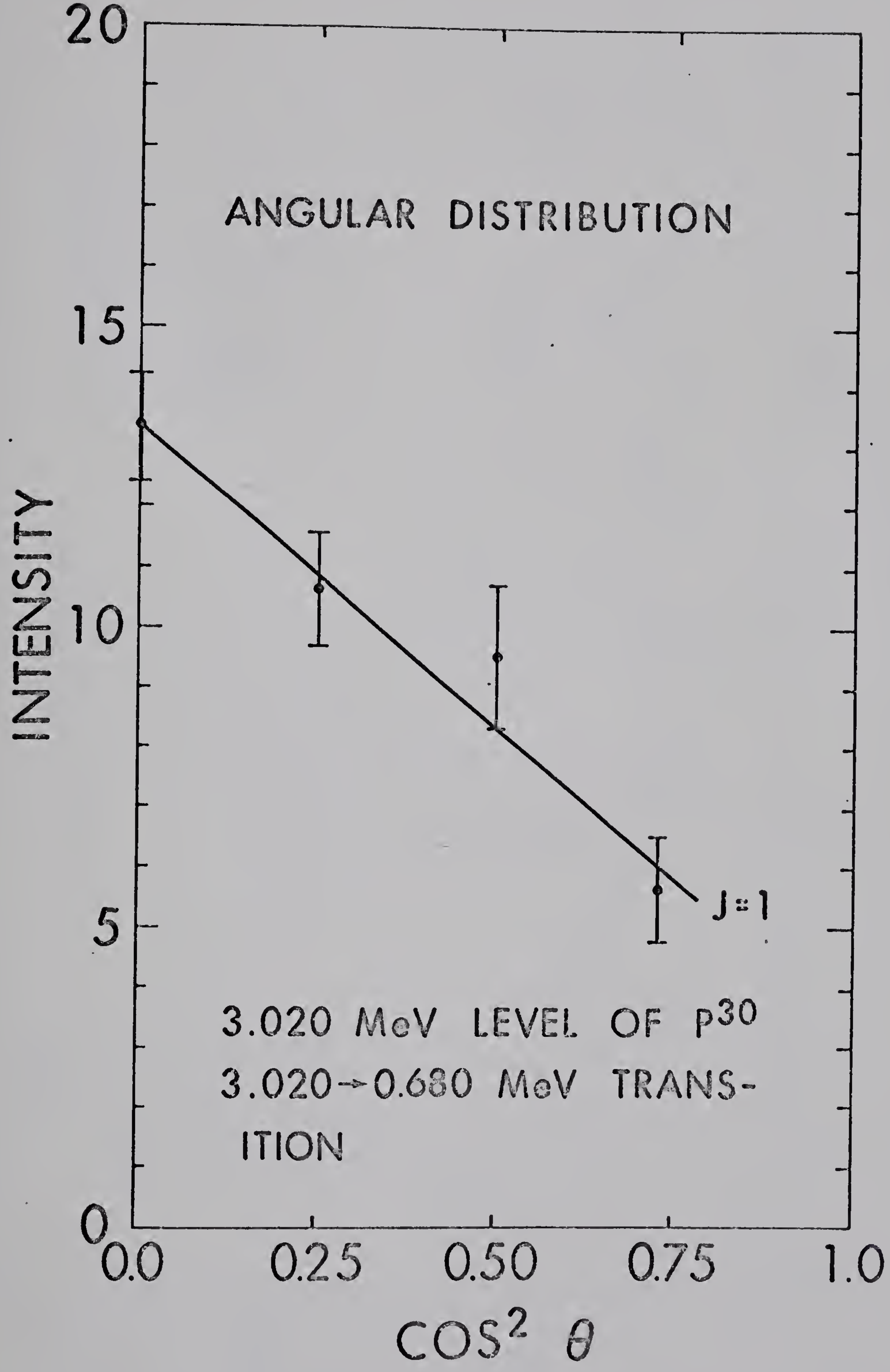

ANGULAR DISTRIBUTION
INTENSITY
20
15
10
5
0
0.0
0.25
0.50
0.75
1.0
COS² θ
J=1
3.020 MeV LEVEL OF P30
3.020→0.680 MeV TRANSITION

Figure 3-19 Gamma-ray Spectrum for the 3.74 MeV Level of ^{30}P.

The points in the simultaneous randoms spectrum are indicated by open circles.

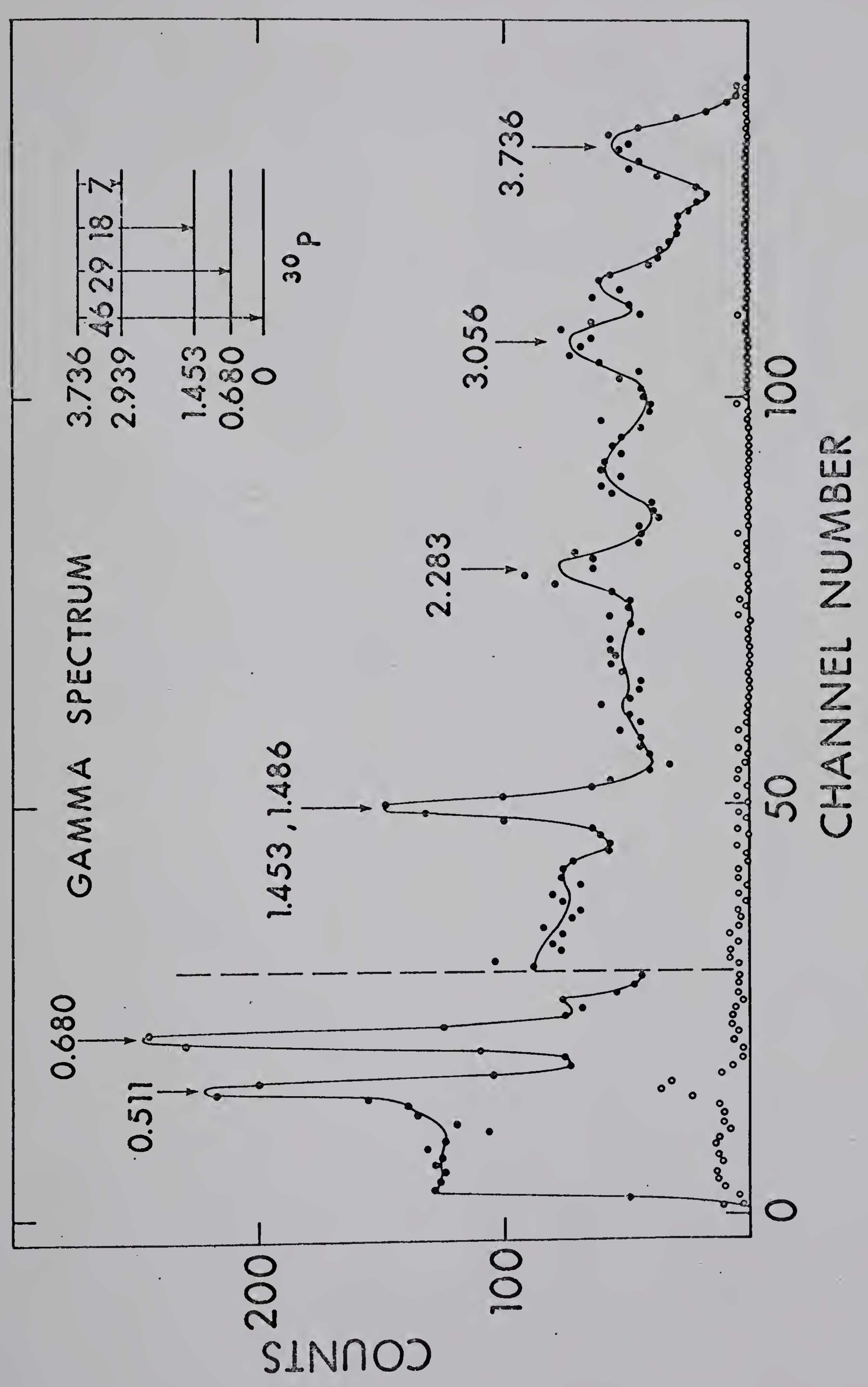
GAMMA SPECTRUM
0.511
0.680
1.453, 1.486
2.283
3.056
3.736
3.736
2.939
1.453
0.680
0
46
29
18
7
^{30}P
COUNTS
100
200
CHANNEL NUMBER
0
50
100

Figure 3-20 Angular Distribution and χ^2-Versus Arc tan x for the 3.74 → 0 MeV Transition.

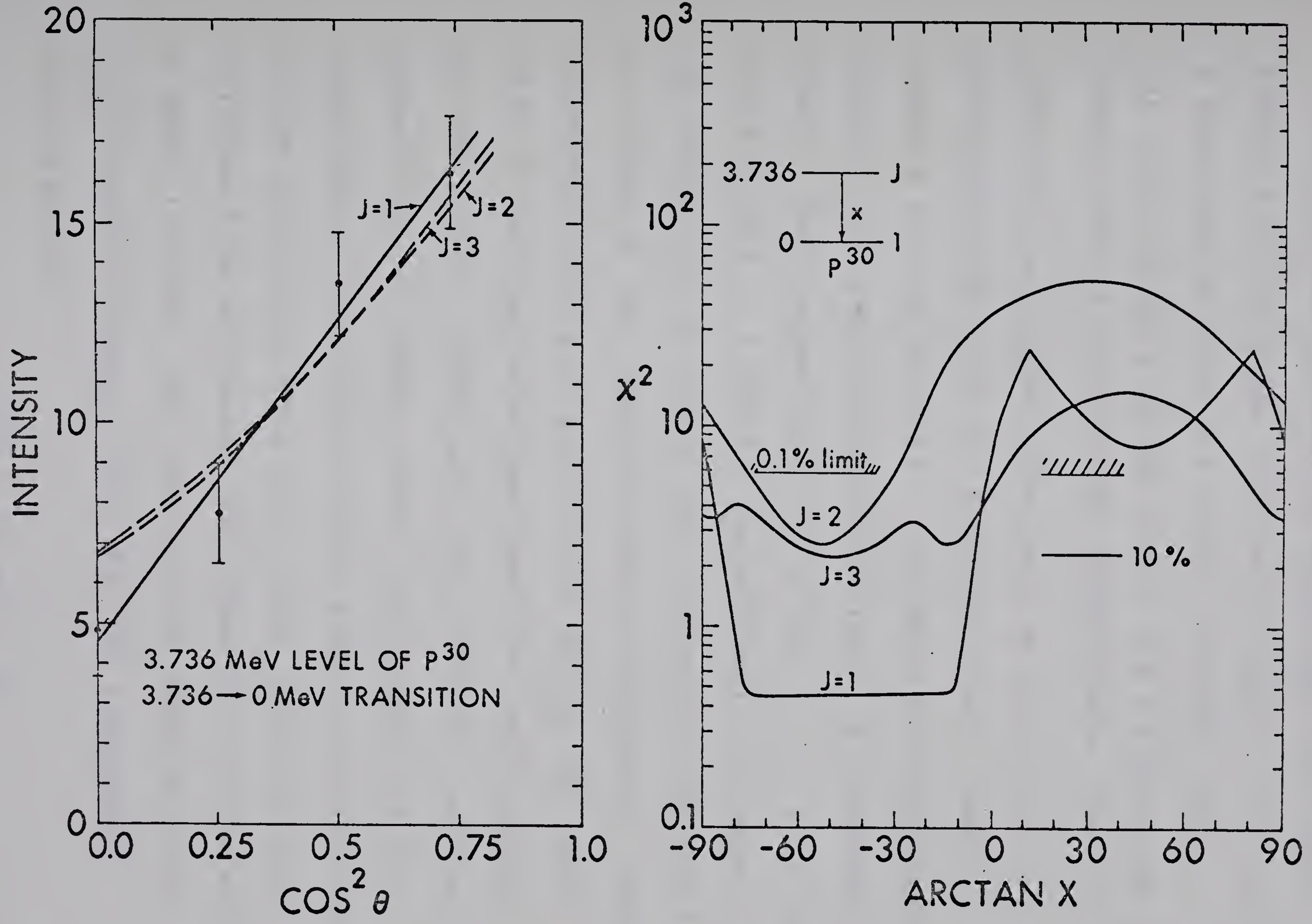
20
15
10
5
0
INTENSITY
0.0
0.25
0.5
0.75
1.0
$\cos^2\theta$
J=1
J=2
J=3
3.736 MeV LEVEL OF P^{30}
3.736→0 MeV TRANSITION
10^3
10^2
10
1
0.1
x^2
3.736
J
x
0
1
P^{30}
0.1% limit
J=2
J=3
J=1
10 %
-90
-60
-30
0
30
60
90
ARCTAN X

k. The 3.84 MeV Level

No previous information exists for this level. Analysis of the gamma spectrum of figure 3-21 yields a branching of (60 ± 6)% to the 2.94 MeV level, (16 ± 4)% to the 1.45 MeV level, (18 ± 9)% to the 0.7 MeV doublet and (6 ± 3)% to the ground state. The 0.7 MeV peak position suggests that most of the 3.84 → 0.7 MeV transition is to the 0.68 MeV level. Least-squares fits to the 3.84 → 2.94 MeV transition shown in figure 3-22 reject spin zero at the 0.1% confidence limit. The minimum values of χ^2 for J = 1, 2, 3 and 4 are 0.9, 0.1, 1.1 and 0.1 respectively. An upper limit of 20 nsec can be set on the lifetime of this level by virtue of the time coincidence conditions. Longer lifetimes would give appreciable tail on the upper side of the time coincident peak that would appear in the randoms window and, thus, lead to a smaller than normal true to randoms ratio. An estimate of the magnitude of this effect can be made by constructing a time coincidence peak for a state with a 20 nsec lifetime from an assumed peak shape for a state with a short lifetime. The construction shown in figure 3-23 involves drawing curves for the exponential decay given by

$$N(t) = N_o \exp(-\frac{t}{20}) \qquad (3\text{-}1)$$

where N(t) is the number of nuclei in the 3.84 MeV

Figure 3-21 Gamma-ray Spectrum for the 3.84 MeV Level of ^{30}P.

The points in the simultaneous randoms spectrum are indicated by open circles.

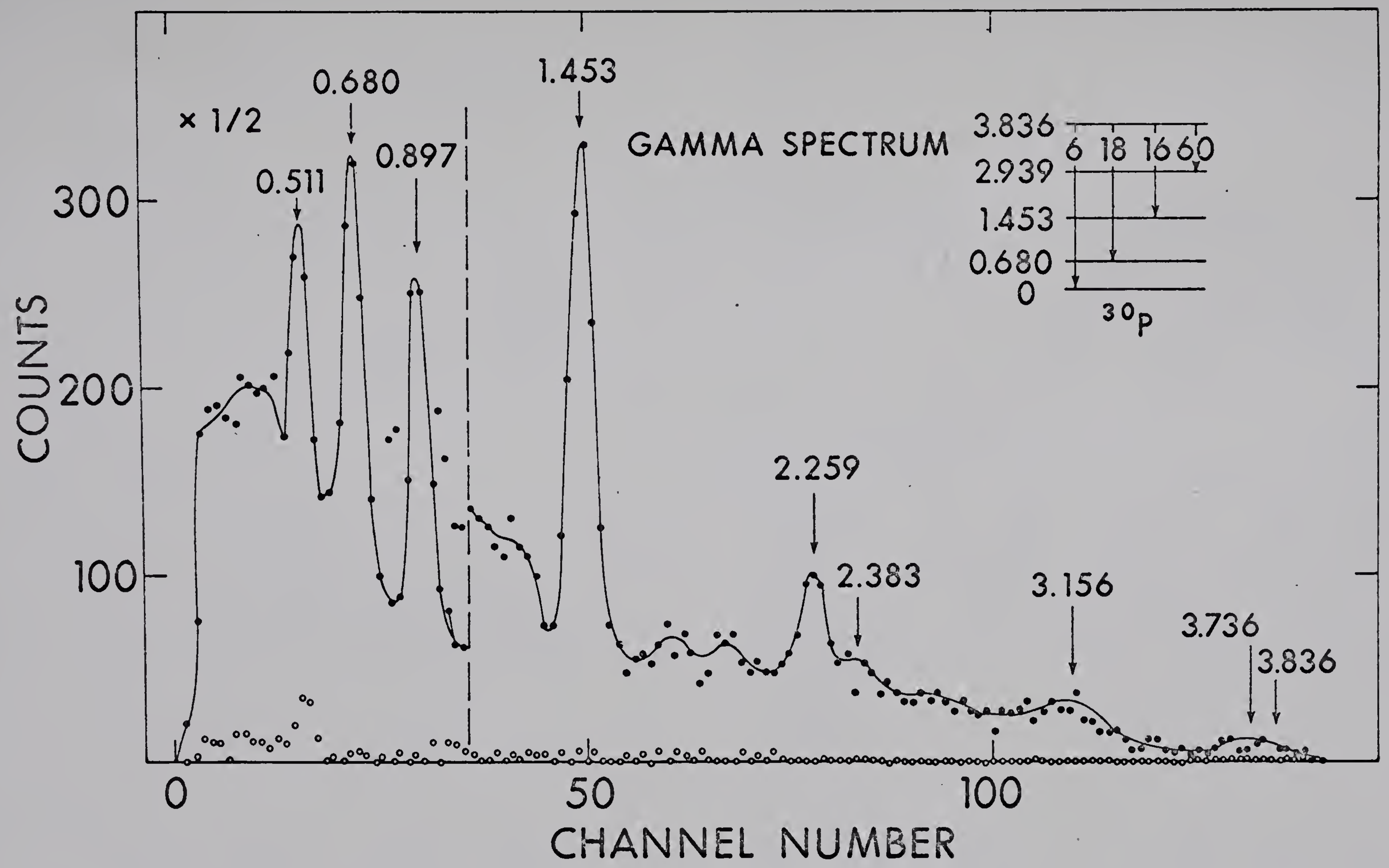
GAMMA SPECTRUM
× 1/2
0.511
0.680
0.897
1.453
2.259
2.383
3.156
3.736
3.836
3.836
2.939
1.453
0.680
0
6
18
16
60
^{30}P
COUNTS
100
200
300
0
50
100
CHANNEL NUMBER

Figure 3-22 Angular Distribution and χ^2-Versus Arc tan x for the 3.84 → 2.94 MeV Transition.

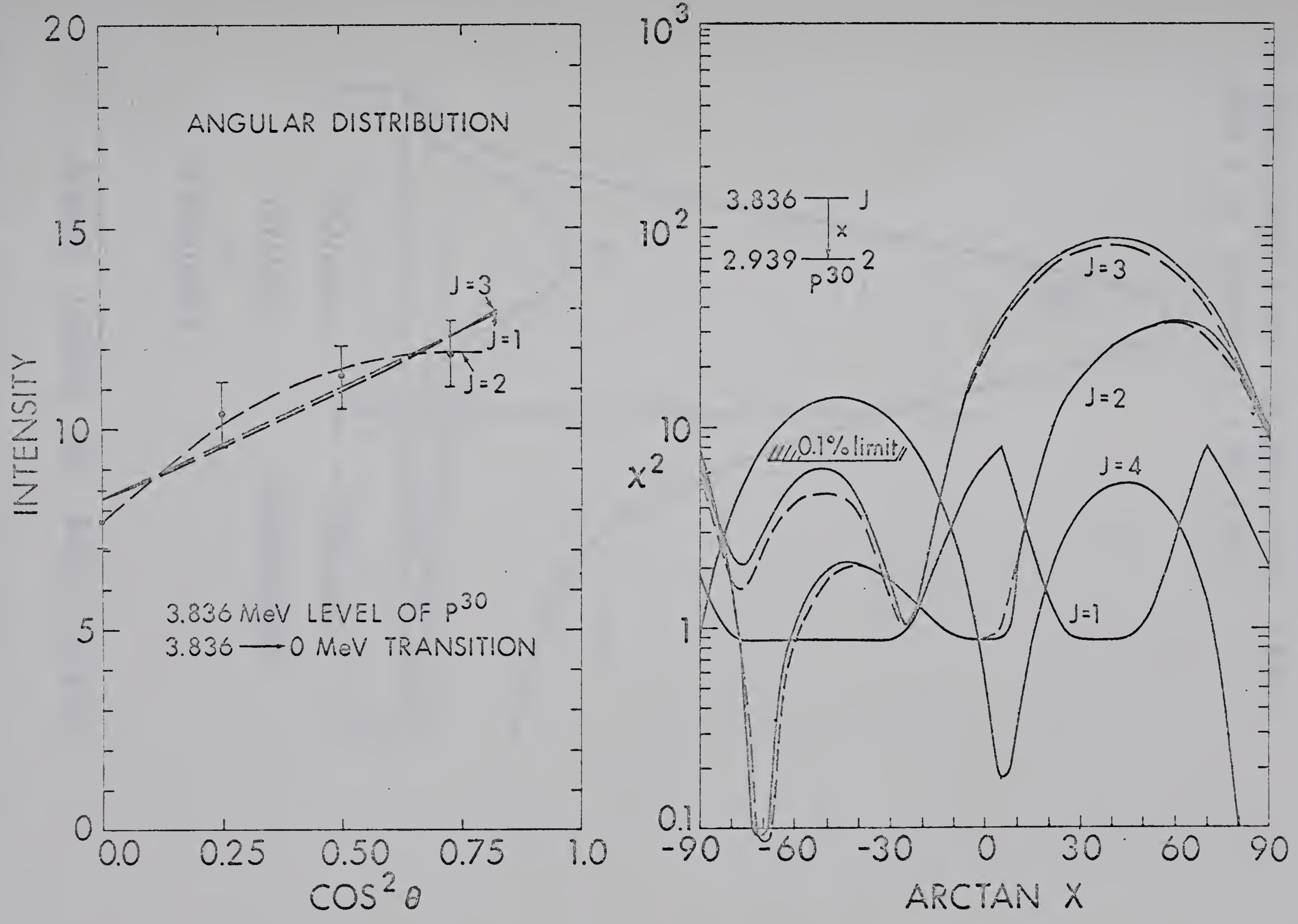
ANGULAR DISTRIBUTION
INTENSITY
20
15
10
5
0
0.0
0.25
0.50
0.75
1.0
COS² θ
J=3
J=1
J=2
3.836 MeV LEVEL OF P³⁰
3.836 ⟶ 0 MeV TRANSITION
10³
10²
10
1
0.1
χ²
-90
-60
-30
0
30
60
90
ARCTAN X
3.836 J
x
2.939 2
P³⁰
0.1% limit
J=3
J=2
J=4
J=1

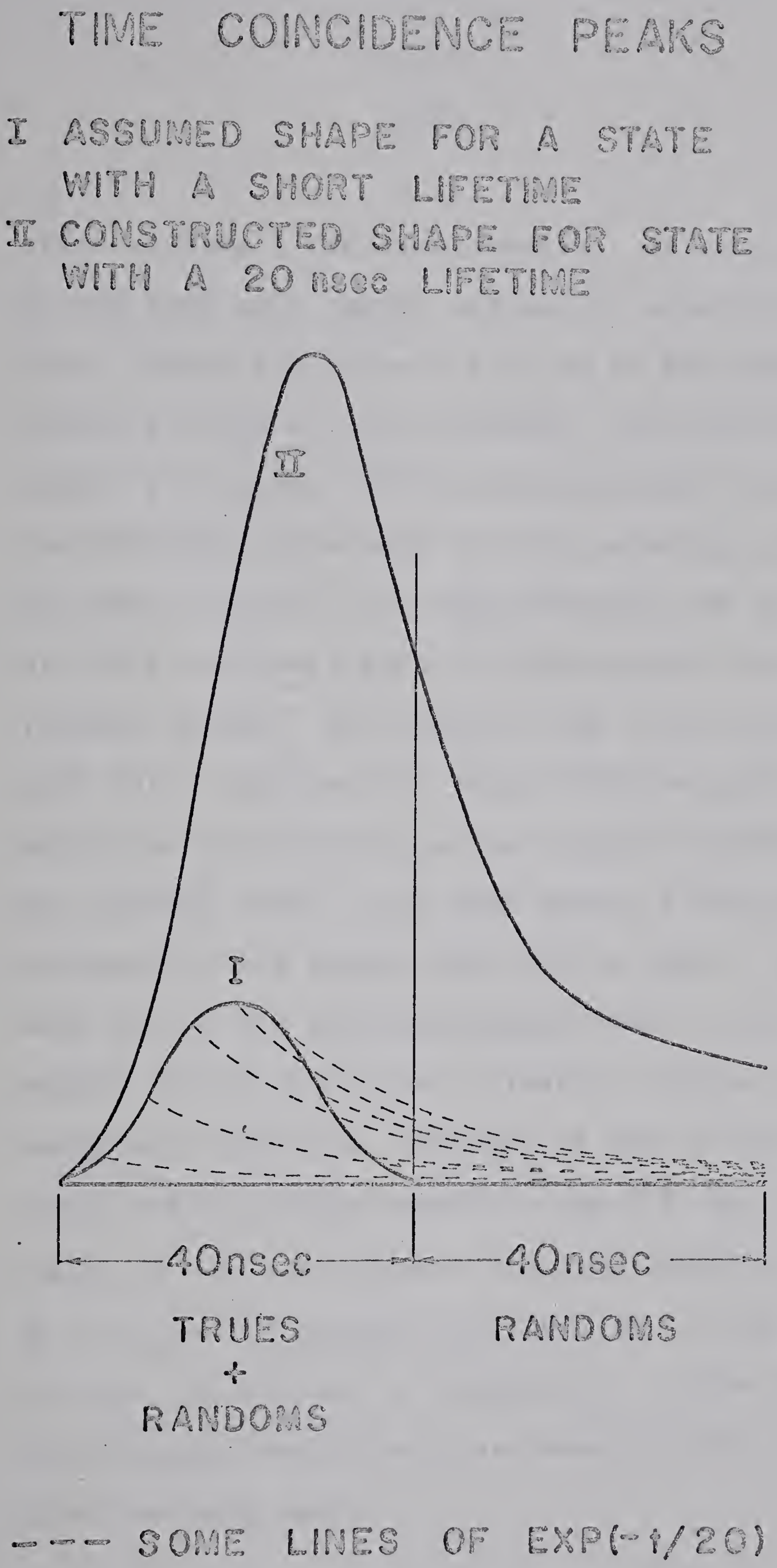
TIME COINCIDENCE PEAKS
I ASSUMED SHAPE FOR A STATE WITH A SHORT LIFETIME
II CONSTRUCTED SHAPE FOR STATE WITH A 20 nsec LIFETIME
II
I
40nsec
40nsec
TRUES + RANDOMS
RANDOMS
--- SOME LINES OF EXP(-t/20)

Figure 3-23 Estimated Time Coincidence Peak for a State with a 20 nsec Lifetime.

state at time t (in nanoseconds). At equal intervals on the time axis curves defined by equation 3-1 were drawn taking the values of No to be the number of counts at each of the intervals. Next the number of counts at a given interval was obtained by summing the contributions from each of the preceding intervals. As seen in figure 3-23 approximately 30% of the amount of the coincidence peak in both windows lies in the randoms window. The shape of the time coincidence peak for a state with a short lifetime,which is dependent mainly on electronics,may be slightly different than the assumed shape. For this reason a conservative estimate of 20% rather than 30% is used. However, even 20% of the time coincidence peak in the randoms window should result in a clearly visible nonrandom background spectrum. Because of the 20 nsec lifetime limit and the large branch to the 0.68 MeV spin zero level, a J = 4 assignment requires $|M(E4)|^2 > 1.5 \times 10^3$ W.u. ($r_o = 1.2$ fermis) for the 3.84 → 0.68 MeV transition and can, therefore, be ruled out. In the latter estimate two standard deviations have been allowed for M3 in the branching ratio.

ℓ. The 3.93 MeV Level

This level has been observed only weakly in proton capture work. A 100% branching to the 0.71 MeV level as suggested by Harris and Hyder (Ha 67A) is clearly not in accord with the observed gamma spectrum as seen in figure 3-24. Analysis of this spectrum indicates a (55 ± 6)% branch to the 2.94 MeV level, a (35 ± 6)% transition to the 1.453 MeV level and a (10 ± 6)% transition to the 0.7 MeV level. Least-squares fits to the 3.93 → 2.94 MeV transition shown in figure 3-25 give spin possibilities of $J = 1$, 2 or 3. The mixing ratio solutions corresponding to these spin values together with values of χ^2 for the best fits are listed in table 3-1. Because of the difficulty in extracting reliable correlations for the other transitions no other peaks in this spectrum were fitted.

m. The 4.14 and 4.18 MeV Level

From the charged-particle spectrum of figure 3-2b

Figure 3-24 Gamma-ray Spectrum for the 3.93 MeV Level of ^{30}P.

The points in the simultaneous randoms spectrum are indicated by open circles.

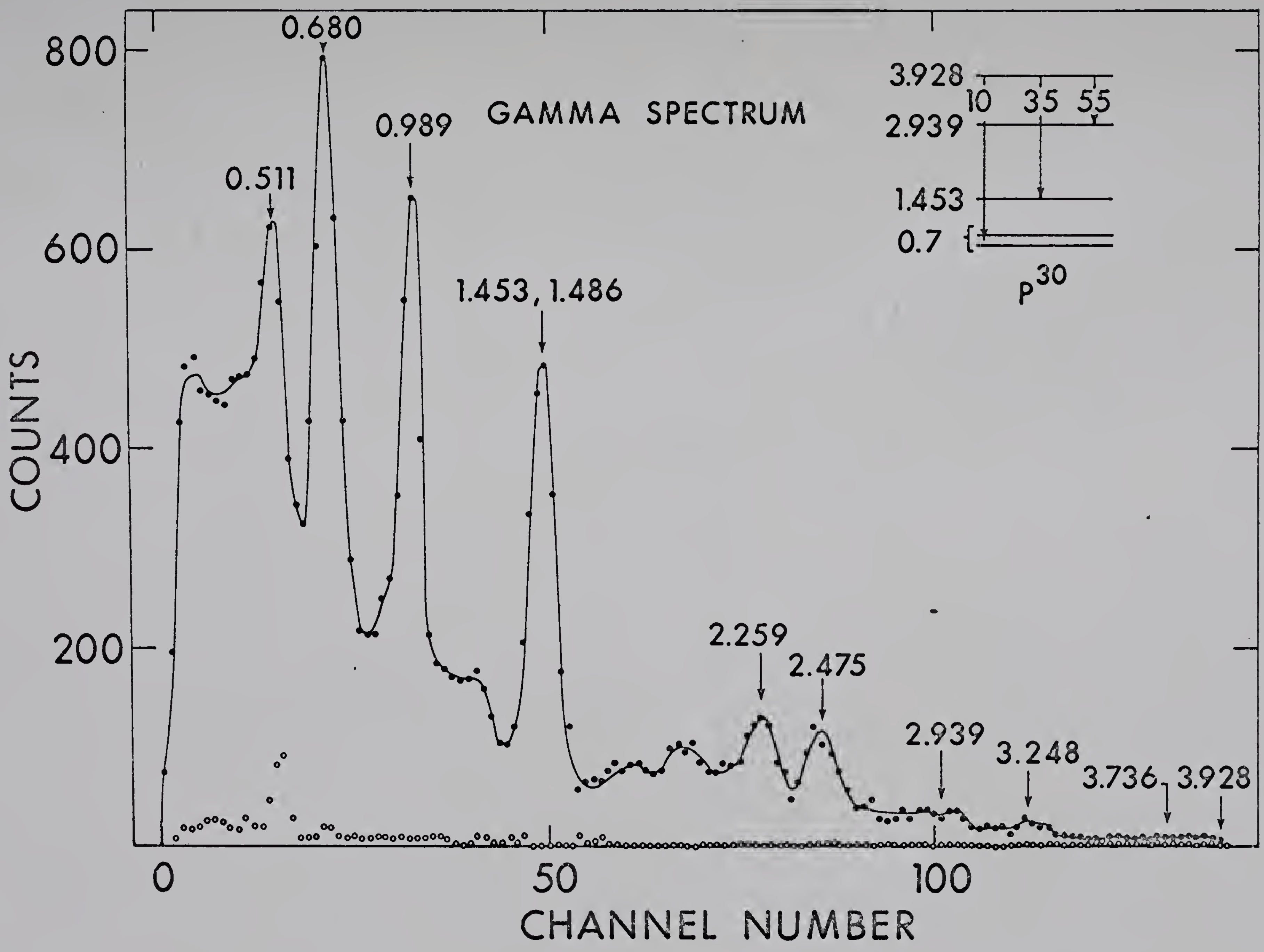
GAMMA SPECTRUM
COUNTS
800
600
400
200
0
50
100
CHANNEL NUMBER
0.511
0.680
0.989
1.453, 1.486
2.259
2.475
2.939
3.248
3.736
3.928
3.928
2.939
1.453
0.7
10
35
55
P^{30}

Figure 3-25 Angular Distribution and χ^2-Versus Arc tan x for the 3.93 → 2.94 MeV Transition.

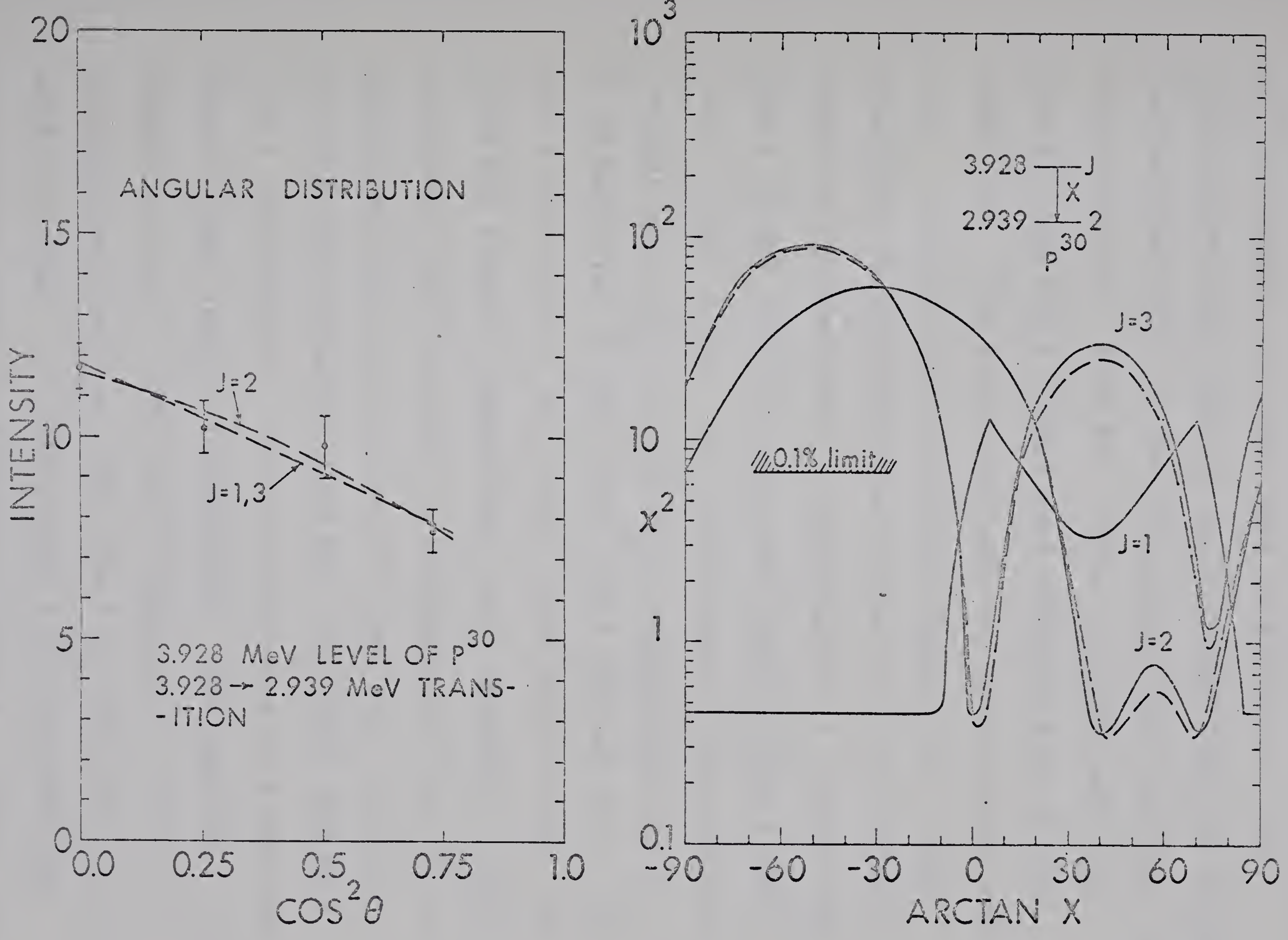
20
15
10
5
0
INTENSITY
0.0
0.25
0.5
0.75
1.0
$\cos^2\theta$
ANGULAR DISTRIBUTION
J=2
J=1,3
3.928 MeV LEVEL OF P^{30}
3.928 → 2.939 MeV TRANS-
-ITION
10^3
10^2
10
χ^2
1
0.1
-90
-60
-30
0
30
60
90
ARCTAN X
3.928 J
X
2.939 2
P^{30}
0.1% limit
J=3
J=1
J=2

it is seen that the 4.14 - 4.18 doublet and the 4.23 MeV peaks are not resolved. It was, however, possible to distinguish the gamma rays of the 4.14 - 4.18 MeV doublet from those of the 4.23 MeV level by setting two adjacent bins in the charged-particle spectrum such that the 4.14 - 4.18 MeV doublet occupied most of one bin and the 4.23 MeV peak occupied most of the other bin. The resulting gamma-ray spectrum for the 4.14 - 4.18 MeV bin is shown in figure 3-26. This procedure enabled branching ratios to be determined. From the charged-particle spectrum it is evident that the 4.18 MeV level is much more weakly excited than the 4.14 MeV level. By subtracting off the effect of overlap with the 4.23 MeV level, branching from the 4.14 MeV level of (70 ± 4)%, (14 ± 5)% and (16 ± 5)% for transitions to the ground state the 0.71 MeV and 1.45 MeV levels, respectively, were obtained. Harris and Hyder (Ha 67A) report a branching of (88 ± 4)% to ground and (12 ± 4)% to the 0.71 MeV for this state For the decay from the 4.18 MeV level they obtained (19 ± 3)% and (81 ± 3)% for transitions to ground and the 0.71 MeV levels, respectively. The weak (14 ± 5)% branch to the 0.71 MeV level indicated by our results is additional evidence that the 4.18 MeV level is very weakly excited. χ^2 fits to the 4.14 MeV gamma-ray correlation shown in figure 3-27 gave J = 1 and 2 as

Figure 3-26 Gamma-ray Spectrum for the 4.14 → 4.18 MeV Levels of ^{30}P.

The points in the simultaneous randoms spectrum are indicated by open circles.

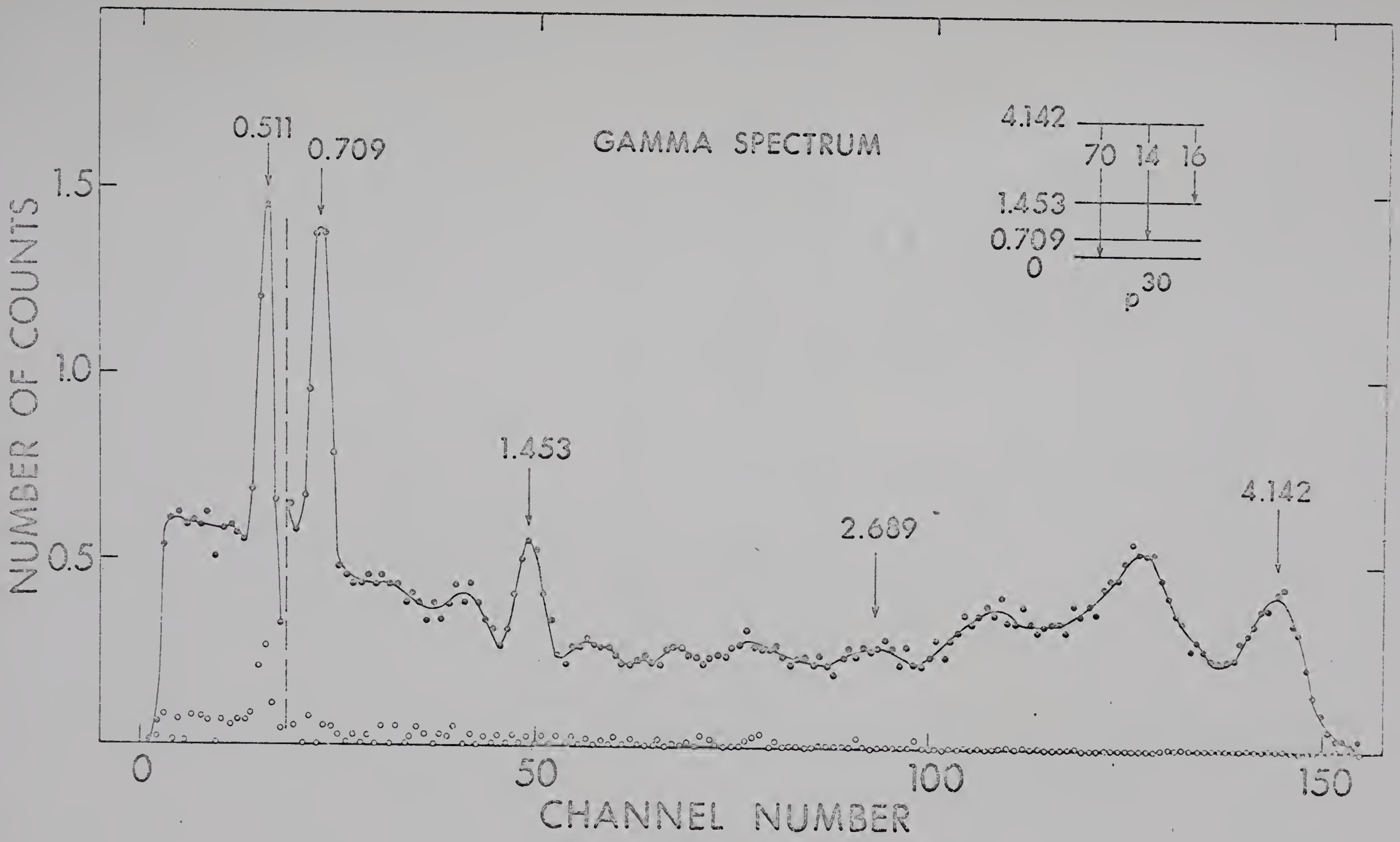
GAMMA SPECTRUM
0.511
0.709
1.453
2.689
4.142
4.142
70
14
16
1.453
0.709
0
P^{30}
NUMBER OF COUNTS
1.5
1.0
0.5
0
50
100
150
CHANNEL NUMBER

Figure 3-27 Angular Distribution and χ^2-Versus Arc tan x for the 4.14 → 0 MeV Transition.

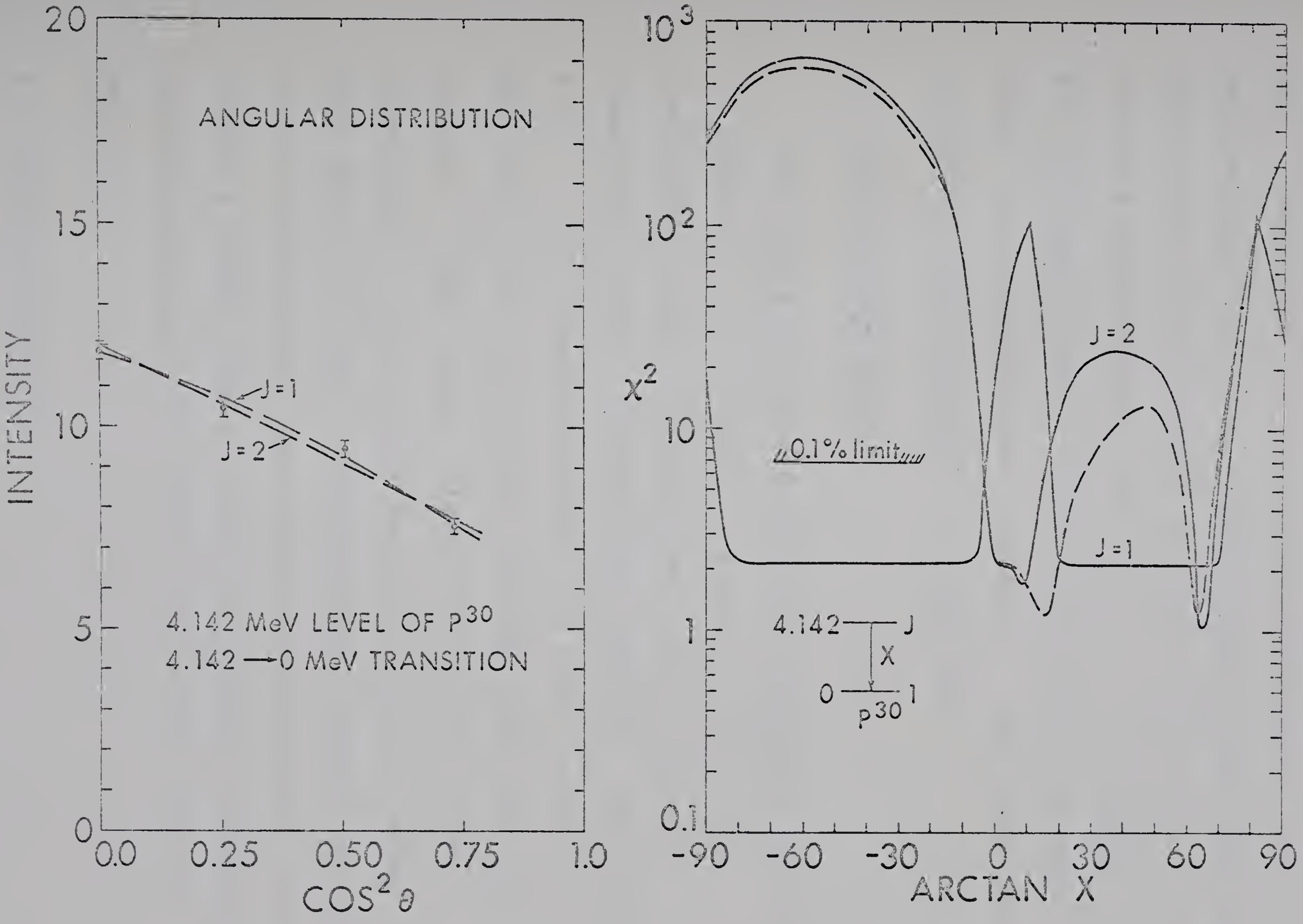
20
15
10
5
0
INTENSITY
ANGULAR DISTRIBUTION
J=1
J=2
4.142 MeV LEVEL OF P30
4.142 ⟶ 0 MeV TRANSITION
0.0
0.25
0.50
0.75
1.0
COS2 θ
10^3
10^2
10
1
0.1
χ2
0.1% limit
J=2
J=1
4.142
J
X
0
1
P30
-90
-60
-30
0
30
60
90
ARCTAN X

the only possible solutions with J = 2 being 5 times more likely than J = 1. Two possible mixing ratios are obtained for J = 2. Taking into account the finite size effect of the annular detector, these are $x = +(0.15^{+0.40}_{-0.22})$ to the 0.1% confidence limit and $x = +(2.14^{+0.22}_{-0.30})$ to the 17% confidence limit. The latter solution is about 1.9 times more probable than the former. This level has previously been assigned J = 2 (Ha 66B).

n. The 4.23 MeV Level

This level has previously been assigned a spin of 4^- with a (3 ± 1)% branch to ground, a (69 ± 2)% transition to the 1.97 MeV level, and a (28 ± 2)% transition to the 2.54 MeV level (Ha 67A). The branching ratios of the present work are (19 ± 4)% to the 2.54 MeV level, (69 ± 4)% to the 1.97 MeV level and (12 ± 5)% to the 1.45 MeV level. Figure 3-28 clearly shows a branching to the 1.45 MeV level not found in other work (Mo 63, Ho 67A). Unfortunately, because the gamma rays from this level were so much less intense than those of the 4.14 MeV level, it was not possible to obtain correlations using the method employed for the 4.14 MeV level.

o. The 4.50 MeV Level

Analysis of the gamma-ray spectrum of figure 3-29

Figure 3-28 Gamma-ray Spectrum for the 4.23 MeV Level of ^{30}P.

The points in the simultaneous randoms spectrum are indicated by open circles.

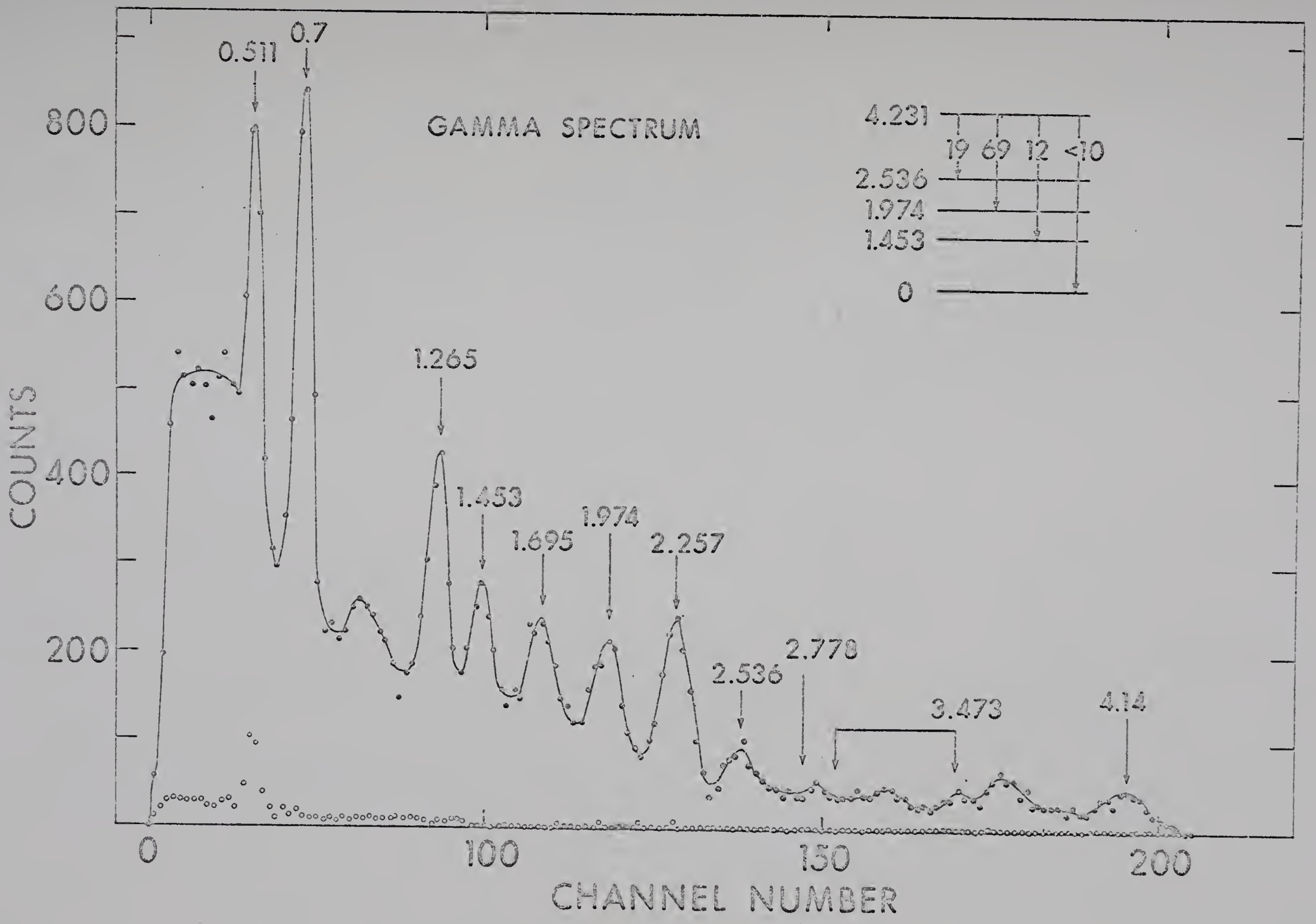
GAMMA SPECTRUM
COUNTS
800
600
400
200
0
100
150
200
CHANNEL NUMBER
0.511
0.7
1.265
1.453
1.695
1.974
2.257
2.536
2.778
3.473
4.14
4.231
2.536
1.974
1.453
0
19
69
12
<10

Figure 3-29 Gamma-ray Spectrum for the 4.50 MeV Level of ^{30}P.

The points in the simultaneous randoms spectrum are indicated by open circles.

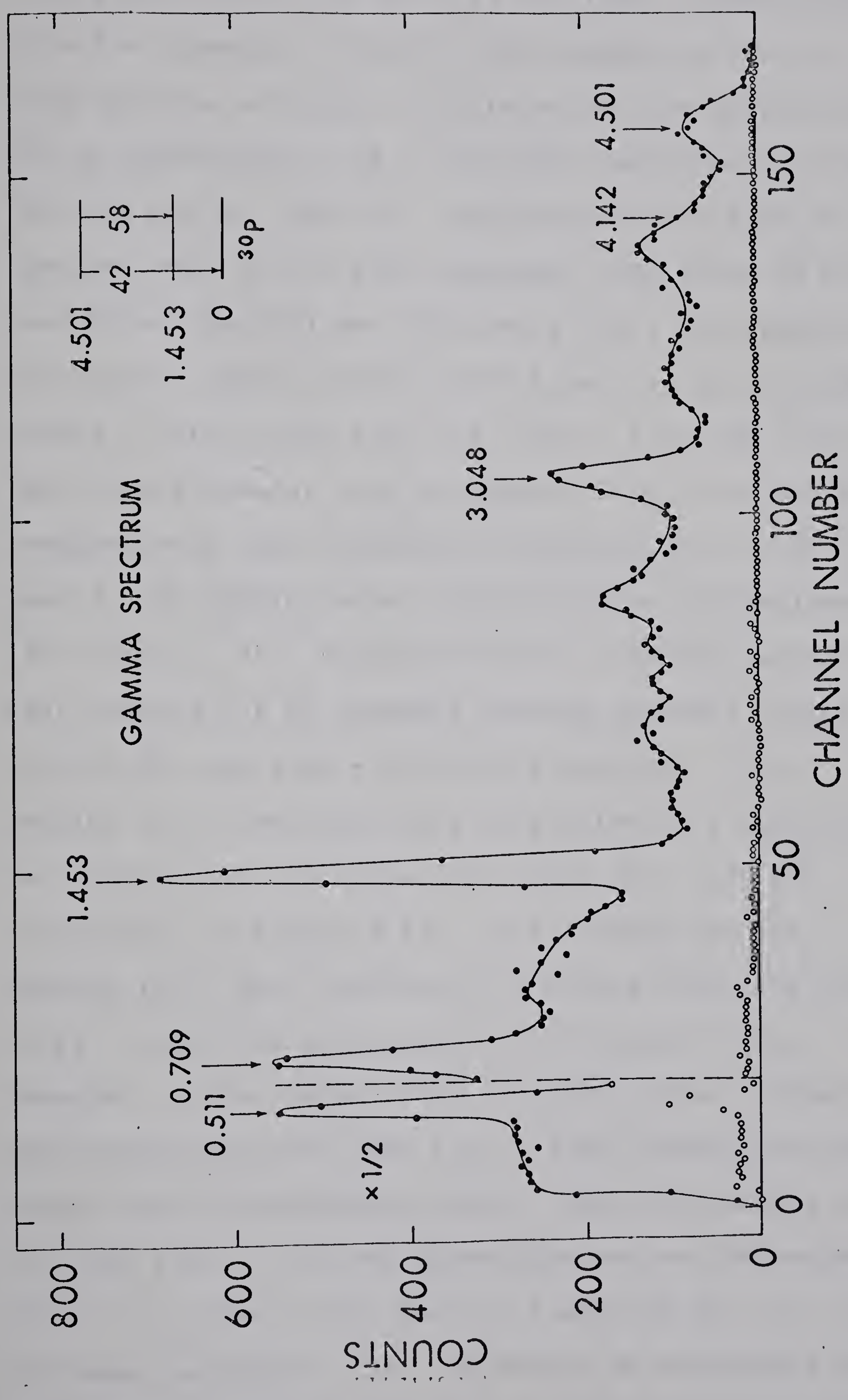
GAMMA SPECTRUM
COUNTS
800
600
400
200
0
CHANNEL NUMBER
0
50
100
150
×1/2
0.511
0.709
1.453
3.048
4.142
4.501
4.501
1.453
0
42
58
30P

gave branching ratios of (42 ± 5)% and (58 ± 5)% to the ground state and the 1.45 MeV level, respectively. The low intensity of the 0.7 MeV gamma ray seen in the spectrum of figure 3-29 rules out the possibility of an appreciable 4.50 → 3.02 MeV transition as reported by Baart *et al.* (Ba 62). Branching ratios from the present work are in poor agreement with those of Harris and Hyder (Ha 67A) who obtained a (70 ± 8)% branch to the ground state and (30 ± 8)% branch to the 1.45 MeV level. Fits to the 4.50 → 0, 4.50 → 1.45 and 1.45 → 0 MeV transitions as seen in figures 3-30, 3-31 and 3-32, respectively gave acceptable solutions for $J = 0, 1$, and 2. To obtain better discrimination, a simultaneous fit of the 1.45 → 0 and the 4.50 → 1.45 MeV transitions was carried out by stepping through possible mixing ratios for the 4.50 → 1.45 MeV transition. The minima in χ^2 for these fits is plotted as a function of mixing-ratio solutions for the 4.50 → 1.45 MeV transition in figure 3-33. In the resultant fits minima in χ^2 were obtained at a mixing ratio for the 1.45 → 0 MeV transition of $x = 0.70$ in all cases. However, in the latter fit χ^2 values for all values of the mixing ratio for the 1.45 → 0 MeV transition were below the 17% confidence limit. Thus, the mixing ratio for the 4.50 → 1.45 MeV transition was not determined for $J = 1$. The χ^2 fit for $J = 1$ and $x(4.50 \rightarrow 0) = 0.18$ is shown in figure 3.34. It should be emphasized that any of the values of $x(4.50 \rightarrow 0)$ are possible so that

Figure 3-30 Angular Distribution and χ^2-Versus Arc tan x for the 4.50 → 0 MeV Transition.

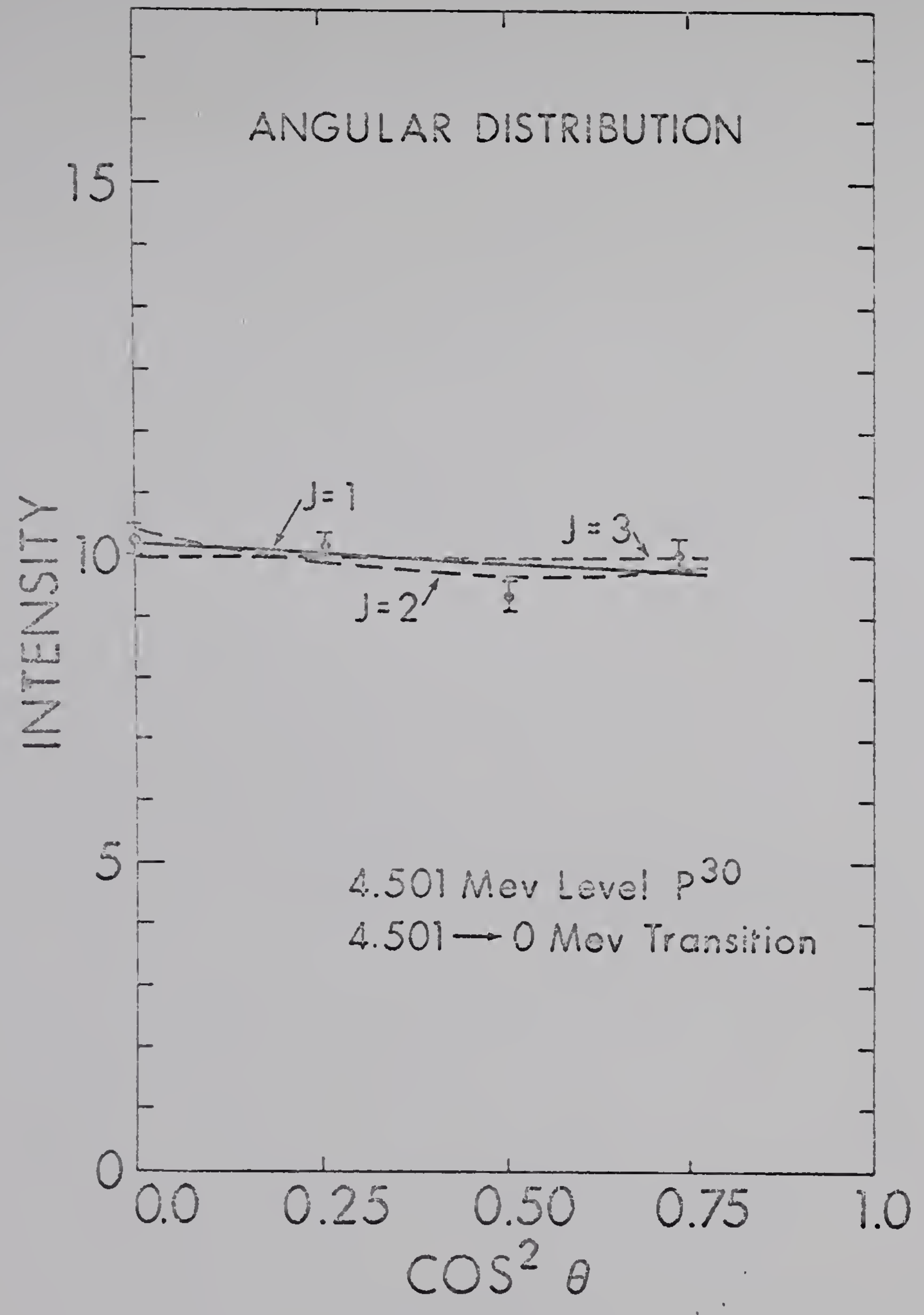
ANGULAR DISTRIBUTION
INTENSITY
15
10
5
0
J=1
J=3
J=2
4.501 Mev Level P^{30}
4.501 → 0 Mev Transition
0.0
0.25
0.50
0.75
1.0
$\cos^2\theta$

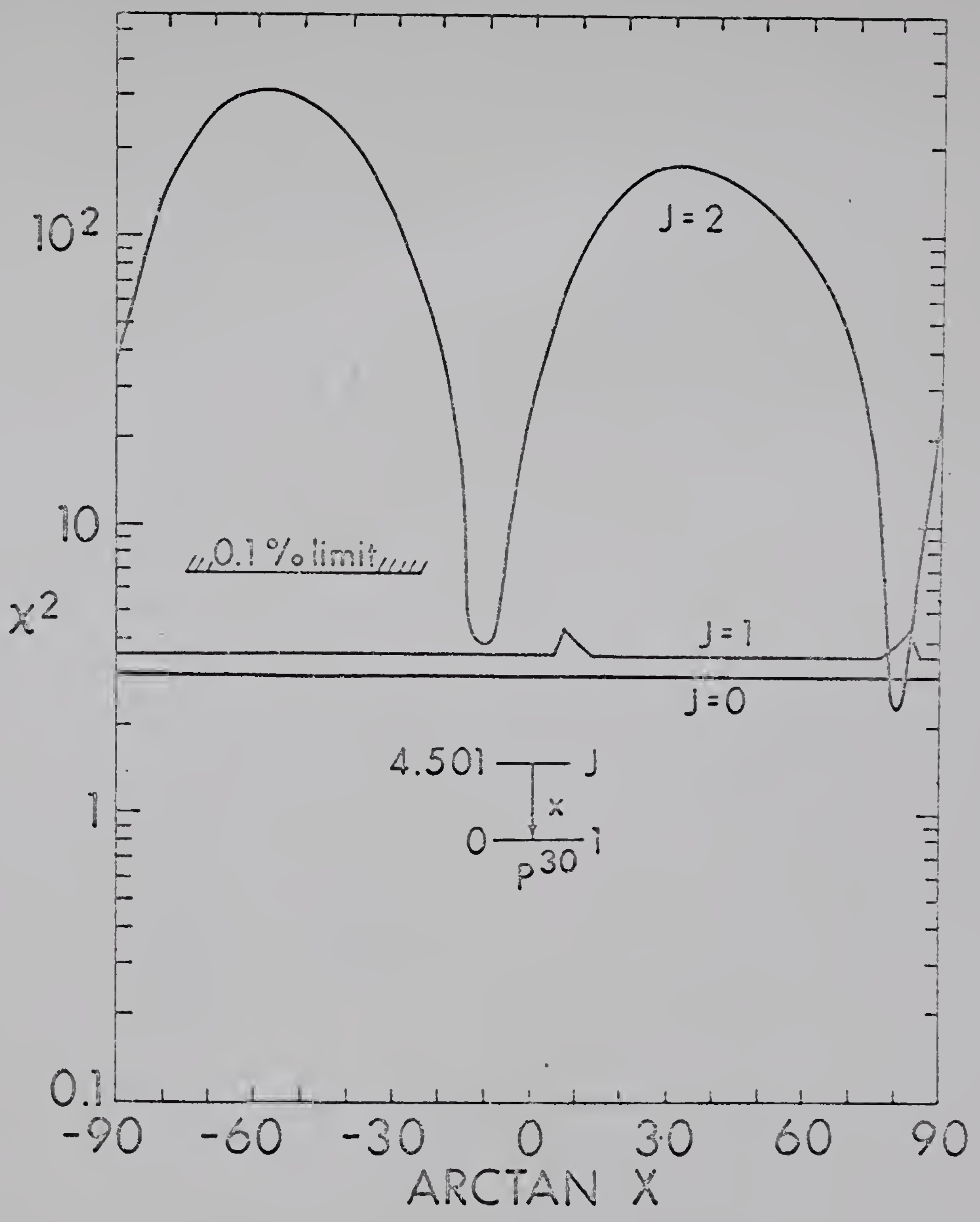
χ^2
10^2
10
1
0.1
J=2
0.1 % limit
J=1
J=0
4.501 — J
x
0 — 1
P^{30}
-90
-60
-30
0
30
60
90
ARCTAN X

Figure 3-31 Angular Distribution and χ^2-Versus Arc tan x for the 4.50 → 1.45 MeV Transition.

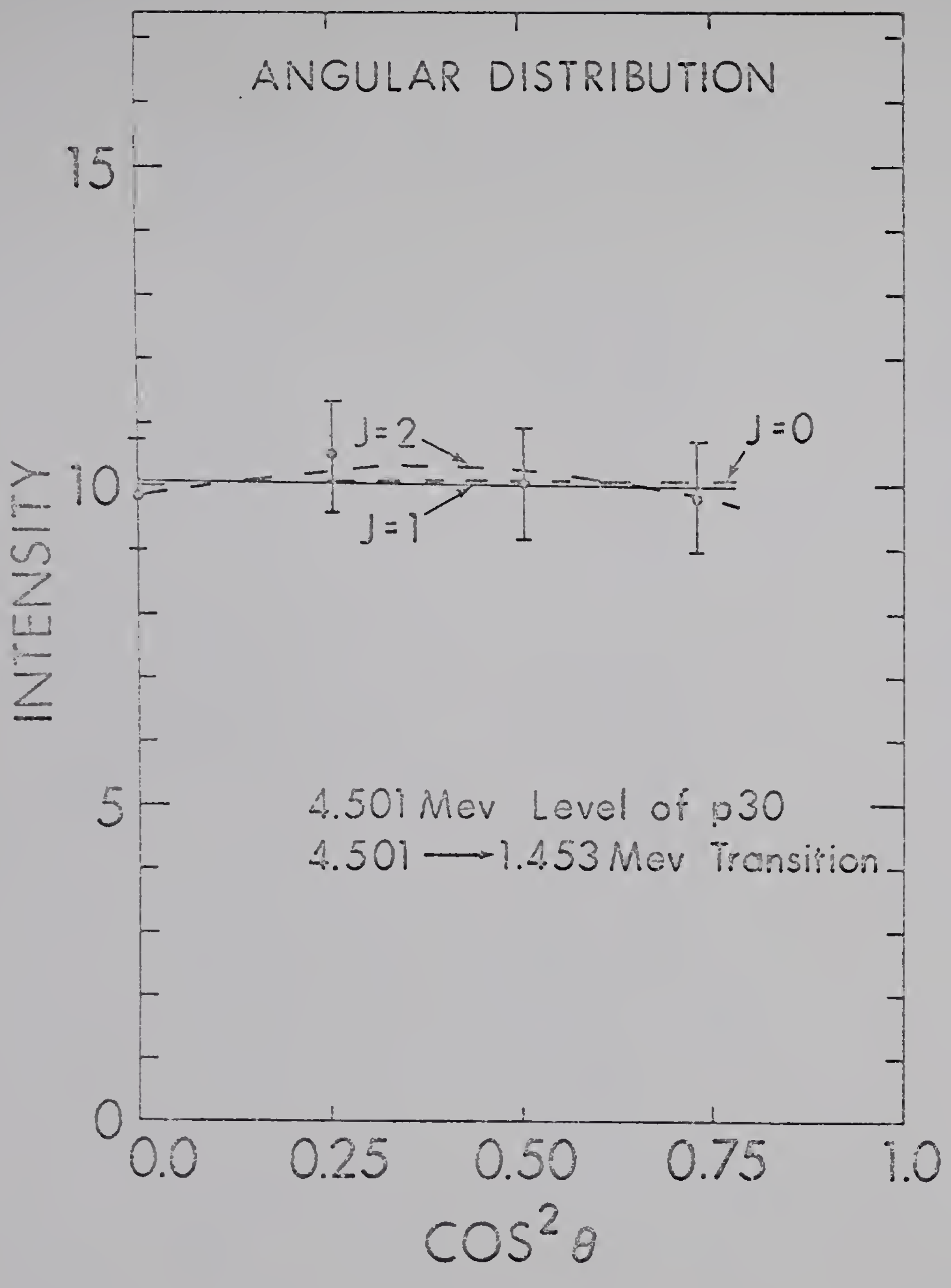
ANGULAR DISTRIBUTION
INTENSITY
15
10
5
0
J=2
J=0
J=1
4.501 Mev Level of p30
4.501 ⟶ 1.453 Mev Transition
0.0
0.25
0.50
0.75
1.0
COS$^2 \theta$

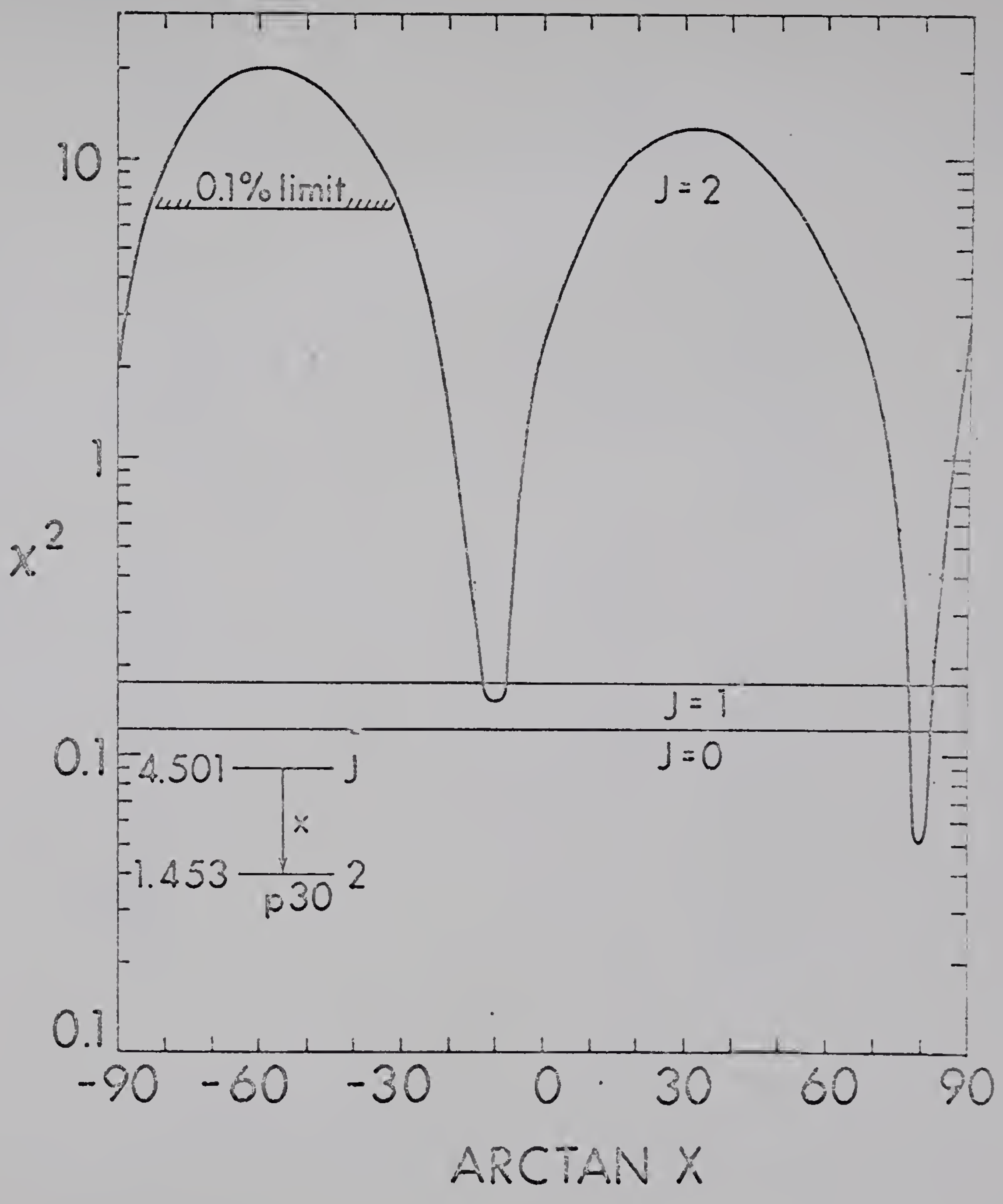
χ^2
10
1
0.1
0.1
0.1% limit
J = 2
J = 1
J = 0
4.501
J
x
1.453
2
p30
-90
-60
-30
0
30
60
90
ARCTAN X

Figure 3-32 Angular Distribution for the 1.45 → 0 MeV Transition Arising from the 4.50 → 1.45 → 0 MeV Cascade.

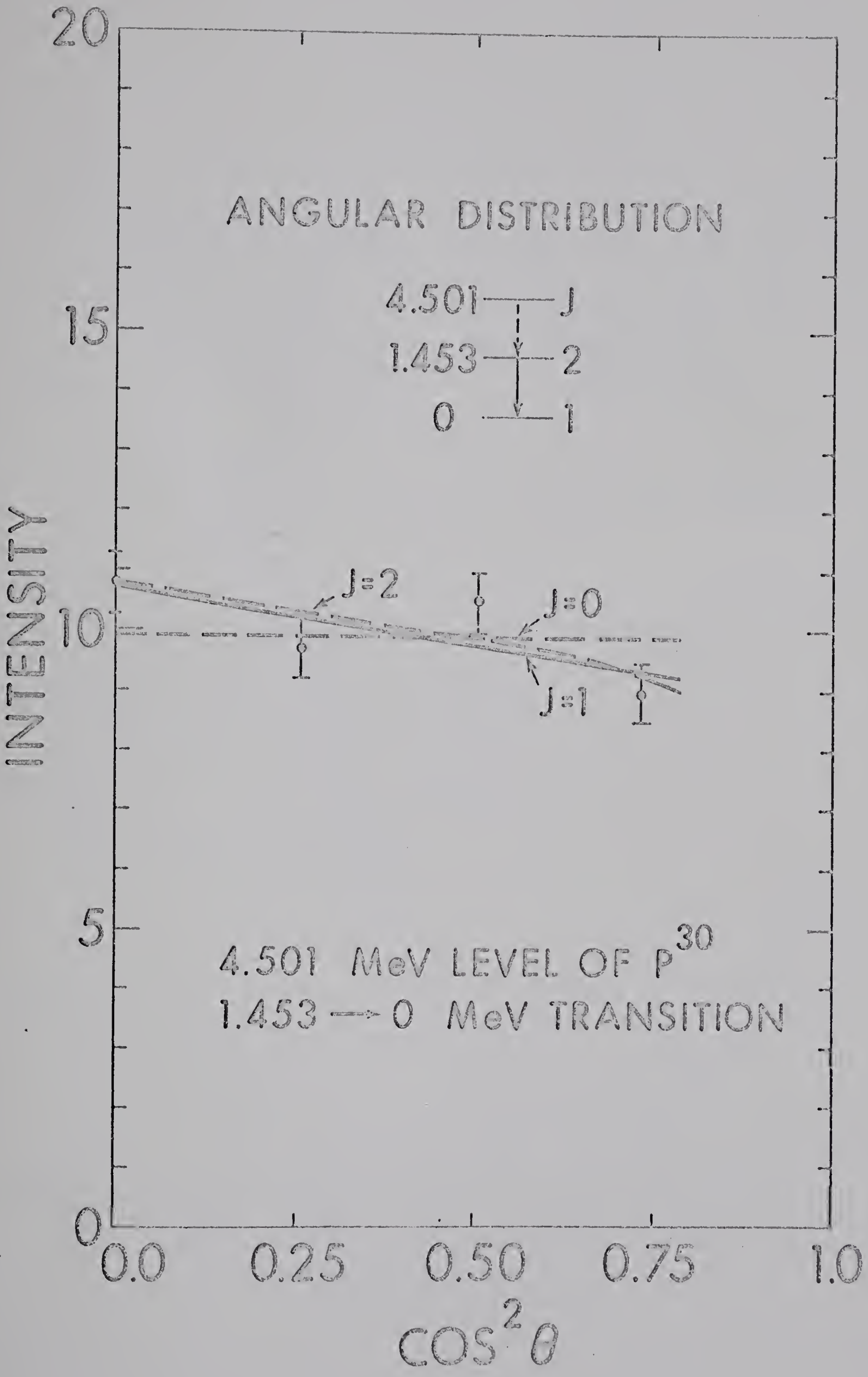
ANGULAR DISTRIBUTION
4.501 — J
1.453 — 2
0 — 1
J=2
J=0
J=1
4.501 MeV LEVEL OF P^{30}
1.453 → 0 MeV TRANSITION
INTENSITY
20
15
10
5
0
0.0
0.25
0.50
0.75
1.0
$\cos^2\theta$

Figure 3-33 Minimum in χ^2-Versus Arc tan x (Mixing Ratio of 4.50 → 1.45 MeV Transition) for 1.45 → 0 MeV Transition that Arises from the 4.50 → 1.45 → 0 MeV Cascade. J(4.50) = 1 is Assumed.

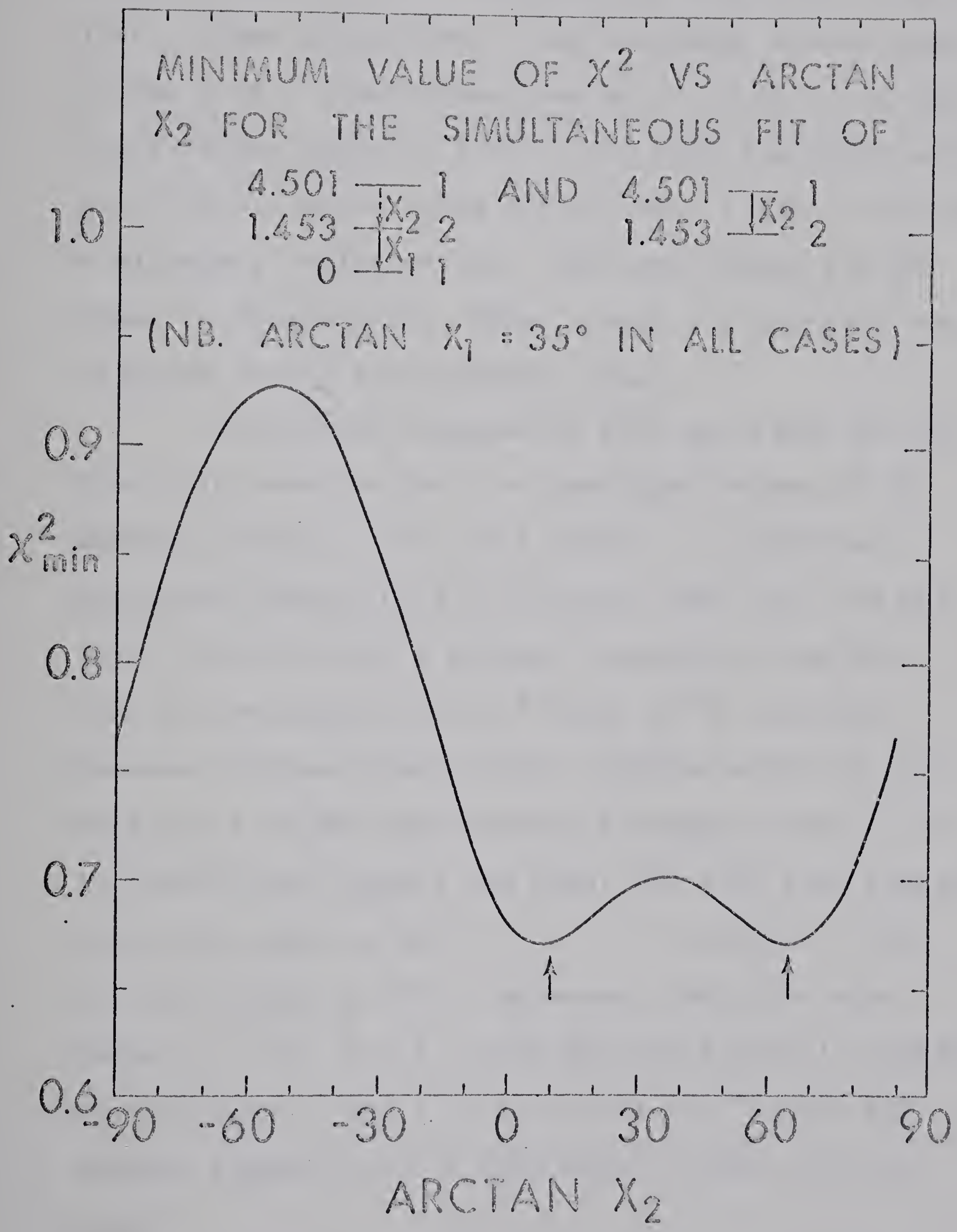
MINIMUM VALUE OF χ^2 VS ARCTAN X_2 FOR THE SIMULTANEOUS FIT OF
4.501 1
1.453 X_2 2
0 X_1 1
AND
4.501 1
1.453 X_2 2
(NB. ARCTAN X_1 = 35° IN ALL CASES)
χ^2_{min}
1.0
0.9
0.8
0.7
0.6
-90
-60
-30
0
30
60
90
ARCTAN X_2

the minimum in χ^2 for J = 1 may range from 0.67 to 0.93. As seen from figure 3-31, for J = 2 the two possible mixing ratio solutions are $x=+(5.7^{+1.44}_{-1.16})$ or $x = -(0.19^{+0.11}_{-0.08})$. Simultaneous fits for both x(4.50 → 1.45) = 5.7 and x(4.50 → 1.45) = -0.19 were made to the 4.50 → 1.45 and 1.45 → 0 MeV transitions. For the known mixing ratio of the 1.45 → 0 MeV transition of x = 0.21 ± 0.03 (Ha 66B)) the fits for x(4.50 → 1.45) = 5.7 gave a minimum value of χ^2 of 4.1 while those for x(4.50 → 1.45) = -0.19 gave a minimum χ^2 value of 3.0. Only the former fit is shown in figure 3-34. Thus, a spin 2 assignment can be rejected at the 1% confidence limit.

It has been proposed by Endt and Paris (En 58) that this level is the T = 1 analogue to one of the doublet levels of ^{30}S, at 3.78 MeV. In addition, Harris and Hyder (Ha 67A) observed that the 4.50 MeV level is excited by a primary transition from the J = 2, 1470 keV resonance in the ^{29}Si(p, γ)^{30}P reaction. Because of these observations together with the fact that the 4.50 MeV level decays strongly to the J = 2, 1.45 MeV level, Harris and Hyder (Ha 67A) have proposed that this state is the T = 1, J = 1 analogue to the 3.77 MeV level of ^{30}Si. Moreover, they have also found a J = 0^+, T = 1, 4.468 MeV level that is probably the analogue to the 3.79 MeV level of ^{30}Si (Ha 67B). Our results support a J = 1 assignment to the 4.50 MeV level.

Figure 3-34 Simultaneous Least-Squares Fit to the 4.50 → 1.45 and 1.45 → 0 MeV Transitions for the 4.50 MeV Level of ^{30}P.

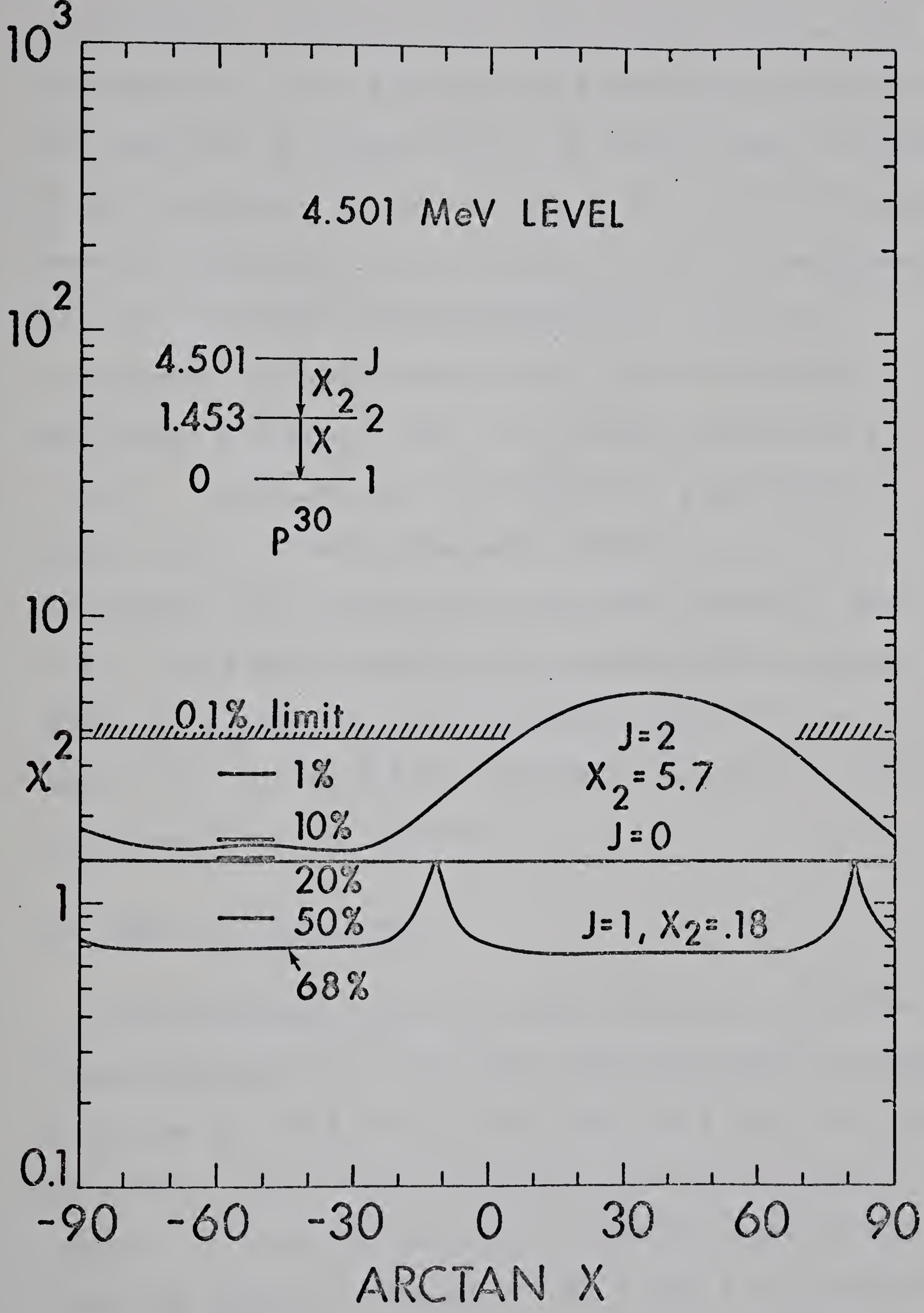

4.501 MeV LEVEL
4.501
1.453
0
J
2
1
X_2
X
P^{30}
0.1% limit
1%
10%
20%
50%
68%
J=2
X_2= 5.7
J=0
J=1, X_2=.18
10^3
10^2
10
1
0.1
X^2
-90
-60
-30
0
30
60
90
ARCTAN X

p. The 4.62 MeV Level

Branching ratios of (59 ± 7)%, (14 ± 6)% and (27 ± 5)% to levels at 1.45, 1.97 and 2.94 MeV were obtained from the spectrum of figure 3-35. As can be seen in figure 3-36, acceptable χ^2 fits to the 4.62 → 1.45 MeV transitions were obtained for J = 1, 2 and 3. A J = 0 assignment is rejected with a 99.7% probability. A $J = 3^-$ assignment has been made to this level by Harris and Hyder (Ha 66B). For J = 3 mixing ratios of x = -(0.04 ± 0.08) and $x = +(5.7^{+8.6}_{-3.0})$ in a probability ratio of 4 : 1 were obtained. Based on a J = 3 assignment the mixing ratio solutions indicate that the 4.62 → 1.45 MeV transition is probably pure dipole. Shown in figure 3-37 is the angular distribution of and χ^2 fit to the 4.62 → 2.94 MeV transition. Table 3-3 summarizes the results.

q. The 4.73 MeV level

The branching ratios for this hitherto unstudied level obtained from the gamma spectrum shown in figure 3-38 are (9 ± 5)%, (15 ± 5)%, (18 ± 5)% and (58 ± 6)% to ground, the 0.7 MeV doublet, 1.45 and 2.94 MeV levels. χ^2 fits to the 4.73 → 2.94 MeV transition shown in figure 3-39 gave J = 1, 2 and 3 as possibilities. Simultaneous least-squares fits to the 4.73 → 2.94 and 2.94 → 0.68 MeV transitions gave possible assignments

Figure 3-35 Gamma-ray Spectrum for the 4.62 MeV Level of ^{30}P.

The points in the simultaneous randoms spectrum are indicated by open circles.

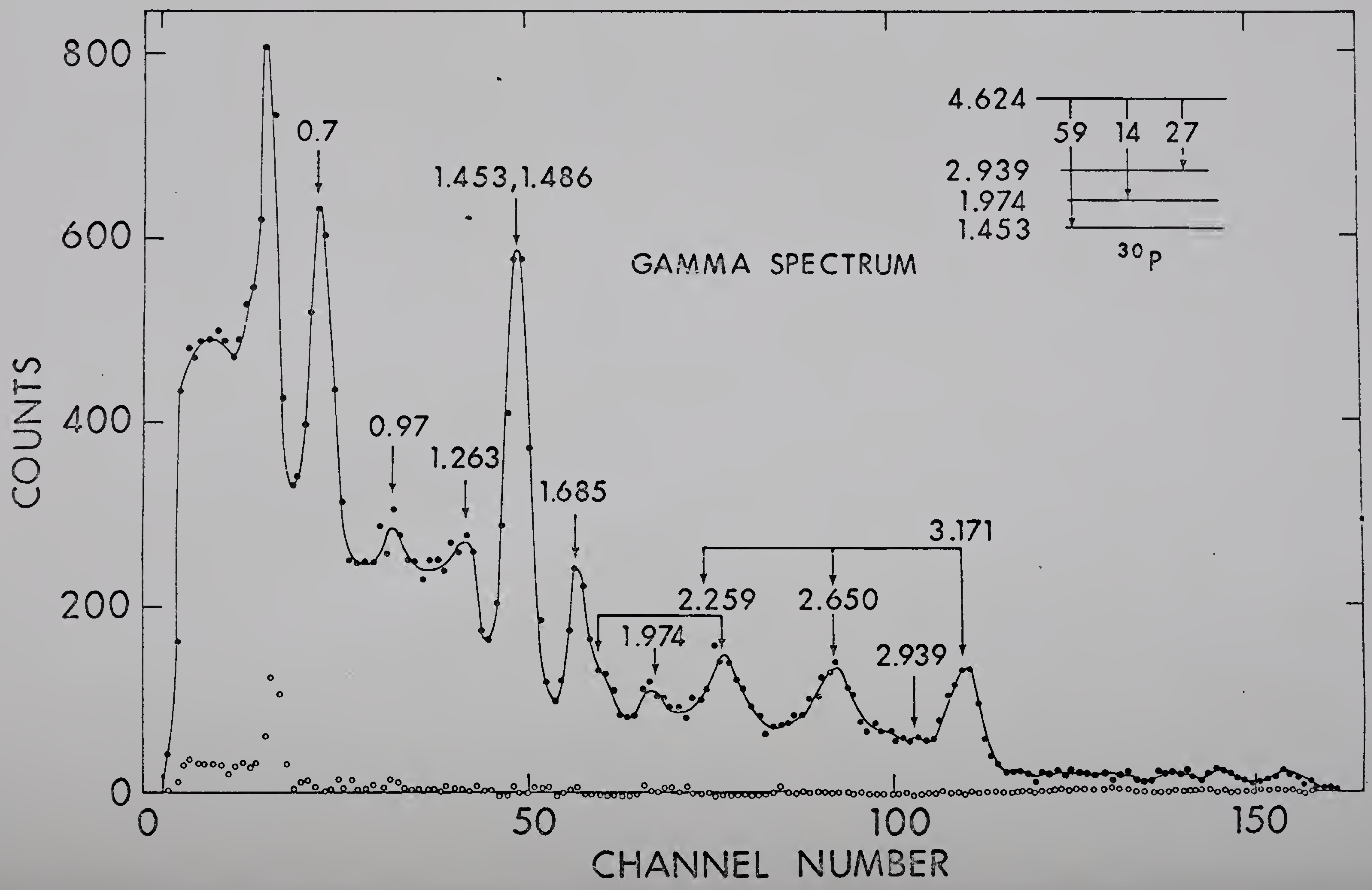
COUNTS
800
600
400
200
0
0
50
100
150
CHANNEL NUMBER
GAMMA SPECTRUM
0.7
0.97
1.263
1.453,1.486
1.685
1.974
2.259
2.650
2.939
3.171
4.624
59
14
27
2.939
1.974
1.453
^{30}P

Figure 3-36 Angular Distribution and χ^2-Versus Arc tan x for the 4.62 → 1.45 MeV Level of ^{30}P.

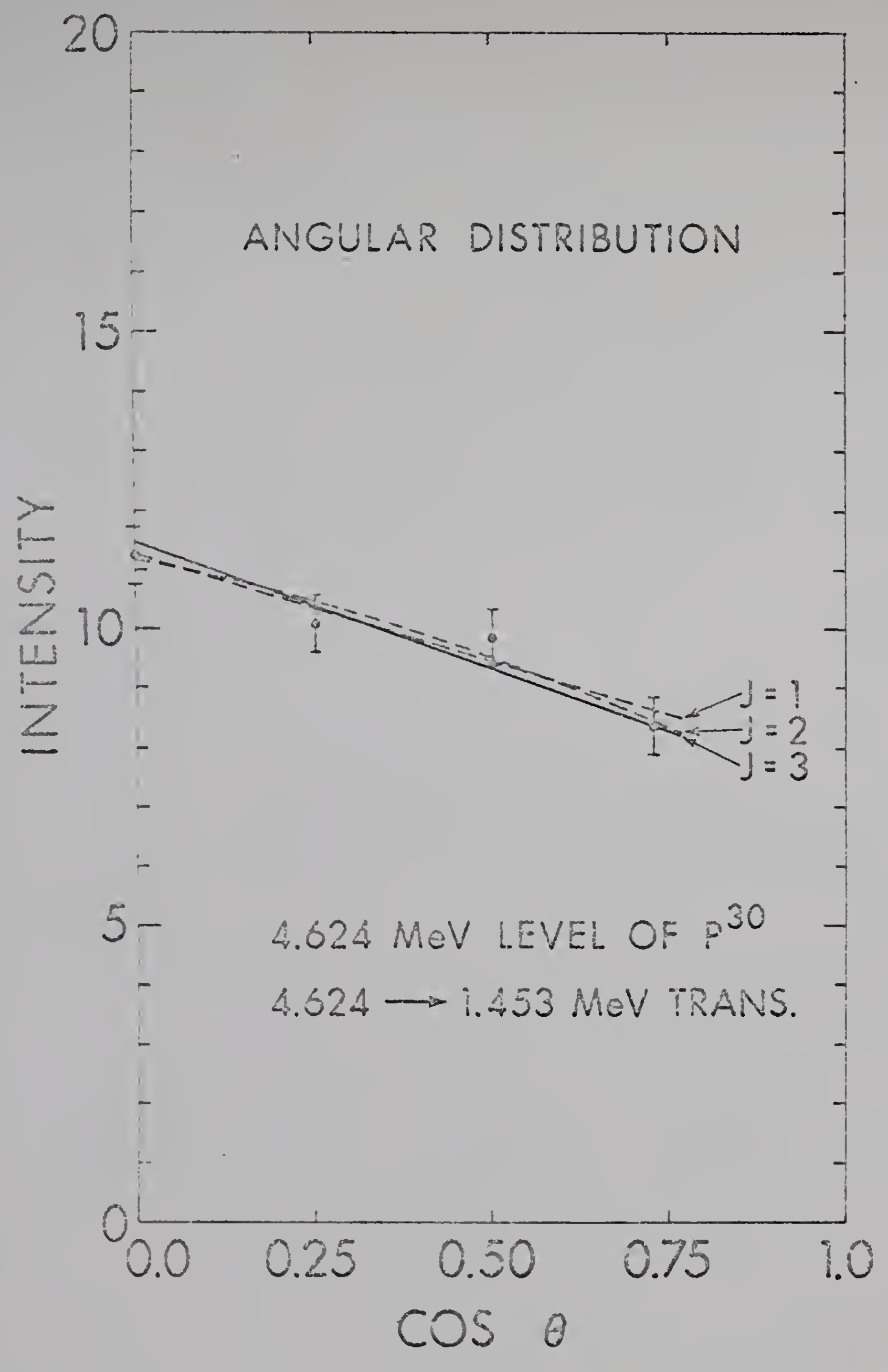
ANGULAR DISTRIBUTION
INTENSITY
20
15
10
5
0
0.0
0.25
0.50
0.75
1.0
COS θ
J = 1
J = 2
J = 3
4.624 MeV LEVEL OF P30
4.624 ⟶ 1.453 MeV TRANS.

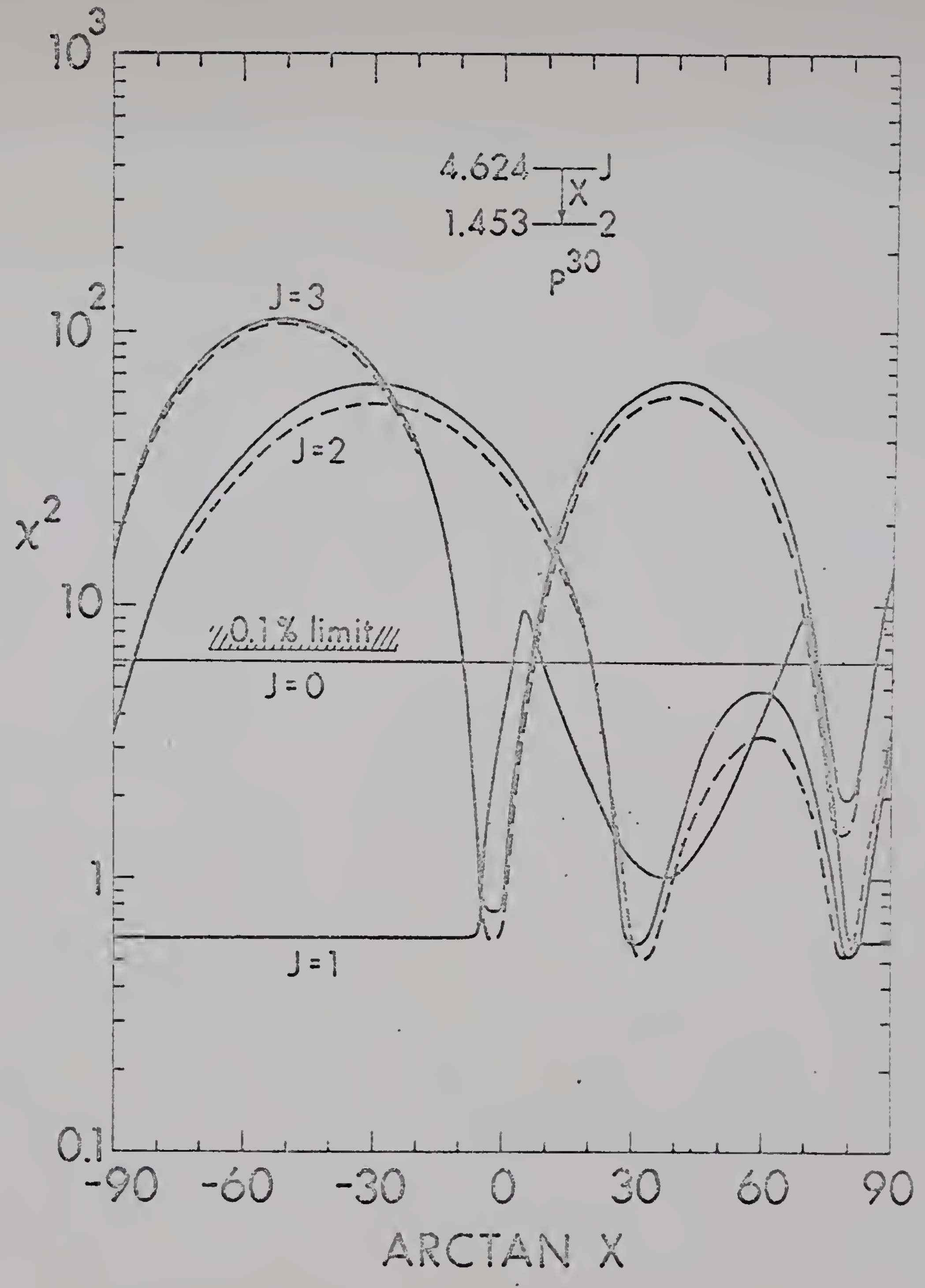
4.624 J
X
1.453 2
P30
J=3
J=2
0.1% limit
J=0
J=1
χ2
10^3
10^2
10
1
0.1
-90
-60
-30
0
30
60
90
ARCTAN X

Figure 3-37 Angular Distribution and χ^2-Versus Arc tan x for the 4.62 → 2.94 MeV Transition.

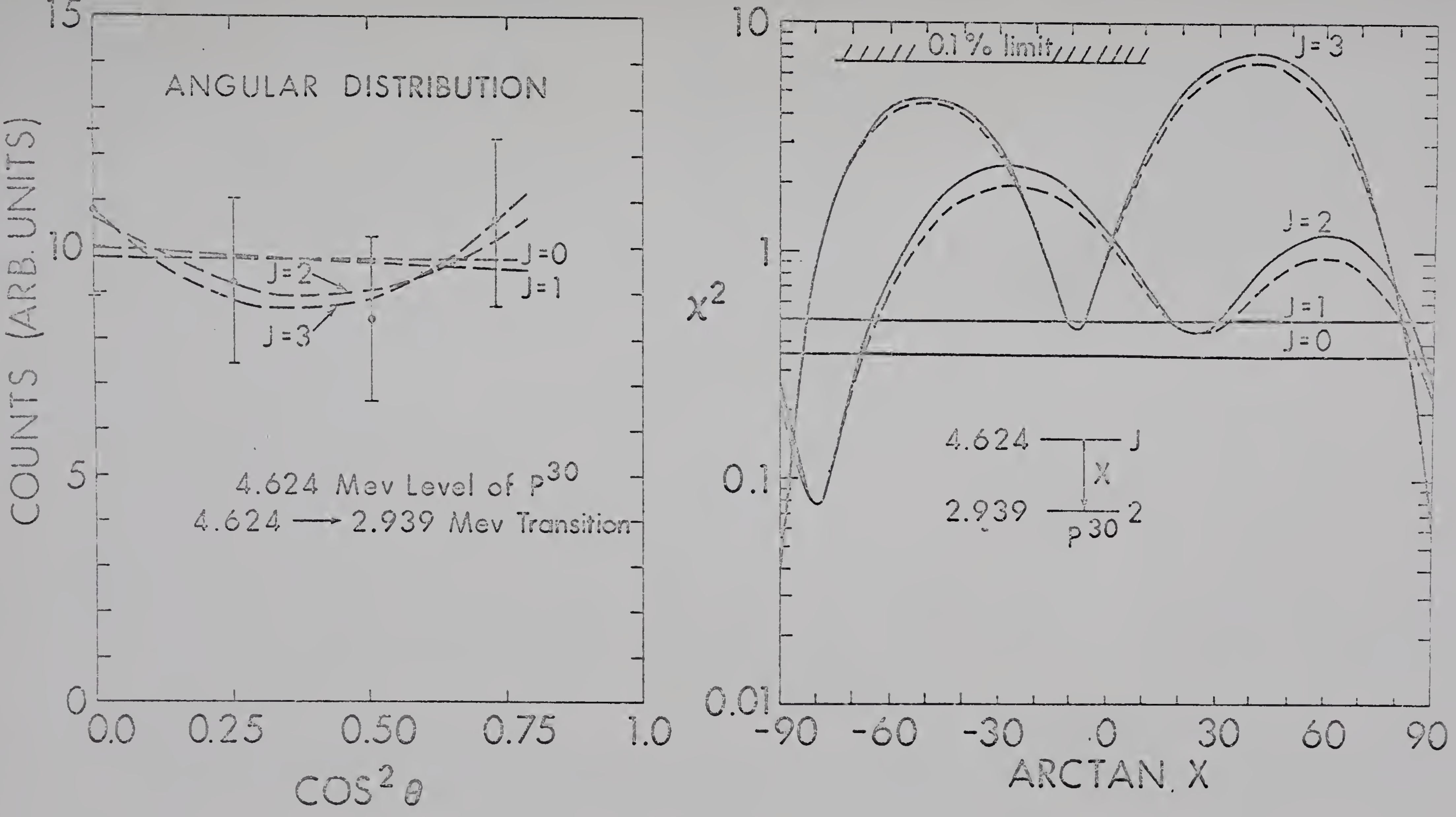
ANGULAR DISTRIBUTION
COUNTS (ARB. UNITS)
15
10
5
0
0.0
0.25
0.50
0.75
1.0
COS² θ
J=0
J=1
J=2
J=3
4.624 Mev Level of P30
4.624 ⟶ 2.939 Mev Transition
10
1
0.1
0.01
χ²
0.1% limit
J=3
J=2
J=1
J=0
4.624
J
X
2.939
P30
2
-90
-60
-30
0
30
60
90
ARCTAN X

Figure 3-38 Gamma-ray Spectrum for the 4.73 MeV Level of ^{30}P.

The points in the simultaneous randoms spectrum are indicated by open circles.

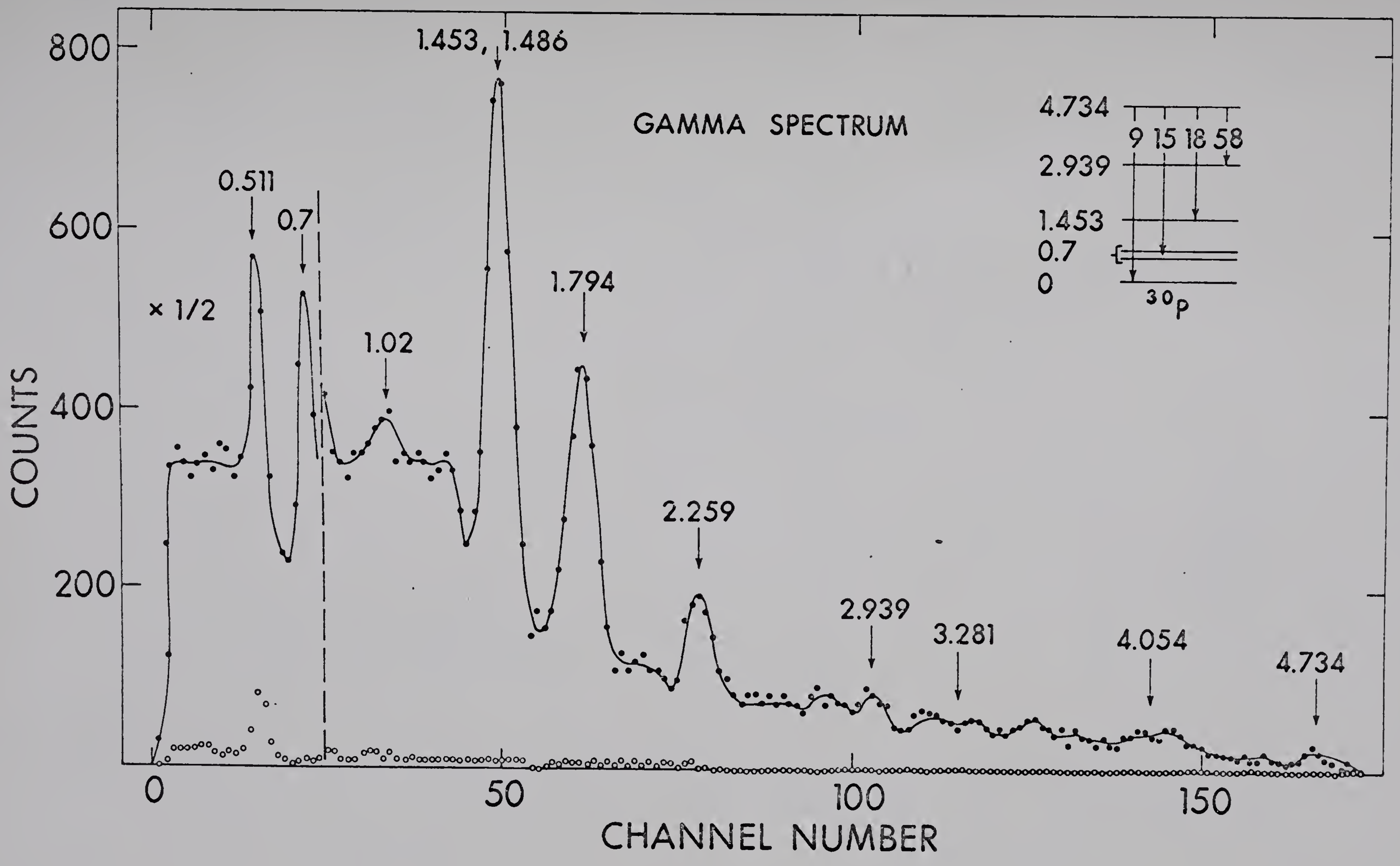
GAMMA SPECTRUM
COUNTS
800
600
400
200
0
50
100
150
CHANNEL NUMBER
× 1/2
0.511
0.7
1.02
1.453, 1.486
1.794
2.259
2.939
3.281
4.054
4.734
4.734
2.939
1.453
0.7
0
9
15
18
58
^{30}P

Figure 3-39 Angular Distribution and χ^2-Versus Arc tan x for the 4.73 → 2.94 MeV Level of ^{30}P.

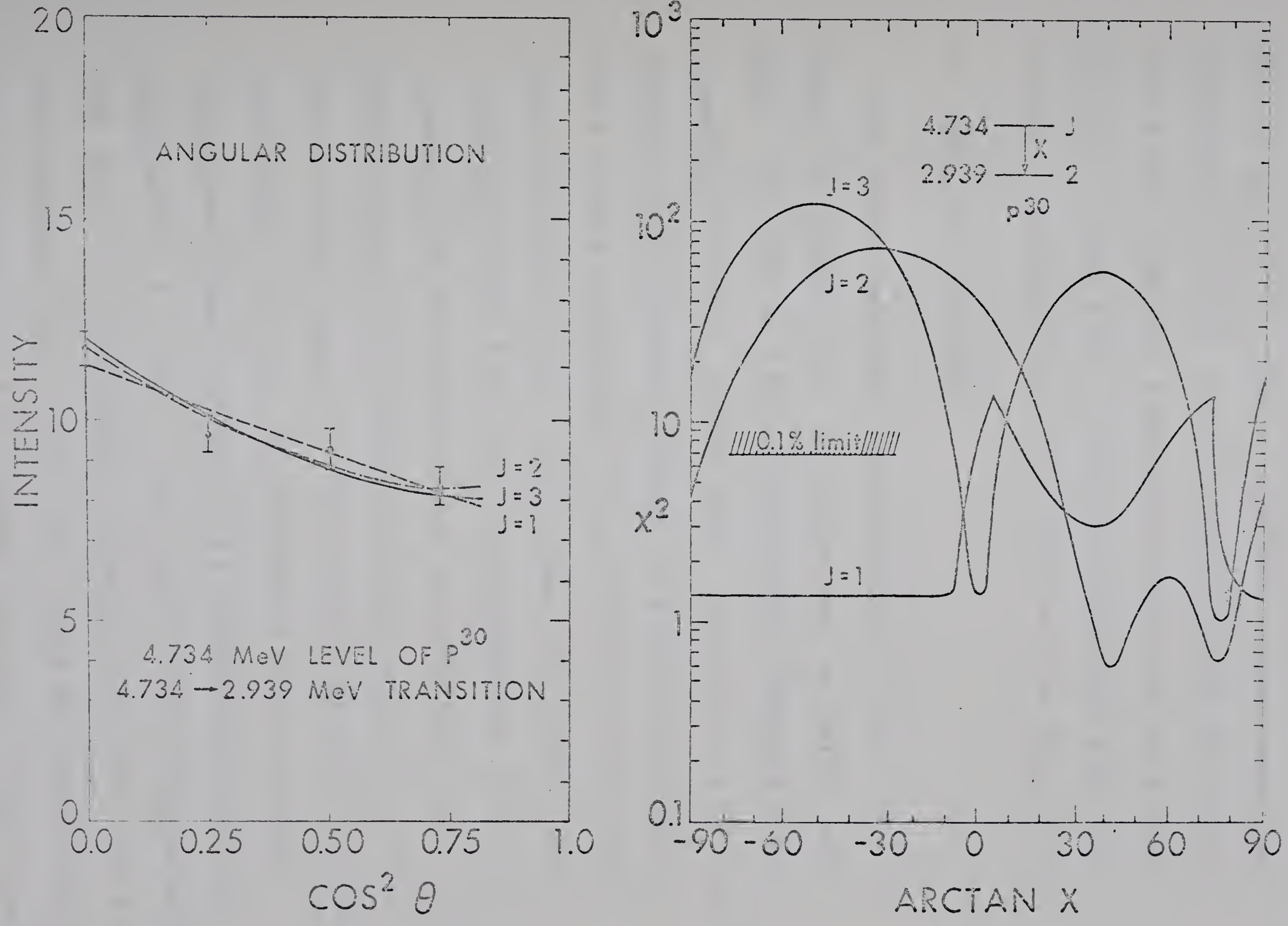
ANGULAR DISTRIBUTION
INTENSITY
20
15
10
5
0
0.0
0.25
0.50
0.75
1.0
COS^2 θ
J = 2
J = 3
J = 1
4.734 MeV LEVEL OF P^{30}
4.734 → 2.939 MeV TRANSITION
10^3
10^2
10
1
0.1
x^2
-90
-60
-30
0
30
60
90
ARCTAN X
4.734 J
X
2.939 2
P^{30}
J = 3
J = 2
J = 1
0.1% limit

of J = 1, 2 and 3 in the probability ratio 2 : 1 : 2 (figure 3-40). Mixing ratio solutions for these possible assignments are given in table 3-3. In the simultaneous fit to the 4.73 → 2.94 → 0.68 MeV cascade only the solution x = (0.02 ± 0.05) obtained from the fit to the 4.73 → 2.94 MeV transition alone was used since the fit to the 2.94 → 0.68 MeV transition from this cascade excluded the other solution (see fig. 3-40b).

r. The 4.92 MeV Level

The gamma spectrum corresponding to this level is shown in figure 3-41. Previous work by Harris and Hyder (Ha 66B, Ha 67A) on this level indicate a 63% branching to the 0.71 MeV level. The results of the present work, however, suggest a strong branching to the 0.68 MeV level rather than to the .71 MeV level. Peak positions of the .7 MeV gamma ray arising from the decay of the 4.92 level as obtained by fits with a gaussian at the eight angles at which data were taken agreed within 0.10 channels with the position of the known 0.68 MeV gamma ray that results from the 3.02 MeV level decay. χ^2 fits to an assumed 4.92 → .71 MeV transition shown in figure 3-43 yielded possible spin assignments of 1 or 2. This result is in disagreement with the J = 3^- assignment of Harris and Hyder (Ha 67A). Least-squares fits to the 4.92 → 0.68 MeV transitions yield a unique J = 1 assignment for the 4.92 MeV level.

Figure 3-40a Simultaneous Least-Squares Fit to the 4.73 → 2.94 and 2.94 → 0.68 MeV Transitions.

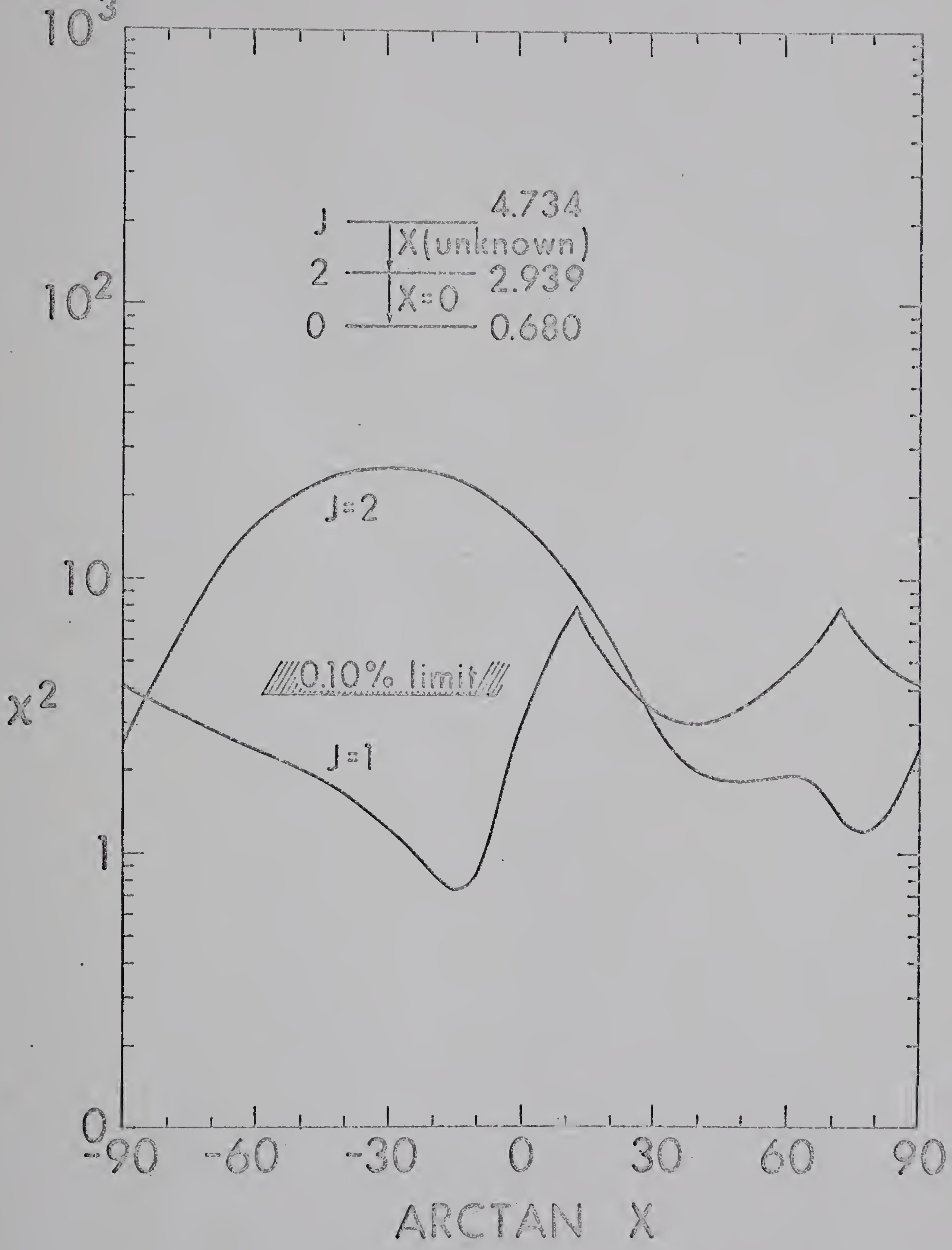

10³
10²
10
1
0
χ²
J
2
0
4.734
X(unknown)
2.939
X=0
0.680
J=2
J=1
0.10% limit
-90
-60
-30
0
30
60
90
ARCTAN X

Figure 3-40b Angular distribution and χ^2-Versus Arc tan x for the 2.94 → 0.68 MeV Transition Arising from the 4.73 → 2.94 → 0.68 Cascade.

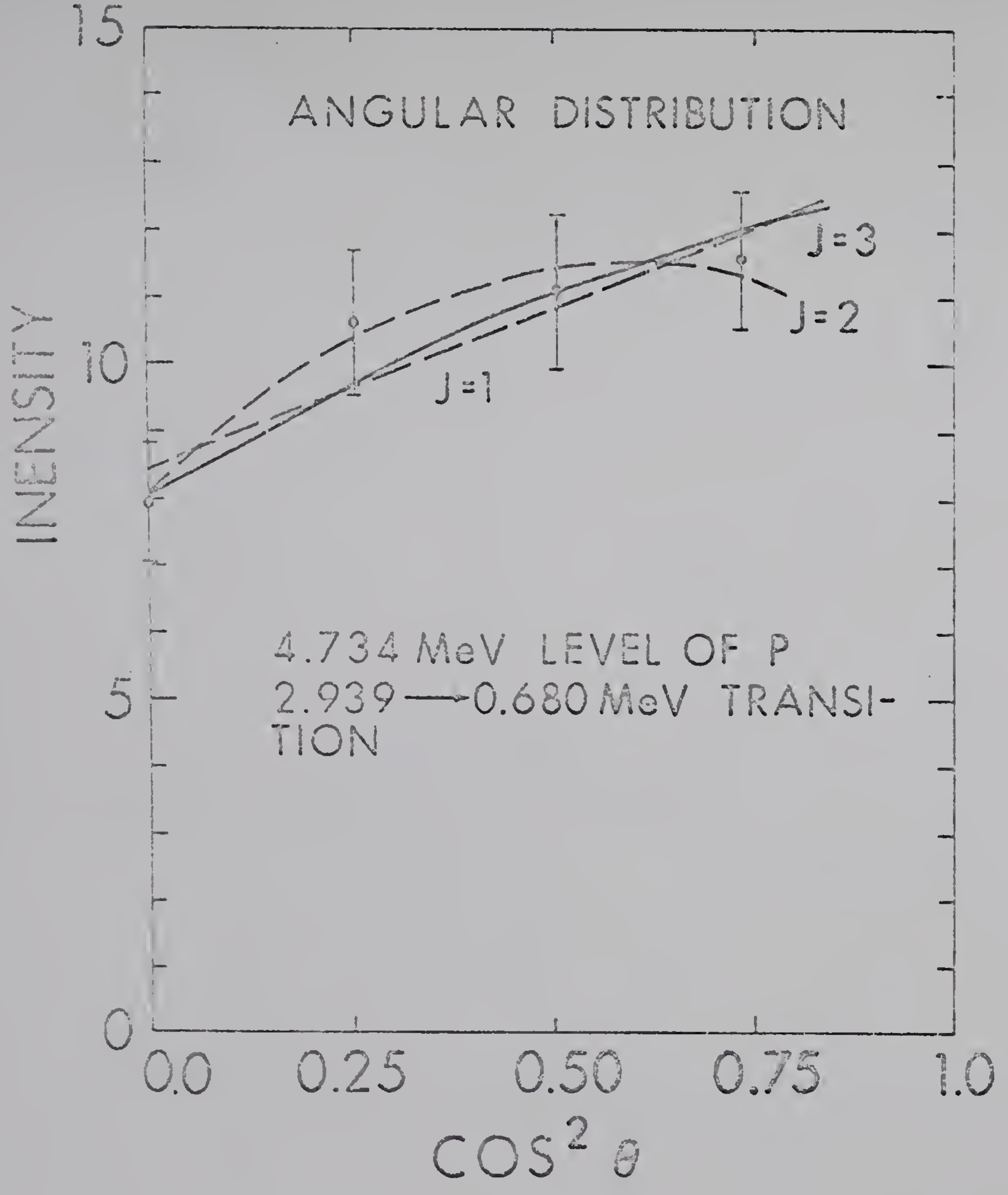
ANGULAR DISTRIBUTION
INENSITY
15
10
5
0
0.0
0.25
0.50
0.75
1.0
COS^2 θ
J=1
J=2
J=3
4.734 MeV LEVEL OF P
2.939 ⟶ 0.680 MeV TRANSI-
TION

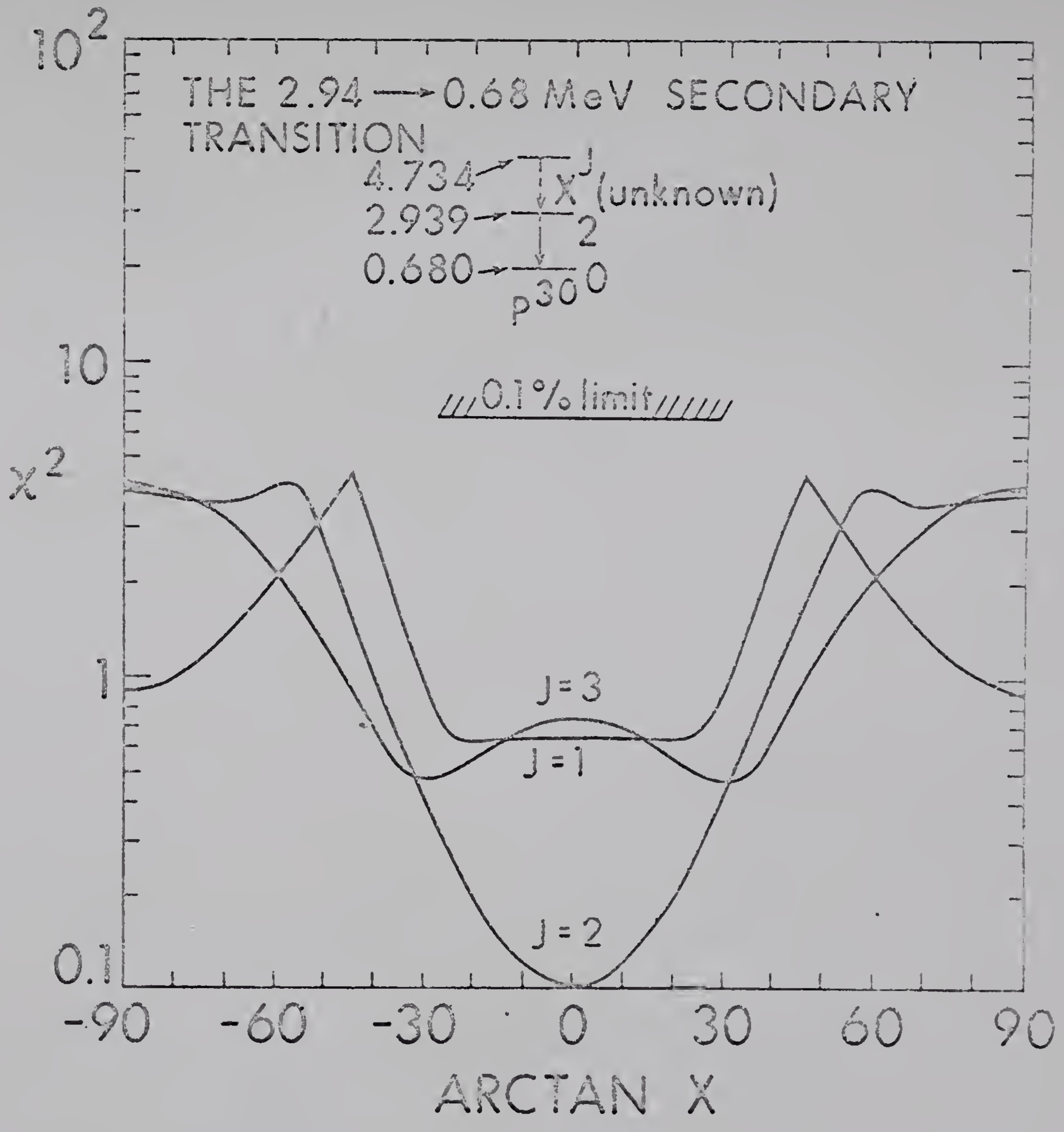
THE 2.94 ⟶ 0.68 MeV SECONDARY
TRANSITION
4.734 → J
X (unknown)
2.939 → 2
0.680 → 0
P^{30}
0.1% limit
10^2
10
1
0.1
χ^2
-90
-60
-30
0
30
60
90
ARCTAN X
J=3
J=1
J=2

Figure 3-41 Gamma-ray Spectrum for the 4.92 MeV Level of ^{30}P.

The points in the simultaneous randoms spectrum are indicated by open circles.

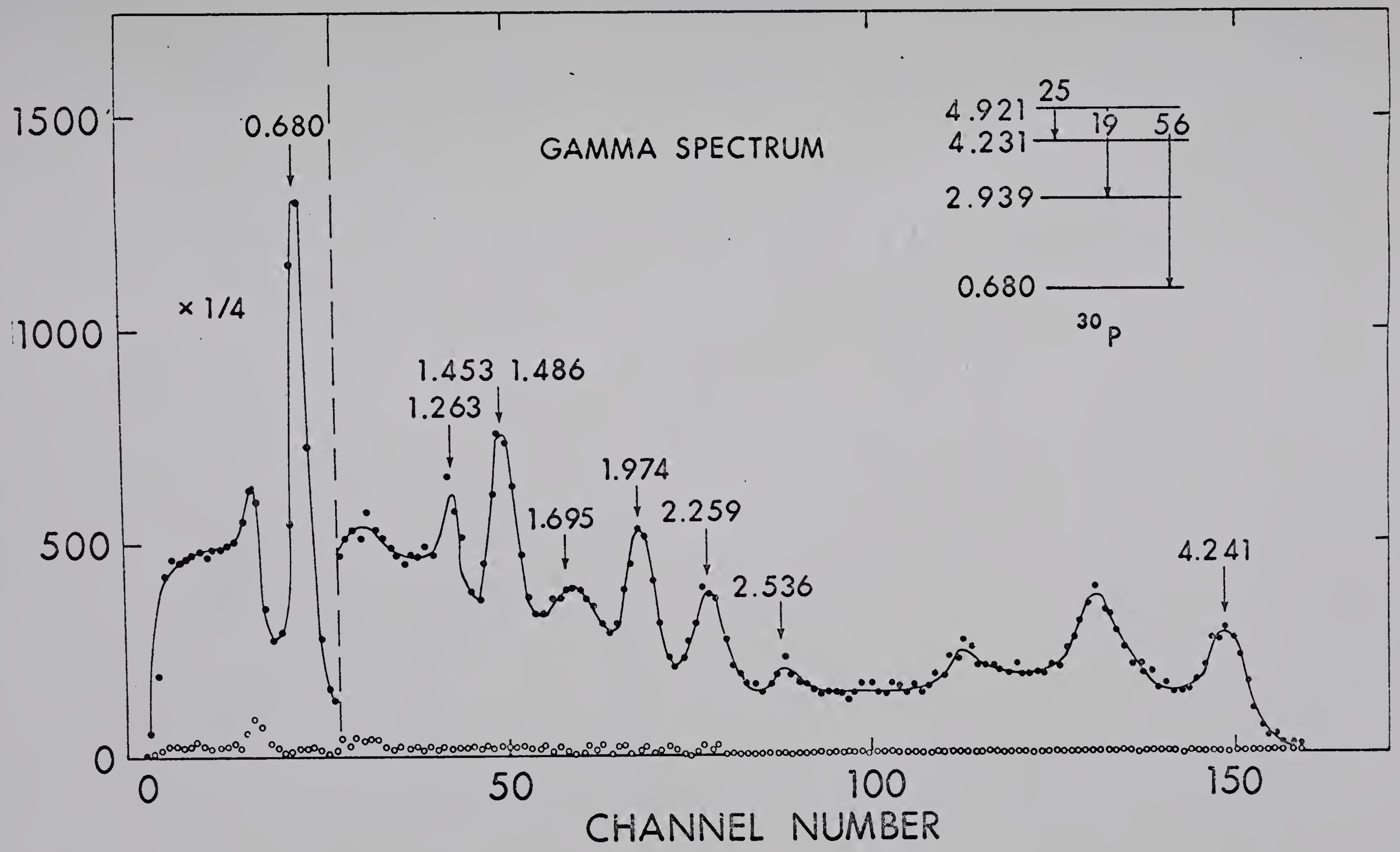

GAMMA SPECTRUM
0.680
× 1/4
1.453 1.486
1.263
1.695
1.974
2.259
2.536
4.241
4.921
4.231
2.939
0.680
25
19
56
^{30}P
1500
1000
500
0
0
50
100
150
CHANNEL NUMBER

Figure 3-42 Angular Distributions of the 4.92 → 0.68 and 4.92 → 2.94 MeV Transitions.

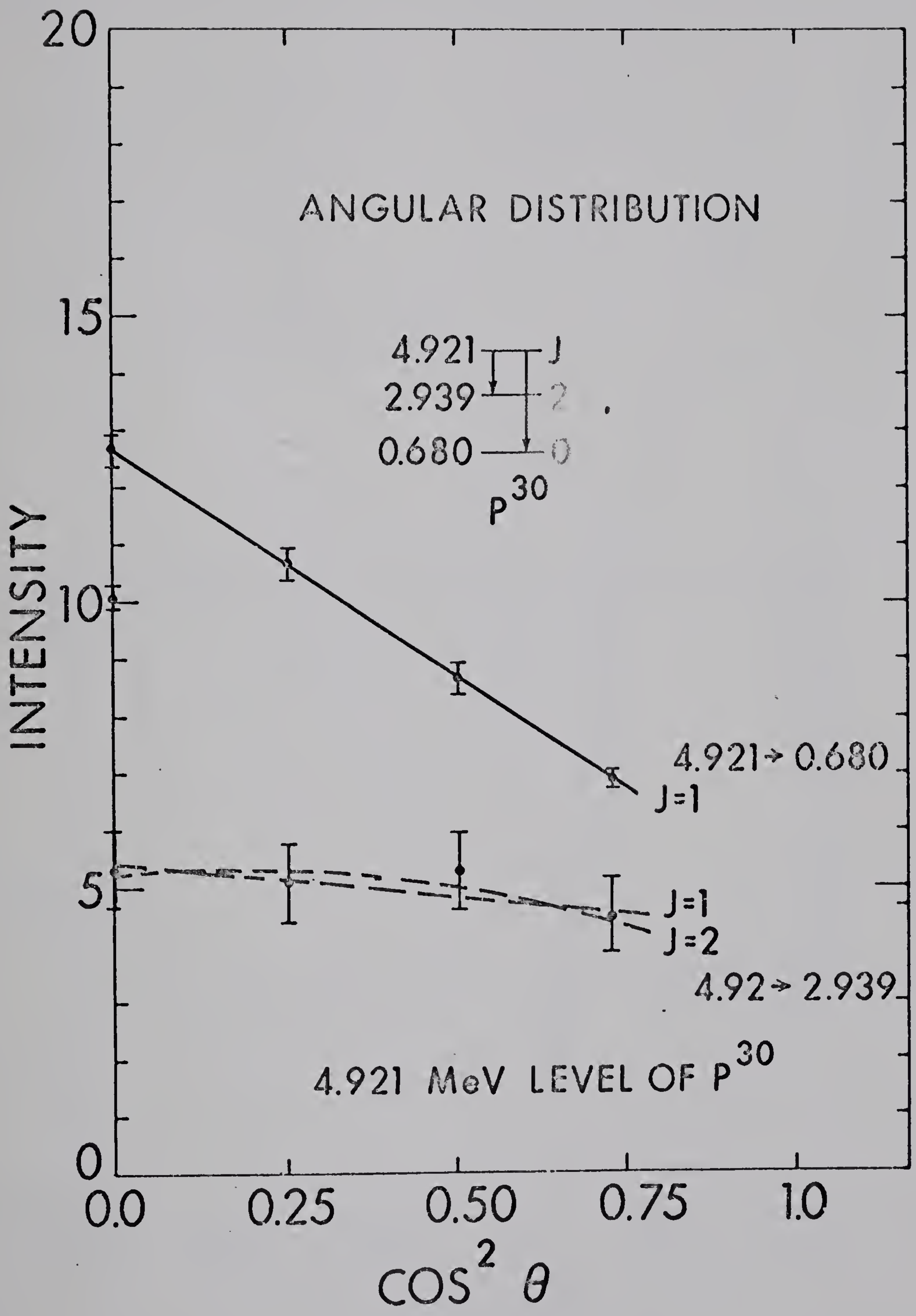
ANGULAR DISTRIBUTION
4.921 J
2.939 2
0.680 0
P^{30}
4.921→0.680
J=1
J=1
J=2
4.92→2.939
4.921 MeV LEVEL OF P^{30}
INTENSITY
0
5
10
15
20
0.0
0.25
0.50
0.75
1.0
$\cos^2\theta$

Figure 3-43 Least-Squares Fit to an Assumed 4.92 → 0.71 MeV Transition for the 4.92 MeV Level of ^{30}P.

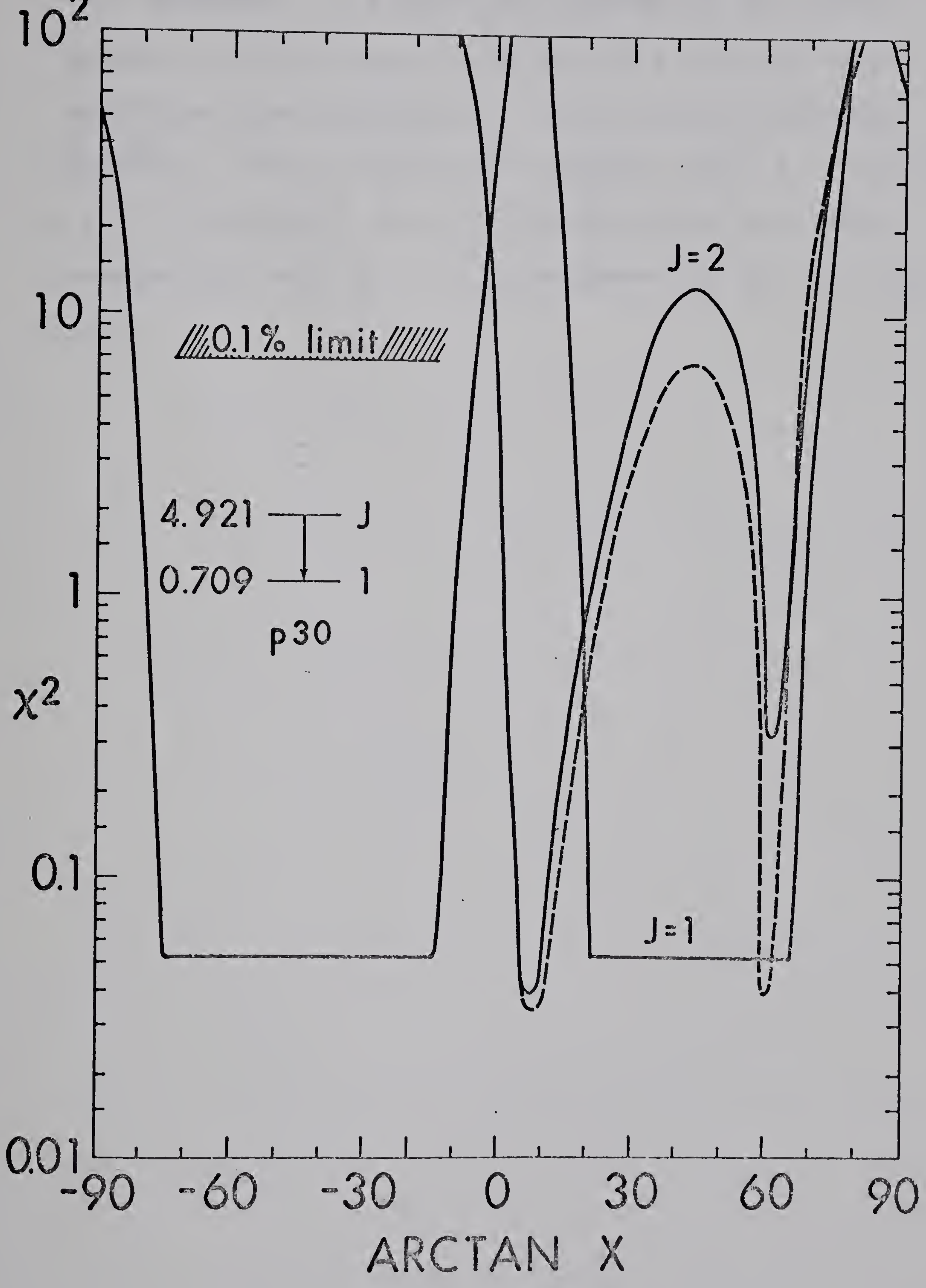

10^2
10
1
0.1
0.01
χ^2
-90
-60
-30
0
30
60
90
ARCTAN X
0.1% limit
4.921 — J
0.709 — 1
p^{30}
J=2
J=1

Branching ratios of (56 ± 7)%, (19 ± 3)% and (25 ± 4)% to the 0.68, 2.94 and 4.23 MeV levels, respectively, were obtained. A surprising feature of the decay scheme is the strong branch to the 4.231 MeV level which has been assigned $J = 4^-$ by Harris and Hyder (Ha 66B). Such a transition requires $|M|^2 > 7 \times 10^3$ for a $J = 1$ assignment to the 4.92 MeV which is clearly incompatible with a $J = 4^-$ assignment to the 4.23 MeV level.

CHAPTER IV MODEL CALCULATIONS

Model calculations by Glaudemans et al. (Gl 64) have led to predicted energies and configurations for a number of energy levels of nuclei in the mass region between ^{29}Si and ^{40}Ca. Their method involved treating 15 matrix elements for the two-particle potentials together with binding energies to the ^{28}Si core of a nucleon in the $2s_{\frac{1}{2}}$ and $1d_{\frac{3}{2}}$ shells as unknown parameters. Of these known levels the states of ^{30}P used were the 0.68, 0.71, 2.54, 2.72 and 2.94 MeV levels. In the present work, the phase consistent formalism of Rose and Brink (Ro 67) was used to calculate mixing ratios and transition probabilities of some of the states of ^{30}P predicted by Glaudemans et al. An outline of the pertinent formalism together with tabulations of intermediate steps are given in Appendix II. These calculations require the radial part of the single-particle wave functions. Since the method of Glaudemans et al. did not require an explicit form for these wave functions it was necessary to assume them. For simplicity harmonic oscillator wave functions of the following form were chosen.

$$U_{n\ell}(r) = N_{n\ell} \exp\left(-\frac{1}{2}\frac{r^2}{b^2}\right) r^{\ell} L_{n\ell}(r)$$

The quantity $N_{n\ell}$ is a normalization factor, $L_{n\ell}$ is an associated Laguerre polynomial and b is an unknown parameter. The value of b was taken from the work of Arima (Ar 58) as 1.826 fermis. More specifically, the normalized U's for the $2s_{\frac{1}{2}}$ and $1d_{\frac{3}{2}}$ shells are

$$U_{2s}(r) = \frac{2}{3}\,\pi^{-\frac{1}{4}}\,b^{-\frac{3}{2}}\left(3 - 2\frac{r^2}{b^2}\right)\exp\left(-\frac{1}{2}\,\frac{r^2}{b^2}\right)$$

$$U_{1d}(r) = \frac{16}{15}\,\pi^{-\frac{1}{4}}\,b^{-\frac{3}{2}}\,\frac{r^2}{b^2}\,\exp\left(-\frac{1}{2}\,\frac{r^2}{b^2}\right)$$

A summary of calculated multipole mixing ratios, branching ratios and lifetimes is presented in figure 4-1 together with experimental data obtained in the present work. It is seen that experimental lifetimes of the 0.68 and 0.71 MeV levels and branching ratios of all states considered except the 2.94 MeV level agree reasonably well with the calculated values. In those cases of agreement with experiment, values calculated using wave functions from Glaudemans' shell model are approximately the same as the values predicted by the Weisskopf single-particle estimates. A factor of 100 was used to decrease the single-particle estimate for the ΔT = 0 transition from the 0.71 MeV level to the ground state because of isospin selection rules. Branching ratio calculations for the 2.94 MeV level

Figure 4-1 A Comparison of Experimental and Calculated Multipole Mixing Ratios, Branching Ratios and Lifetimes for 5 Low Lying States of ^{30}P.

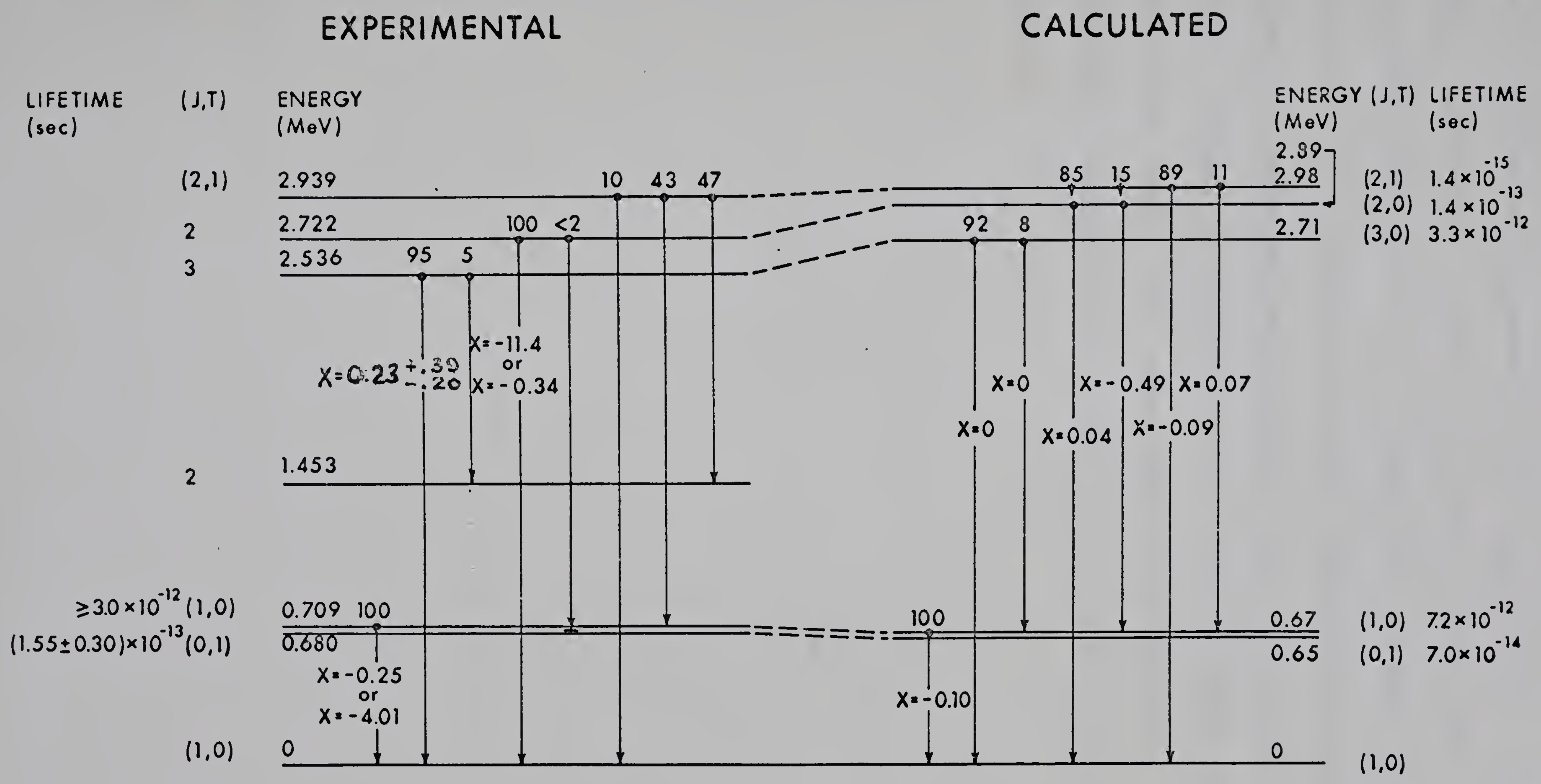
EXPERIMENTAL
CALCULATED
LIFETIME (sec)
(J,T)
ENERGY (MeV)
(2,1) 2.939
2 2.722
3 2.536
2 1.453
≥3.0×10^-12 (1,0) 0.709
(1.55±0.30)×10^-13 (0,1) 0.680
(1,0) 0
95 5
100 <2
10 43 47
100
X=0.23 +.39 -.20
X=-11.4 or X=-0.34
X=-0.25 or X=-4.01
ENERGY (MeV) (J,T) LIFETIME (sec)
2.89
2.98 (2,1) 1.4×10^-15
(2,0) 1.4×10^-13
2.71 (3,0) 3.3×10^-12
0.67 (1,0) 7.2×10^-12
0.65 (0,1) 7.0×10^-14
0 (1,0)
85 15 89 11
92 8
100
X=0
X=0
X=0.04
X=-0.49
X=-0.09
X=0.07
X=-0.10

^{30}P

are in marked disagreement with experiment. The only mixing ratio that agrees reasonably well with experiment are those for the 0.71 → 0 and 2.54 → 0 MeV transitions. For the 2.72 → 0 MeV transition there is a significant difference between experimental and calculated mixing ratios. Thus, it appears that a shell model which assumes an inert ^{28}Si core does not adequately describe radiative properties of the [illegible] 2.72 or 2.94 MeV levels of ^{30}P.

CHAPTER V CONCLUSION

The following spin possibilities have been obtained for 5 previously unassigned excitated states of ^{30}P:

Energy (MeV)	J
2.839	2,3,(1)
3.736	1,(2,3)
3.836	1,2,3
3.928	1,2,3
4.734	1,2,3

In addition, confirmation or consistency with previous spin assignments to states at 1.453, 1.974, 2.536, 2.722, 3.020, 4.142, 4.501, and 4.634 MeV excitation energy has resulted. However, both the spin assignment to and branching ratios for the 4.921 MeV level are in serious disagreement with the work of Harris and Hyder (Ha 67A). Moreover, the 25% branch to the 4.231 MeV level indicated by our results rules out the possibility of a $J=4^-$ assignment to the 4.231 MeV level (the assignment made to the 4.231 MeV level by Harris and Hyder) if our assignment to the 4.921 MeV level is correct. The branching ratios from the present work for the 2.839, 3.736, 3.836, 3.928, and 4.501 MeV levels are also in disagreement with those of previous investigators (Mo 63, Ha 67A). The branching ratios for the remaining states investigated showed general agreement with previous results.

A test of the shell model of Gaudemans' et al. (Gl 64) in predicting radiative properties of the 0.680, 0.709, 2.536, 2.722, and 2.939 MeV levels showed it to be inadequate for describing the 2.722, and 2.939 Mev levels. It appears that a model which includes core effects is required.

REFERENCES

Ar 58 A. Arima, Progress of Theoretical Physics, 19 (1958) 421.

Ba 62 E. E. Baart, L. L. Green and J. C. Willmott, Proc. Phys. Soc. 79 (1962) 237.

Bd 58 C. Broude, L. L. Green and J. C. Willmott, Proc. Phys. Soc. 72 (1958) 1122.

Bd 67 C. Broude, P. J. M. Smulders and T. K. Alexander, Nucl. Phys. A90 (1967) 321.

Bo 67 M. C. Bouten, J. P. Elliot and J. A. Pullen, Nucl. Phys A97 (1967) 113.

Br 57 D. A. Bromley, H. E. Gove and A. E. Litherland, Can.J. Phys. 35 (1957) 1057.

Ej 64 H. Ejire, Y. Nakjima, K. Horie, S. Matsumoto, and Y. Nogami, Nucl. Phys. 51 (1964) 470.

En 58 P. M. Endt and C. H. Paris, Phys. Rev. 110 (1958) 89.

En 62 P. M. Endt and C. Van der Leun, Nucl. Phys. 34 (1962)1.

Gl 64 P. W. M. Glaudemans, G. Weichers and P. J. Brussard, Nucl. Phys. 56 (1964) 529; P. W. M. Glaudemans, G. Weichers and P. J. Brussard, Nucl. Phys. 56 (1964) 548.

Go 56 H. E. Gove, G. A. Bartholomew, E. B. Paul and A. E. Litherland, Nucl. phys. 2 (1956) 132; A. E. Litherland, H. McManus, E. B. Paul,

D. A. Bromley and H. E. Gove, Can. J. Phys. 36 (1958) 378.

Ha 66A G. I. Harris, A. K. Hyder, Jr., and L. W. Seagondollar, Bull. Am. Phys. Soc. 11 (1966) 65.

Ha 66B G. I. Harris and A. K. Hyder, Jr., Phys. Letters 22(1966) 159.

Ha 67A G. I. Harris and A. K. Hyder, Jr., Phys. Rev. 157 (1967) 958.

Ke 67 E. F. Kennedy, D. H. Youngblood, and A. E. Blaugrund, Phys. Rev. 158 (1967) 897.

Li 58 Litherland, M^{c}Manus, Paul, Bromley and Gove, Canad. J. Phys. 36 (1958) 378.

Li 61 A. E. Litherland and A. J. Ferguson, Can. J. Phys. 39 (1961) 788.

Mo 63 R. A. Moore, Thesis, University of Kansas, 1963 (unpublished).

Mp 54 G. Morpurgo, Nuovo Cimento 12 (1954) 60.

Mp 58 G. Morpurgo, Phys. Rev. 110 (1958) 721.

Ph 65 P. A. Phelps, E. A. Milne, and H. E. Handler, Phys. Rev. 138 (1965) B1088.

Pi 66 J. Picard and A. G. De Pinho, Nuovo Cimento 41B (1966) 239.

Po 65 A. R. Poletti and E. K. Warburton, Phys. Rev. 137 (1965) B595.

Pu 67 N. G. Puttaswamy, D. S. Gemmell, L. Meyer-

Schutzmeister and H. Ohnuma, Bull. Am. Phys. Soc. 12 (1967) 665.

Ra 52 L. A. Radicati, Phys. Rev. 87 (1952) 521.

Ro 67 H. J. Rose and D. M. Brink, Rev. Mod. Phys. 39 (1967) 306.

Si 59 J. J. Singh, Phys. Rev. 115 (1959) 445.

Sm 64 P. J. M. Smulders, Phys. Letters 9 (1964) 155.

Th 60 V. K. Thankappan and S. P. Pandya, Nucl. Phys. 19 (1960) 303.

Th 62 V. K. Thankappan and S. P. Pandya, Nucl. Phys. 39 (1962) 394.

Va 58 C. Van der Leun and P. M. Endt, Phys. Rev. 110 (1958) 96.

Ve 67A C. W. Vermette, D. A. Hutcheon, D. H. Sykes and W. C. Olsen, Bull. Am. Phys. Soc. 12 (1967) 571.

Ve 67B C. W. Vermette, D. A. Hutcheon, D. H. Sykes and W. C. Olsen, Phys. Rev. (in press).

Wa 58 E. K. Warburton, Phys. Rev. Letters 1 (1958) 68.

Yu 62 Yu. P. Antuf'ev, A. K. Vel'ter, A. N. L'vow, E. G. Koponets and S. P. Tsytko, Zh. Eksperim. i. Teor. Fiz. 42 (1962) 386; Soviet Phys. - JETP 15 (1962) 268.

APPENDIX I

LEAST-SQUARES ANALYSIS

The following is a development of the least-squares method of analysis used in the present work.

Equation 1-1 can be restated as

$$W(\theta) = \sum_{\substack{k\alpha \\ k \text{ even}}} \sum_{n=0}^{2} U(k,n,\alpha) \frac{x^n}{1+x^2} P(\alpha) P_k(\cos\theta) \qquad \text{(A1-1)}$$

where

$$U(k,0,\alpha) = \rho_k(a\alpha) F_k(\mathrm{LLab}) Q_k$$

$$U(k,1,\alpha) = -2\rho_k(a\alpha) F_k(\mathrm{LL{+}1ab}) Q_k \qquad \text{(A1-2)}$$

$$U(k,2,\alpha) = \rho_k(a\alpha) F_k(\mathrm{L{+}1L{+}1ab}) Q_k .$$

The quantity x is the mixing ratio, $P(\alpha)$ is the population parameter of the magnetic substate α and P_k is the Legendre polynomial of order k. The angular distribution at each angle θ_i in matrix form is given by

$$\begin{pmatrix} W(\theta_1) \\ W(\theta_2) \\ \vdots \\ W(\theta_N) \end{pmatrix} = \overbrace{\begin{pmatrix} 1 & P_2(\cos\theta_1) & P_4(\cos\theta_1)\dots \\ 1 & P_2(\cos\theta_2) & P_4(\cos\theta_2)\dots \\ \vdots & \vdots & \vdots \\ 1 & P_2(\cos\theta_N) & P_4(\cos\theta_N)\dots \end{pmatrix} \begin{pmatrix} \sum\limits_n U(0,n,1)\frac{x^n}{1+x^2} & \dots & \sum\limits_n U(0,n,c)\frac{x^n}{1+x^2} \\ \vdots & & \\ \sum\limits_n U(4,n,1)\frac{x^n}{1+x^2} & \dots & \sum\limits_n U(4,n,c)\frac{x^n}{1+x^2} \\ & & \vdots \end{pmatrix}}^{\Lambda}$$

$$\times \overbrace{\begin{pmatrix} P(\alpha_1) \\ P(\alpha_2) \\ \vdots \\ P(\alpha_c) \end{pmatrix}}^{X} \tag{A1-3}$$

or in more compact notation by

$$W = \Lambda X$$

If Y is a column vector of measured values, then (Y - W) is a column vector of residues. In matrix notation, therefore, the function χ^2 (equation 1-14) can be written as

$$\chi^2 = (Y - W)^T \, \omega(Y - W) \tag{A1-4}$$

Here Z^T denotes the transpose of Z and ω is the matrix of weighting values which in the present case is diagonal with elements given by

$$\omega(I,I) = \frac{1}{E^2(\theta_I)} \tag{A1-5}$$

The quantity $E^2(\theta_I)$ is the uncertainty in the number of

counts at angle θ_I. Expanding equation (A1-4) gives

$$\chi^2 = Y^T\omega Y - Y^T\omega W - W^T\omega Y + W^T\omega W$$

Substituting equation (A1-3) in the above yields

$$\chi^2 = Y^T\omega Y - Y^T\omega AX - X^TA^T\omega Y + X^TA^T\omega AX$$

The set of equations defined by $\frac{\partial\chi^2}{\partial P(\alpha)} = 0$ can be shown to give

$$2[A^T\omega AX - A^T\omega Y] = 0$$

or

$$X = (A^T\omega A)^{-1}A^T\omega Y \qquad \text{(A1-6)}$$

Defining the normal matrix, N, as

$$N = A^T\omega A \qquad \text{(A1-7)}$$

gives

$$X = N^{-1}A^T\omega Y \qquad \text{(A1-6)}$$

It is a general result of statistics that the variance-covariance matrix of the fitted parameters is the inverse of the normal matrix. Thus the standard deviation of the i^{th} element of X is given by

$$\sigma_i = (N^{-1})_{ii} \qquad \text{(A1-8)}$$

which in this case is the uncertainty in the population parameters $P(\alpha_i)$. After solving for X one can compute

W for a given value of the mixing ratio, x, from equation A1-3 and, hence, compute the value of χ^2.

In simultaneously fitting two transitions both of which arise from a given level decay one replaces A1-3 by the matrix equation

$$(W_1 + W_2) = (A_1 + A_2)X \qquad \text{(A1-9)}$$

where the subscripts 1 and 2 denote transitions 1 and 2 respectively. This formulation is possible since the unknown population parameters (contained in X) are the same for both transitions. Extension to three or more transitions involves replacing both W and A of A1-3 by the sum of the component W's and A's corresponding to each transition. The additional requirement(s) of having to fit two or more distributions will generally result in fewer possible values for the population parameters and, hence, more restricted mixing ratio solutions together with better discrimination between possible spin values.

APPENDIX II

CALCULATION OF REDUCED MATRIX ELEMENTS FOR TRANSITIONS BETWEEN TWO-PARTICLE STATES

Formulas from the Rose and Brink phase consistent formalism for calculating multipole mixing ratios, branching ratios and lifetimes for transitions between two-particle states are given in the following presentation. These formulas are followed by a tabulation of intermediate steps in the calculations for two-particle states in the $2s_{1/2}$ and $1d_{3/2}$ shells. The symbols are the same as those used by Rose and Brink (Ro 67).

The essential problem in predicting radiative properties of transitions between two-particle states involves calculating reduced matrix elements of the form

$$<\ell_1 \ \tfrac{1}{2} \ j_1 || T_L^{<\pi>} || \ell_2 \ \tfrac{1}{2} \ j_2>$$

The ket $|\ell \ \tfrac{1}{2} \ j>$ is the wave function for a spin-$\tfrac{1}{2}$ particle with spin-orbit coupling in a central field (i.e. $\vec{\ell} + \vec{\tfrac{1}{2}} = \vec{j}$) and denotes the type of interaction (i.e. electric or magnetic). The $T_{LM}^{<\pi>}$ are one-particle operators defined by

$$T_{LM}^{e} = \alpha_L^{e} \ (Q_{LM} + Q'_{LM}) \qquad \text{(A2-1)}$$

$$T_{LM}^{m} = \alpha_L^{m} \ (M_{LM} + M'_{LM}) \qquad \text{(A2-1')}$$

The multipole expansion coefficients, $\alpha_L^{<\pi>}$ are listed up to L = 3 in Table A2-1.

TABLE A2-1 Multipole Expansion Coefficients

L	α_L^e	α_L^m
1	ik	k
2	$-k^2/2\sqrt{3}$	$ik^2/2\sqrt{3}$
3	$-ik^3\sqrt{2}/15\sqrt{3}$	$-k^3\sqrt{2}/15\sqrt{3}$

For convenience Rose and Brink have replaced the operator Q_{LM} by $(Q_{LM})_{eff}$ $(=eg_\ell r^L C_{LM})$. Here e denotes electronic charge, r is magnitude of the vector $\vec{r}$ which describes the particle's position, g_ℓ is zero for a neutron and 1 for a proton, C_{LM} is related to spherical harmonics, Y_{LM}, by

$$C_{LM} = \frac{4\pi}{(2L+1)^{\frac{1}{2}}} Y_{LM}$$

For a transition from a single-particle state $|\lambda>$ to another single-particle state $|\mu>$ by emission of a gamma ray (i.e. $E_\lambda > E_\mu$) the matrix element of Q_{LM} is given by

$$<\lambda|Q_{LM}|\mu> = 2g_\ell\left(\frac{m\beta}{\hbar^2 k}\right)(E_\lambda - E_\mu)<\lambda|r^L C_{LM}|\mu>$$

and that for $(Q_{LM})_{eff}$ is given by

$$<\lambda|(Q_{LM})_{eff}|\mu> = eg_{\ell}<\lambda|r^{L}C_{LM}|\mu>.$$

The quantity m denotes the mass of a nucleon β is the nuclear magneton and k is the photon wave number. Since the photon wave number is given by

$$k = \frac{E_{\lambda} - E_{\mu}}{\hbar c},$$

in this case

$$<\lambda|Q_{LM}|\mu> = <\lambda|(Q_{LM})_{eff}|\mu>$$

However, when the single-particle energies E_{λ} and E_{μ} are such that $E_{\lambda} < E_{\mu}$, one must change the sign of $<\lambda|(Q_{LM})_{eff}|\mu>$.

The single-particle reduced matrix elements corresponding to the operators $(Q_{LM})_{eff}$, Q'_{LM}, M_{LM} and M'_{LM} are given by

$$<\ell_1 \tfrac{1}{2} j_1||(Q_L)_{eff}||\ell_2 \tfrac{1}{2} j_2> = eg_{\ell}I(L)b_{12} \quad (A2-2)$$

$$<\ell_1 \tfrac{1}{2} j_1||Q'_L||\ell_2 \tfrac{1}{2} j_2> = \tfrac{1}{2} g_s\beta kI(L)(a_1-a_2)\frac{b_{12}}{L+1} \quad (A2-2')$$

$$<\ell_1 \tfrac{1}{2} j_1||M_L||\ell_2 \tfrac{1}{2} j_2> = 2\beta g_{\ell} i^{\ell_1-\ell_2}(-)^{j_1+\frac{1}{2}}I(L-1)(\ell_1\ell_2 01|L1)$$
$$\times W(j_1\ell_1j_2\ell_2;\tfrac{1}{2} L)[(2j_2+1)(2\ell_1+1)(2\ell_2+1)\ell_2(\ell_2+1)L]^{\frac{1}{2}}$$
$$\times [(2L+1)(L+1)]^{-\frac{1}{2}} \quad (A2-2'')$$

$$<\ell_1 \tfrac{1}{2} j_1||M_L'||\ell_2 \tfrac{1}{2} j_2> = \tfrac{1}{2} g_s \beta I(L-1)(L-a_1-a_2)b_{12} \qquad \text{(A2-2''')}$$

where I(L) is the radial integral

$$I(L) = \int U_1(r) r^{L+2} U_2(r) dr \qquad \text{(A2-3)}$$

and

$$b_{12} = i^{\ell_1-\ell_2}(-)^{j_1-\frac{1}{2}}(2j_2+1)^{\frac{1}{2}}(2L+1)^{-\frac{1}{2}}(j_1 j_2 \tfrac{1}{2} -\tfrac{1}{2}|L0) \qquad \text{(A2-4)}$$

$$a_1 = (\ell_1 - j_1)(2j_1 + 1) \qquad \text{(A2-5)}$$

The quantity g_s is 5.585 or -3.826 for a proton or neutron, respectively.

Clebsch-Gordan and Racah coupling coefficients are denoted by $(j_1 j_2\ \ell_1 \ell_2|j_3 \ell_3)$ and $W(j_1 j_2\ \ell_2 \ell_1;j_3 \ell_3)$, respectively. To conserve parity $L+\ell_1+\ell_2$ must be even for electric operators and odd for magnetic ones. The U 's are radial components of the single-particle wave functions. A tabulation of I(L) values for harmonic oscillator wave functions is given in Table A2-2.

Reduced matrix elements for transitions between two-particle states can be expressed in terms of those for one-particle states by the expression

$$<j_a j_b\ JT||T_L(1)+T_L(2)||j_c j_d J'T'> = (-)^{L+j_c-j_b}(2J'+1)^{\frac{1}{2}}$$

$$\times \tfrac{1}{2}\{[1+\delta(j_a j_b)]][1+\delta(j_c j_d)]\}^{-\frac{1}{2}}$$

TABLE A2-2 Summary of I(L) Values for Harmonic Oscillator Wave Functions as a Function of the Parameter b.

States	L = 1	L = 2	L = 3
$2s_{\frac{1}{2}}$, $2s_{\frac{1}{2}}$	$\frac{3}{\sqrt{\pi}}\ b$	$\frac{7}{2}\ b^2$	$\frac{14}{\sqrt{\pi}}\ b^3$
$2s_{\frac{1}{2}}$, $1d_{\frac{3}{2}}$	$-\sqrt{\frac{32}{\pi}}\ b$	$-\sqrt{10}\ b^2$	$-4\sqrt{\frac{10}{\pi}}\ b^3$
$1d_{\frac{3}{2}}$, $1d_{\frac{3}{2}}$	$\frac{16}{5\sqrt{\pi}}\ b$	$\frac{7}{2}\ b^2$	$\frac{64}{5\sqrt{\pi}}\ b^3$

$$\times\ \{\delta(j_b j_d)(-)^{J}(2j_a+1)^{\frac{1}{2}}W(j_a j_c JJ';Lj_b)M(j_a j_c)$$

$$+\ \delta(j_a j_c)(-)^{J'+T+T'}(2j_b+1)^{\frac{1}{2}}W(j_b j_a JJ';Lj_a)M(j_b j_d)$$

$$+\ \delta(j_a j_d)(-)^{T+1}(2j_b+1)^{\frac{1}{2}}W(j\ \ j\ \ JJ';Lj_a)M(j_b j_c)$$

$$+\ \delta(j_b j_c)(-)^{J+J'+T'+1}(2j_a+1)^{\frac{1}{2}}W(j_a j_d JJ';Lj_b)M(j_a j_d)\}] \tag{A2-6}$$

where

$$M(j_a j_c) = [<j_a||T_L(1)||j_c> + (-)^{T+T'}<j_a||T_L(2)||j_c>] \tag{A2-7}$$

The symbol T denotes isospin and J is such that $\vec{J} = \vec{j}_a + \vec{j}_b$. It is arbitrary in the case of a neutron-proton two body problem whether nucleon "1" is the proton and "2" the neutron or vice versa.

From two-particle reduced matrix elements calculated in the above way one can determine reduced matrix elements for different two-particle configurations. The predicted configurations are obtained from model calculations. Using the latter reduced matrix matrix elements one can calculate both the sign and the magnitude of multipole mixing ratios from the definition

$$\delta_L^{<\pi>} = \frac{<J_1||T_L^{<\pi>}||J_2>/(2L+1)^{\frac{1}{2}}}{<J_1||T_{\bar{L}}^{<\bar{\pi}>}||J_2>/(2\bar{L}+1)^{\frac{1}{2}}} \tag{A2-8}$$

The symbols $\bar{L}$ and $\bar{\pi}$ denote the lowest-order multipolarity occurring in the transitions $J_1 \rightarrow J_2$. One can also calculate the speeds for given transitions and lifetimes of nuclear states. The transition speed, τ_i^L, for a given type of radiation (i.e. electric or magnetic) with multipolarity L is given by

$$\frac{1}{\tau_i^L} = \frac{4k}{\hbar} \left|\langle J_1 || T_L^{\langle\pi\rangle} || J_2 \rangle\right|^2 / (2L+1) \qquad \text{(A2-9)}$$

The total transition speed τ_i for a given transition with a mixing ratio δ is

$$\frac{1}{\tau_i} = (1 + \delta^2)\frac{1}{\tau_i^L} \qquad \text{(A2-10)}$$

where L refers to the lowest multipole component. Finally, the lifetime of a nuclear state "a" is given by the sum

$$\frac{1}{\tau} = \sum_i \frac{1}{\tau_i} \qquad \text{(A2-11)}$$

where i refers to all transitions that go from state "a" to lower lying states. Branching ratios are obtained from the ratios $\frac{\tau}{\tau_i}$.

A summary of values for the various matrix elements of equations (A2-2) (as applied to the $2s_{1/2}$ and $1d_{3/2}$

shells) is given in Table A2-3. On this tabulation the integral I(L) between states f and h is denoted by $(I(L))_{fh}$. The sign of the $2s_{1/2} \rightarrow 1d_{3/2}$ matrix element of $(Q_2)_{eff}$ has been changed since $E_{2s_{1/2}} < E_{1d_{3/2}}$. Next a summary of two-particle matrix elements for both M1 and E2 multipoles for T + T' even is given in Table A2-4. A summary of calculated configurations for five states of ^{30}P as obtained by Glaudemans _et_ _al_. (Gl 6) is given in Table A2-5.

TABLE A2-3a Proton Single-Particle Matrix Elements

$<\ell_1 \tfrac{1}{2} j_1 || (Q_L)_{eff} || \ell_2 \tfrac{1}{2} j_2>$

Initial State	Final State	L = 1	L = 2	L = 3
$2s_{\frac{1}{2}}$	$2s_{\frac{1}{2}}$	0	0	0
$2s_{\frac{1}{2}}$	$1d_{\frac{3}{2}}$	0	$0.633\ e(I(2))_{sd}$	0
$1d_{\frac{3}{2}}$	$2s_{\frac{1}{2}}$	0	$0.447\ e(I(2))_{sd}$	0
$1d_{\frac{3}{2}}$	$1d_{\frac{3}{2}}$	0	$-0.447\ e(I(2))_{dd}$	0

TABLE A2-3b Single Particle Matrix Elements

$<\ell_1 \tfrac{1}{2} j_1 || Q'_L || \ell_2 \tfrac{1}{2} j_2>$

Particle	Initial State	Final State	L = 1	L = 2	L = 3
Proton	$2s_{\frac{1}{2}}$	$2s_{\frac{1}{2}}$	0	0	0
	$2s_{\frac{1}{2}}$	$1d_{\frac{3}{2}}$	0	$1.766\beta k(I(2))_{sd}$	0
	$1d_{\frac{3}{2}}$	$2s_{\frac{1}{2}}$	0	$1.249\beta k(I(2))_{sd}$	0
	$1d_{\frac{3}{2}}$	$1d_{\frac{3}{2}}$	0	0	0
Neutron	$2s_{\frac{1}{2}}$	$2s_{\frac{1}{2}}$	0	0	0
	$2s_{\frac{1}{2}}$	$1d_{\frac{3}{2}}$	0	$-1.210\ \beta k(I(2))_{sd}$	0
	$1d_{\frac{3}{2}}$	$2s_{\frac{1}{2}}$	0	$-0.856\ \beta k(I(2))_{sd}$	0
	$1d_{\frac{3}{2}}$	$1d_{\frac{3}{2}}$	0	0	0

TABLE A2-3d Single-Particle Matrix Elements

$<\ell_1\ \tfrac{1}{2}\ j_1||M'_L||\ell_2\ \tfrac{1}{2}\ j_2>$

Particle	Initial State	Final State	L = 1	L = 2	L = 3
Proton	$2s_{\frac{1}{2}}$	$2s_{\frac{1}{2}}$	4.84 β	0	0
	$2s_{\frac{1}{2}}$	$1d_{\frac{3}{2}}$	0	0	0
	$1d_{\frac{3}{2}}$	$2s_{\frac{1}{2}}$	0	0	0
	$1d_{\frac{3}{2}}$	$1d_{\frac{3}{2}}$	-2.16 β	0	1.416 $\beta(I(2))_{dd}$
Neutron	$2s_{\frac{1}{2}}$	$2s_{\frac{1}{2}}$	-3.31 β	0	0
	$2s_{\frac{1}{2}}$	$1d_{\frac{3}{2}}$	0	0	0
	$1d_{\frac{3}{2}}$	$2s_{\frac{1}{2}}$	0	0	0
	$1d_{\frac{3}{2}}$	$1d_{\frac{3}{2}}$	1.48 β	0	-0.970 $\beta(I(2))_{dd}$

TABLE A2-3c Proton Single Particle Matrix Elements

$$\langle \ell_1 \tfrac{1}{2} \; j_1 || M_L || \ell_2 \tfrac{1}{2} \; j_2 \rangle$$

Initial State	Final State	L = 1	L = 2	L = 3
$2s_{\frac{1}{2}}$	$2s_{\frac{1}{2}}$	0	0	0
$2s_{\frac{1}{2}}$	$1d_{\frac{3}{2}}$	0	0	0
$1d_{\frac{3}{2}}$	$2s_{\frac{1}{2}}$	0	0	0
$1d_{\frac{3}{2}}$	$1d_{\frac{3}{2}}$	2.324β	0	$-1.014\beta(I(2))_{dd}$

TABLE A2-4a E2 Two-Particle Matrix Elements for T + T' Even.

in the $2s_{\frac{1}{2}}$ and $1d_{\frac{3}{2}}$ Shells.

Final / Initial	$\vert s_{\frac{1}{2}}^2\rangle$	$\vert s_{\frac{1}{2}} d_{\frac{3}{2}}\rangle$	$\vert d_{\frac{3}{2}}^2\rangle$
$\vert s_{\frac{1}{2}}^2\rangle$	0	$[0.0913e+0.0803\beta k]$ $k^2(I(2))_{sd}$	0
$\vert s_{\frac{1}{2}} d_{\frac{3}{2}}\rangle$	$-[0.0913e+0.0803\beta k]$ $k^2(I(2))_{sd}$	$0.0457ek^2(I(2))_{dd}$	$[0.0289e+0.0254\beta k]$ $k^2(I(2))_{sd}$
$\vert d_{\frac{3}{2}}^2\rangle$	0	$-[0.0289e+0.0254\beta k]$ $k^2(I(2))_{sd}$	$-0.0730k^2(I(2))_{dd}$

TABLE A2-4b M1 Two-Particle Matrix Elements for T + T' Even in the $2s_{\frac{1}{2}}$ and $1d_{\frac{3}{2}}$ Shells.

Final / Initial	$\vert s_{\frac{1}{2}}^{2}\rangle$	$\vert s_{\frac{1}{2}} d_{\frac{3}{2}}\rangle$	$\vert d_{\frac{3}{2}}\rangle^{2}$
$\vert s_{\frac{1}{2}}^{2}\rangle$	1.244βk	0	0
$\vert s_{\frac{1}{2}} d_{\frac{3}{2}}\rangle$	0	0.444βk	0
$\vert d_{\frac{3}{2}}^{2}\rangle$	0	0	0.600βk

TABLE A2-5 Shell Model Two-Particle Configurations of Predicted ^{30}P states.

J	T	Level Energy (MeV)		Amplitudes		
		Expt'l	Predicted	$\vert s_{\frac{1}{2}}^{2}\rangle$	$\vert s_{\frac{1}{2}} d_{\frac{3}{2}}\rangle$	$\vert d_{\frac{3}{2}}^{2}\rangle$
1	0	0	0	+0.482	+0.865	+0.138
0	1	0.680	0.65	-0.852	+0.0	+0.523
1	0	0.709	0.67	-0.876	+0.471	+0.100
3	0	2.536	2.71	+0.000	+0.000	+1.000
2	0	2.722	2.89	0.000	+1.000	+0.000
2	1	2.939	2.98	0.000	-0.971	+0.239

LIST OF SYMBOLS

A	matrix related to P_k's, U(k,n,)'s and x's
A_i	corrected photopeak area corresponding to B_i
A_k	coefficients in a Legendre polynomial expansion of order k
e	electronic charge
E_λ	single-particle energy of state $\|\lambda>$
$F_k(ab)$	coefficients in the expression for W(θ) which depend only on the gamma-ray transition from state 'a' to state 'b'
$F_k(LL'ab)$	coefficients in the expression for W(θ) related to the above F's
i	imaginary unit
I(L)	integral involving single-particle radial wave functions
ℓ	single-particle angular momentum
k	wave number (=2π/λ) where λ is the wave length of a photon
ℓ	orbital quantum number
L	multipolarity of a gamma-ray transition
$L_{n\ell}$	associated Laguerre polynomial
M	magnetic quantum number corresponding to L
$\|M\|^2$	strength of a transition (gamma) in Weisskopf units
N	number of degrees of freedom in χ^2
P(α)	population parameter of α^{th} magnetic substate

$P_k(\cos\theta)$	Legendre polynomial of order k
Q_k	attenuation coefficients for the gamma-ray detector
Q_{LM}, Q'_{LM}	electric multipole operators
T_{LM}	general interaction operator
$U_k(ab)$	coefficients similar to $F_k(ab)$
$U(k,n,\alpha)$	coefficients in $W(\theta)$ related to $F_k(LL'ab)$, Q_k and $\rho_k(a\alpha)$
$U_{n\ell}$	radial part of harmonic oscillator wave function
$W(\theta)$	angular distribution of a gamma ray
X	column vector whose elements are the population parameters
x	mixing ratio of a gamma-ray transition
$Y(\theta)$	gamma-ray yield at angle θ
Y_{LM}	spherical harmonic
α	magnetic quantum number
α_L	multipole expansion coefficient
β	nuclear magneton
χ^2	chi-square
ω	matrix of weighting values in the expression for χ^2
$\rho_k(a)$	statistical tensor describing the population of the α^{th} magnetic substate of state 'a'
$\rho_k(a\alpha)$	coefficients occurring in the expansion of $\rho_k(a)$ in terms of the population parameters
σ	standard deviation

τ	transition speed in seconds
δ_L	the Rose and Brink notation for a gamma-ray mixing ratio
$(\ell_1 m_1 \ell_2 m_2 \| \ell m)$	Clebsch-Gordan coefficient
$w(abcd;ef)$	Racah coefficient
$<a\|\|H\|\|b>$	a reduced matrix element of the operator H between states 'a' and 'b'

B29880